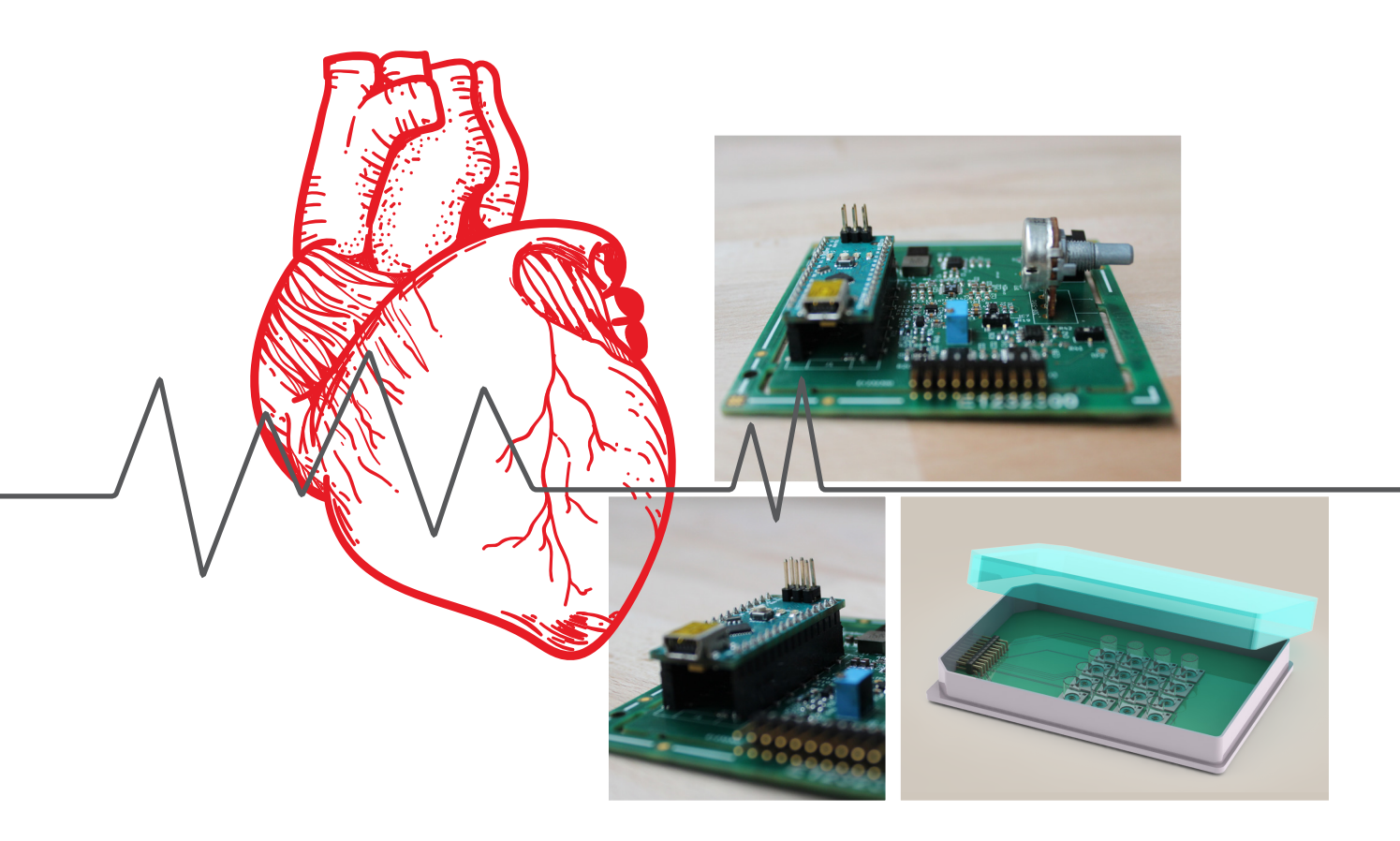


Design and Fabrication of Electrical Stimulation Set up for EHT platform

by Androniki Diakou





Design and Fabrication of an Electrical Stimulation Set Up for EHT platform



Androniki Diakou

In partial fulfillment of the requirements for the degree of

Master of Science

in Biomedical Engineering, at the Delft University of Technology, to be defended publicy on Monday September 28, 2020 at 12:00 AM.

Supervisor: Dr. Massimo Mastrangeli Daily Advisor: Milica Dostanic Committee Members: Prof. Dr. Lina Sarro(chair) Prof. Dr. Wouter Serdijn

Preface

The current thesis project is the final step for the completion of my studies in Biomedical Engineering in the Technical University of Delft. It is a period of my life full of personal and educational development which started with the diploma of Electrical & Computer Engineering in the Technical University of Volos in Greece (equivalent to Master) and concludes with the Master degree of Science in Biomedical Engineering at TU Delft.

However, I would not be able to do so without the psychological and materialistic support of my parents(Anestis and Evdokia), my brothers(Nikolaos and Kostantinos), my beloved boyfriend Gerasimos and my friends. Thank you for providing me with unfailing support and continuous encouragement throughout my studies. This accomplishment would not have been possible without you.

I would also like to thank my supervisor Massimo Mastrangeli who trusted me for this project and for his guidance throughout my thesis. I feel happy that we collaborated for this project.

Special thanks to my daily advisor and PHD candidate Milica Dostanic for her guidance, patience and help throughout my project. Microfabrication was a completely new world for me and I learned a lot from you. Thank you for all.

Furthermore, I would like to thank Prof. Lina Sarro, who also gave me the opportunity to become part of her team for these months and for the time she will spend to read and evaluate my effort. Thank also Prof. Wouter Serjin for being member of the committee.

During all these years I was given the opportunity to expand my knowledge and my experience in a broad range of topics. Now, I feel confident that I can apply my knowledge for the benefit of the society and the common good.



Abstract

The overarching goal of Engineered Heart Tissues (EHTs) is to develop functional 3D heart tissues in vitro with the potential to find drug targets, identify drug toxicity and predict the effects of the drugs in the body. This 3D model of the cardiac tissue consists of a bunch of cells, self-assembled around specific anchoring points the main aim of which is to support tissue formation. Although this model is very promising, still has to overcome an important drawback which is the lack of maturation of iPSC-derived cardiomyocytes (CM). This obstacle leads to limited recreation of the adult human cardiac tissue physiology.

It has been shown that electrical stimulation of cardiac cells is one of the most important factors for cardiomyocyte's maturation. Therefore, the principal goal of this thesis is to design and fabricate an electrical stimulator device and integrated electrodes in an existing EHT platform for electrical stimulation of cardiomyocytes. In the beginning, a literature study was conducted on different electrical stimulation methods and existing electrical stimulation devices for this purpose.

For the first part of the thesis which was the design and fabrication of electrical stimulator, the electrical stimulation parameters that must be fulfilled by this device, were specified. Various hardware design approaches were studied in detail and compared before the design and implementation of the final idea. Simulations of the selected method using the LTSpice software tool were performed in order to study the behavior of the electrical stimulator design. The device is a 16-channel electrical stimulator that provides perfect rectangular biphasic pulses in the range of $\pm 15V$ with adjustable voltage amplitude, frequency and duty cycle. A user-friendly interface allows the user to select the desired channel of stimulation and the signal is distributed providing electrical stimulation to a total of EHT platforms. Therefore, this device was designed in a way to be connected with a second Printed Circuit Board(PCB) which hosts 16-EHT with integrated electrode chips. The 16-EHT holder (PCB) was also designed to suit in a 96-well plate, used by biologists for cardiac-cell culturing inside the incubator. The characterization of the electrical stimulator took place in the measurement room of the EKL lab. The results of the measurements verify the precision and efficiency of the electrical stimulator circuit as they are in excellent agreement with the simulations.

The second part of the thesis includes the fabrication of integrated electrode-chips. The fabrication was conducted at EKL lab, in the Microelectronics Department of TUD using clean room microfabrication techniques. The selected electrode material was TiN due to its unique mechanical properties and the electrodes were fabricated on PDMS, encapsulated between two layers of polyimide. The main steps required for the integration of these electrodes in the existing EHT platform have been also carried out.

Keywords: Engineered Heart Tissue; cardiomyocytes (CM); 96-well plate; electrical stimulation; electrical stimulator; integrated electrodes

_CONTENTS

Li	st of	symbols	i
Li	st of	figures & tables	ii
1	Intr	roduction	1
	1.1	Organ-on-Chip Technology	1
	1.2	Chronology and Current State	2
	1.3	Main Sources of Cells for Organ-On-chip	3
	1.4	Main Applications of Organ-On-Chip	3
		1.4.1 Blood-brain barrier	3
		1.4.2 Liver-on-Chip	4
		1.4.3 Lung-on-Chip	5
		1.4.4 Heart-on-Chip	6
	1.5	Summary	6
	1.6	Engineered Heart Tissue(EHT)	6
		1.6.1 Introduction	6
		1.6.2 Advantages over 2-D structures	7
		1.6.3 EHT as a promising solution	7
	1.7	Importance of Electrical Stimulation in EHT maturation	11
	1.8	Parameters for Electrical stimulation of Cardiomyocytes	11
		1.8.1 Shape of pulse (Biphasic/Monophasic)	12
		1.8.2 Faradaic versus Non Faradaic charge transfer	12

		1.8.3	Type of electrodes used for electrical stimulation	14
		1.8.4	Equivalent Circuit model for electrode-electrolyte interface	14
	1.9	Goal	of the Thesis and Research Statement	14
		1.9.1	Goal of the thesis	14
		1.9.2	Research Statement	15
	1.10	Thesis	S Outline	16
2	Elec	ctrical	Stimulation Methods for Cardiomyocytes	17
	2.1	Metho	ods for electrical stimulation of 2D cell cultures and design of stimulator systems	17
	2.2	Metho	ods for electrical stimulation of 3D cardiac tissues	19
		2.2.1	Training the cardiac tissue by using electromechanical stimulation	19
		2.2.2	Current Techniques: Bioreactors	20
		2.2.3	Current Techniques: Fabrication of 3D electrodes	20
		2.2.4	3D pillar electrode for 3D cardiac tissues	21
		2.2.5	Summary	21
	2.3	Hardv	vare designs of Electrical Stimulators	22
		2.3.1	Introduction	22
		2.3.2	Voltage-Controlled Voltage Source (VCVS) vs Current Controlled (CCS)	22
		2.3.3	H-Bridge for Biphasic pulse Generation	22
	2.4	Oper	ational Amplifier for biphasic pulse generation	23
	2.5	Volta	ge Source to Current Source Conversion	24
		2.5.1	Wilson Current Mirror Technique	24
		2.5.2	Voltage to Current Converter	26
	2.6	Hardv	vare designs conclusions	27
3	Des	ign of	a Pulse Generator System	28
	3.1	Introd	luction	28
	3.2	Impor	tant Parameters for the circuit design	29
		3.2.1	Equivalent circuit of electrode and cardiac cells interface	29
	3.3	Syster	n's specifications	30
	3.4	Design	n of Power Supply System	31
		3.4.1	Description of Charge Pump Converter	32

5	4.4 4.5 4.6 4.7 4.8	The proposed circuit design can provide a wide spectrum of frequencies Testing and Measurement of Duty Cycle 4.5.1 Measurement and verification of current measurement circuit Measurement and verification of voltage Measurement Circuit 4.6.1 Voltage Controlled Mode 4.6.2 Current Controlled Mode Testing of Howland Converter Circuit Conclusion rication of Integrated Electrodes in an EHT platform	
	4.5 4.6 4.7	The proposed circuit design can provide a wide spectrum of frequencies	54 55 56 58 58 62 65
	4.5	The proposed circuit design can provide a wide spectrum of frequencies	54 55 56 58 58 62
	4.5	The proposed circuit design can provide a wide spectrum of frequencies	54 55 56 58 58
	4.5	The proposed circuit design can provide a wide spectrum of frequencies Testing and Measurement of Duty Cycle	54 55 56 58
	4.5	The proposed circuit design can provide a wide spectrum of frequencies	54 55 56
		The proposed circuit design can provide a wide spectrum of frequencies	54 55
		The proposed circuit design can provide a wide spectrum of frequencies	54
	4.4		
		4.5.1 Testing the functionality of the potentionieter	54
		4.3.1 Testing the functionality of the potentiometer	
	4.3	Testing Procedure of the Biphasic Pulse generation unit	53
	4.2	Testing procedure of the Power Supply circuit	53
	4.1	Description of Measurement set up	51
4	Mea	asurement and Results	51
	3.13	Conclusions	50
	3.12	Design of a PCB for 16- integrated electrode chips	48
		3.11.1 Current Source	45
	3.11	Voltage to Current Source Stimulation	45
	3.10	Current Source Electrical Stimulation	44
	3.9	Circuit for Measuring the applied voltage amplitude	43
	3.8	Measuring the current through the electrodes	42
	3.7	Demultiplexing the rectangular biphasic signal to the output	41
		3.6.1 Opamp for biphasic pulse generation	39
	3.6	MCU unit and PWM generation	37
		3.5.1 Analysis of Selected Method	36
	3.5	Uni-phasic to Bi-phasic pulse converter system	36
		Calculation of Peak inductor current	36
		Calculation of Minimum Value of the output inductor	35
		3.4.2 Description of Buck Converter	34

	5.2	PDMS	S on Silicon	. 68
	5.3	TiN as	s a material for electrodes fabrication	. 68
	5.4	Microf	fabrication of the EHT platform	. 69
		5.4.1	Introduction	. 69
		5.4.2	Manufacturing process of EHT platform	. 69
		5.4.3	Filling the Pillars with PDMS	. 75
		5.4.4	Etching PDMS	. 75
		5.4.5	Al etching for Contact Pads	. 76
		5.4.6	First Layer of Polyimide	. 76
	5.5	Fabric	ation Process for Test Electrode structures	. 80
		5.5.1	Conclusion	. 83
6	Disc	cussion	1	84
	6.1	Design	n of 16-channel Electrical Stimulator	. 84
	6.2	Integra	ated Electrodes and read-out interface	. 85
7	Con	clusio	n and Recommendations	86
	7.1	Conclu	asion	. 86
	7.2	Future	e Recommendations	. 87
Re	efere	nces		87
A	Sch	ematic	s and PCB layout	93
	A.1	Design	Schematics of Electrical Stimulator	. 93
В	Pro	gramn	ning code in C/C++ for controlling the electrical stimulator	98
\mathbf{C}	Sim	ulation	a Circuit of second method of biphasic pulse generation	101
D	List	s with	Electronic Component Selection	102

____LIST OF SYMBOLS

Symbol	Description	Units
\overline{f}	Frequency	$_{ m Hz}$
T	Period	S
V_{i}	Input voltage	V
V_o	Output voltage	V
I	Current	A
VCS	Voltage Controlled Stimulation	
CCS	Current Controlled Stimulation	

_LIST OF FIGURES

1.1	Brain on Chip model: (a) 1. top part of the device, 2. Membrane, 3. the bottom part of the Brain on Chip, 4. Pt integrated electrodes and (b) the figure of the assembled device. (c) Illustration of Brain on chip made in PDMS [14]	4
1.2	Multiple layers of PLCs were deposited on PDMS membrane to form a biological template and hexagonal coutour [17]	5
1.3	Illustration of the lung-on-chip device with a PDMS membrane which separates the two microchannels forming a barrier between alveolar and capillaries. The right figure depicts the applied vacuum to the chambers aiming to introduce the desirable mechanical stretching[18]	5
1.4	Schematic representation of the proposed set up for EHT. Picture (a) illustrates the assembly of a casting mold. Specifically, tubing (T) was attached to the substrate made by glass. Then the disks (D) and the cylinders (C) function as spacers while the casting mold is prepared. Picture (b) depicts the creation of EHT around the cylinders. Picture (c) shows the transfer of EHT in a stretch device which provides the desirable stretch contributing to further development of EHT. Picture (d) shows the EHT in a thermostated organ bath. Scale Bars=10mm [26]	8
1.5	In the left figure a general design of Heart-Dyno is provided, and in the right Figure the formation and the culture of cardiac tissue in this device is illustrated [29]	9
1.6	Schematic representation of EHT platform developed at ECTM group in TU Delft. Pictures (a),(b),(c), shows the three scale down chips. The first one (a) can fit up to 16000 cells, the second one (b) up to 31.000 cells and the third one (c) up to 47000 cells.(d) illustrates the etched silicon wafer and the (e) illustrates the final PDMS structures of the EHT platform [30]	10
1.7	Schematic of all the possible methods that cause maturation to cardiomyocytes. The introduction of mechanical stimuli such as cyclic or static stretch, the electric field by using electrical stimulation of cardiomyocytes, the change of extracellular matrix properties and the mix of cardiomyocytes with fibroblasts or endothelial cells are some of the most important factors[32]	11
1.8	Illustration of biphasic pulse generator and the circuity of the electrode. As the figure shows the anodic amplitude of the pulse is followed by a cathodic amplitude of the pulse but in the opposite polarity. The symbol TF represents the train frequency of the pulse and the symbol TD represents the duration of the pulse [38]	12

1.9	Comparison between Faradaic and Non-Faradaic processes which take place at an electrode[39]	13
1.10	Rendel's model as a representation of the electrode-electrolyte interface which is created by inserting an electrode in contact with $\operatorname{cells}[40]$	14
2.1	Schematic representation of MEA chip for 2D cell culture. The MEA chip is glued and wire-bonded to the PCB. The electronic circuit which provides electrical stimulation to MEA chip is also presented.[47]	18
2.2	Demonstration of electrical stimulation for MEA[49]	18
2.3	(A) Demonstration of the general set up of the electrical stimulation system (Block Diagram). (B), (C) An illustration of the electric field during the electrical stimulation (D) In detail illustration of container for six MEAS with cells culture on them [50]	19
2.4	(A) Electrical stimulation of cardiac tissue using the proposed bioreactor. B) Mini bioreactor with electrodes and PDMS base for gene expression tests. C) The result from electrical stimulation with biphasic square pulse measured with an oscilloscope [55]	20
2.5	Fabrication of the interdigitated array of Pt electrodes and application of electric field stimulation of C2C12 myotubes [39]. The interdigitated array of Pt- electrodes used for the stimulation of 3D arrays of engineered muscle tissue, made by a hydrogel called gelatin methacrylate (GelMA). GelMA hydrogel consists of gelatin modified with methacrylic anhydride. This hydrogel is very useful for tissue engineering applications[56].	21
2.6	Illustration of 3D pillar electrode for 3D cardiac tissues [57]	21
2.7	(a) Schematic representation of H-Bridge method for generating biphasic pulse. (b) The relation among S1-S4 in order to produce the pulse. (c) Illustration of biphasic balanced current pulse $[62][63]$	23
2.8	Depiction of a constant current biphasic stimulator for neural applications. It consists of a microcontroller (MSP430) which produces a PWM at a very high frequency (up to 40 kHz). The electronic circuit consists also of a second amplifier which generates negative DC voltage, (C) an inverter amplifier that produces a positive DC voltage, (D) multiple analog switches and (E) a converter which converts the voltage source to current source [64].	24
2.9	Illustration of Wilson current mirror technique: The current in the output is equal to the input current[67]	25
2.10	Two current mirror as a technique to produce biphasic current pulses for electrical stimulation[67]	26
2.11	Circuit design of voltage to current converter implemented in electrical stimulator for robotic $\operatorname{system}[67]$	27
3.1	Randell's circuit for modelling the load of the pulse generator circuit[70]	29
3.2	TiN electrodes shape and contact pads illustration CAD model	29
3 3	Block diagram of Power Supply system of the pulse generator circuit	31

3.4	Block diagram of Complete Electrical Stimulator for EHT platform. The Power management System which supplies power all sub-units is illustrated together with the main unit of biphasic pulse generation.	31
3.5	Schematic of the dual charge pump circuit that generates ± 12 Volts for the power supply of amplifiers[73]	33
3.6	Schematic of the dual charge pump circuit that generates ± 12 Volts for the power supply of amplifiers[73]	33
3.7	$Schematic \ diagram \ of \ Buck \ Converter \ which \ supplies \ with \ voltage \ the \ microcontroller \ [74].$	35
3.8	Schematic representation of the proposed method for biphasic pulse generation	36
3.9	PWM waveforms for different values of Duty Cycle. For 0 Duty cycle the PWM signal is off, for 50 Duty cycle half of the signal is OFF and half of the signal is ON, 75 Duty Cycle 75 is ON and 25 is OFF and 100 Duty cycle means that the PWM is ON. [75] .	37
3.10	Control the clock frequency of the microcontroller to achieve low frequencies in the range of $0.5\text{-}5\text{Hz}$	38
3.11	Schematic design of the amplifier circuit that will use in our case	39
3.12	Circuit design for the simulations in LTSpice software tool	40
3.13	Output from the simulation of the first amplifier which takes as an input two biphasic pulses with an amplitude of 5V and converts them to $\pm 12V$ biphasic pulse	40
3.14	Output from the simulation of the second in series amplifier (buffer amplifier) which purpose is to improve the quality and consistency of the signal. The black line in the signal indicates the difference in comparison with the first signal	41
3.15	Output from the simulation of the third amplifier in parallel of which a potentiometer was placed	41
3.16	Conceptualized schematic of microcontroller and demultiplexing unit	42
3.17	Schematic of circuit which measures the amount of current passing through the connected electrodes	43
3.18	Schematic design of the circuit for measuring the applied voltage	44
3.19	A practical current source	45
3.20	The Improved Howland Current Pump Method for current controlled stimulation [83] [84] [84]	5]. 46
3.21	Howland circuit with the used values of resistors. The Rload of this circuit tested for different values $(300\Omega, 500\Omega, 1k\Omega)$	47
3.22	The Improved Howland Current Pump Method for Voltage Controlled Charge-Balanced method. The current remains stable at 7mA and independent of the load	47
3.23	The updated power supply system consists of an external charger (30V) and a power management system. The power management system includes a buck converter which supplies the microcontroller and a dual charge pump converter which supplies the biphasic generation unit and the measurement circuits	48
3.24	3D CAD Model of Pulse Generator Circuit for Electrical Stimulation of Cardiomyocytes in an EHT platform.	48

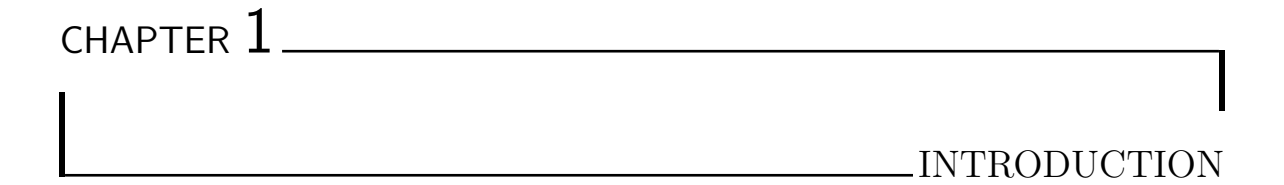
3.25	3D CAD model of PCB holder for one electrode chip	49
3.26	$3\mathrm{D}$ model of PCB holder for 16-electrode chips. The 6mm holes in the PCB enable the transparency and observation of the cardiac cell cultures during the experiments	49
3.27	3D model of holder structure for 16-electrode chips. The bottom of the holder was designed in KiCad (see Figure 3.26). Then this PCB was integrated with the entire case for the EHT platforms and was designed in Solidworks by M. Dostanic	50
4.1	Simple set up for testing the microcontroller output using a digital oscilloscope	51
4.2	Fabricated version of PCB	52
4.3	Entire measurement set up which includes the power supply of 30V, an oscilloscope, a multimeter and the testing PCB	52
4.4	The output of the first amplifier which creates the threshold of $\pm 15 \text{Volts}$. The biphasic pulse reaches up to 14.8V and the period of the signal is T=1sec	53
4.5	The pulse generator circuit for EHT electrical stimulation purposes has the ability to alter the voltage amplitude by simply rotating a knob to be adjusted in the experiment needs. The Figure illustrates various voltage amplitudes (0.7V, 6.31V, 14.26V, 14.8V).	54
4.6	The design electrical stimulator provides biphasic pulses in various frequencies in the range of 0.3-4Hz. The results from the measurements verify the precision in the achievement of low frequencies. The user can change the frequency by step of 0.1Hz. (a) 0.5Hz, (b) 1hZ, (C) 1.5HZ, (d) 4HZ	55
4.7	Illustration of biphasic pulse with (a) 2.5% duty cycle. (b) 5% duty cycle, (c) 10% duty cycle and (d) 40% duty cycle	56
4.8	The blue graph represents the Voltage Input to the current sense amplifier and the red graph represents the measured signal in the ADC output of the microcontroller	57
4.9	The (a) graph illustrates the voltage input to the current measurement circuit while the graph b represents the measured current in the pin A7 of the microcontroller. The measured value was 4.3 mA something that verifies the accuracy of the measurement circuit.	58
4.10	This schematic demonstrates the new values of the loads. The gain and the offset of the voltage measurement circuit were calculated according to these values	59
4.11	Results from simulation circuit behavior in LTSpice	59
4.12	The blue dot and the grey dot represent the points where the signal was measured. The A6 label indicated the output of the amplifier which is sent to A6 pin of the microcontroller to measure the voltage	60
4.13	The blue line represents the applied voltage in the blue dot while the red line represents the measured voltage by the microcontroller.	60
4.14	The blue line represents the applied voltage in the blue node while the red line represents the measured voltage by the $microcontroller(VA6)$	61
4.15	The voltage was measured in the yellow node of the circuit and in the brown node (A6)	62
4.16	The blue line represents the voltage amplitude at the yellow node, while the red line represents the voltage in the grey node(A6)	63

4.17	TP2: Applied Voltage A6: Measured Voltage	64
4.18	Voltage measurement graph: The blue line represents the voltage amplitude as it was measured at the yellow node (TP2), while the red line represents the voltage in the grey node A6 (the pin of microcontroller that measured the voltage)	64
4.19	Illustration of the circuit and the test points where the oscilloscope measures the signal.	65
4.20	Measured Voltage Waveform at TP2 node for three different values of loads (220 Ω , 500 Ω and 1 k Ω)	66
4.21	Stability of the output current, independent of the load changing, verifying the accuracy of Howland converter.	66
5.1	Sketch of the flowchart for TiN electrodes integration in EHT platform	70
5.2	Silicon oxide deposition (step 1) and patterning oxide in the front side (step 2)	71
5.3	Schematic of PECVD reactor [90]	72
5.4	3D illustration of pillar's depth after observing under the microscope	73
5.5	Profile of etched structures in Si wafers. The total depth of pillars after etching was measured at 663um.	73
5.6	Growth Si oxide as a stopping layer	74
5.7	Wet etching of oxide from the backside of the wafer	74
5.8	Filling the pillars structures with PDMS	75
5.9	Deposition of Al layer on the PDMS	76
5.10	TiN openings for electrodes and PDMS etching at TiN openings	76
5.11	Al etching for contact pads creation	76
5.12	First layer of polyimide (PI)	77
5.13	TiN metal sputtering above the first layer of PI	78
5.14	Deposition of second layer of PI above the TiN metal	78
5.15	The last steps of the microfabrication process including the release of membrane and the reveal of PDMS pillars	78
5.16	The last steps of the microfabrication process including the release of membrane and the reveal of PDMS pillars	79
5.17	Optical picture of electrode structure after the first layer of polyimide	81
5.18	Illustration of two TiN contact of Electrode encapsulated between two layers of polyimide above PDMS polymer	82
5.19	Illustration of two TiN contact of Electrode encapsulated between two layers of polyimide above PDMS polymer	82
5.20	Illustration of two TiN contact of Electrode encapsulated between two layers of polyimide above PDMS polymer	83

A.1	Schematic of the buck converter chip which converts 30V to 8V and supplies the microcontroller
A.2	Schematic of the Charge Pump Converter which converter which converts 30V to +-15V and supplies the amplifiers
A.3	Entire Schematic of Electrical Stimulator Circuit
A.4	3D Version of Electrical Stimulator
A.5	The KiCad schematic of the front layer of the PCB
A.6	The KiCad schematic of the second layer of the PCB
A.7	The KiCad schematic of the third layer of the PCB
A.8	The KiCad schematic of the back layer of the PCB
B.1	Set up and initialization of parameters
B.2	Set up and initialization of parameters
B.3	Channel selection-automated the user just type the desired channel of stimulation in the serial monitor and the pulse is directed to it
B.4	Channel selection-automated the user just type the desired channel of stimulation in the serial monitor and the pulse is directed to it
B.5	Voltage Measurement and Current Measurement circuits and
B.6	Safety Module
C.1	Simulation circuit of second method of biphasic pulse generation
C.2	Result from simulation of second method of biphasic pulse generation

LIST OF TABLES

3.1	Specifications of Pulse Generator Circuit
4.1	Tested load values and Values of the output current after the voltage-to-current converter 67
D.1	Component List fo DC Buck Converter
D.2	Component List fo DC Buck Converter
D.3	Component List for Biphasic Pulse Generation Unit
D.4	Component List for Howland Converter
D.5	Component List for Voltage Measurement and Microcontroller



1.1 Organ-on-Chip Technology

A major problem in the development of effective drugs for the treatment of serious diseases is the absence of reliable models to recognize the drug targets, identify the drug toxicity [1] and predict the effects of drugs in the human body [2]. Conventional animal models or 2D cell cultures fail to precisely emulate human physiology and consequently to predict human responses to drug treatments. This problem represents one of the main causes of drug failures during the period of clinical trials and the lack of medical treatments for specific serious diseases [2]. Furthermore, ethical concerns that stem from the use of animals in drug testing lead to the willingness of minimization of animal experiments or their replacement with other alternative methods [3][4]. Due to the aforementioned reasons, the need to find an alternative method that simulates both the function of human organs and tests the efficiency of specific drugs becomes essential.

Organ-on-chip technology aims to create miniaturized microfluidic in vitro systems whose purpose is to mimic the crucial biological and physiological behavior of in vivo environment of specific organs [5]. These in vitro models aim to become an alternative to conventional static cell culture in the future, bridging the gap between the animal models for drug testing and the human body[6]. Although there is a wide spectrum of organ-on-chip applications (some of the most significant are illustrated below), this introduction chapter is directed more towards the Engineered Heart Tissue (EHT) model. Its development has undergone impressive progress during last decades and it has been driven by three motivations. The first one is to generate cardiac tissue outside of the biological environment for cardiac repair. The second one is to create in vitro models of heart function, and the third one to observe and study a cardiac muscle beating on a dish [6].

One of the most important challenges that the heart-on-chip models face is the lack of maturation of iPSC-derived cardiomyocyte (CM)[7]. This obstacle leads to limited recreation of the physiology of adult human cardiac tissue. The maturation of CMs can be induced by different factors such as mechanical or electrical stimulation of tissue [7]. The study of these factors stimuli and their role in the CMs maturation will set the foundations for the development of an environment that emulates the functions of the heart efficiently. Due to the fact that the electrical stimulation has a role of the utmost importance for the growth and maturation of cardiomyocytes, the first introduction chapter analyses important electrical stimulation parameters leading to worth-mentioning conclusions and at the same time explains existing electrical stimulation methods and devices.

1.2 Chronology and Current State

In the past, scientists were working for years to develop new drugs for the treatment of serious diseases [8]. Animals have been used as preclinical models to emulate the processes that takes place in human body.

However, animals as models for drug testing cannot capture faithfully the human physiology. The fundamental translation problem dominates leading to some drugs work well on animals but not to humans. Furthermore, animal experiments for drug testing are subjected to scepticism for ethical reasons [3][8]. As a result of this, scientists started looking for other alternative solutions to this problem [9].

Later, the advance of science and technology led to the development of *in vitro* two-dimensional cell cultures, in plastic Petri dishes, in order to test the drug toxicity. These traditional *in vitro* models have been used until nowadays in many laboratories aiming to study the cell responses to stimulation from biophysical and chemical signals [10]. It is proven that 2D cell culture in a Petri dish has undoubtedly improved the understanding of cellular behavior and growth by the scientists [10]. Nevertheless, they have not yet sufficiently simulated the interactions between cells or between a cell and a matrix [11].

The progress of microfabrication, tissue engineering and biology led to the development of microfluidic devices called organ-on-chip (OOC). In OOC models, cells are cultured on a chip which hosts the environment where the cells are grown and interact with each other[3]. Those chips are small in dimension and constituted of one or more chambers, where the cells are located. The basic material of the chip is usually transparent which allows easy optical imaging of the cells. The surface of a micro-chamber can be made of various materials, such as natural or synthetic polymers [3].

The OOC is a promising technology providing a more precise view regarding the human responses to drugs compared to conventional models. Some of the most worth mentioning properties that an ideal OOC should have are the following [2][3]:

1. Tissue Structure

• One of the most important parameters which ensure the tissue structure is the contact between cells and the interface between tissues. An ideal OOC model should offer an environment that allows the study of tissue-tissue interface and the biological processes that would be difficult to be controlled in animal experiments.

2. Good conditions in the micro-environment

• Due to the fact that OOC models represent a sub-unit of an organ and emulate the physiology and its main functions, it is essential to provide a micro-environment which really mimics the natural environment where an organ lives and matures. Thus, the control of conditions of the cellular micro-environment can be achieved by the control of dynamics such as electrical and mechanical stimulation. Furthermore, the integration of perfusion systems and the control of flow which ensure the oxygenation and nutrition of the organs, are important parameters for healthy tissues. Therefore, an ideal OOC device should include the aforementioned systems in order to simulate with more precision the natural cellular micro-environment.

3. Main Functions

• The primary function of an ideal OOC is to recapitulate the physiology of a human organ and mimic basic functions. In addition, an ideal OOC model should emulate the biological properties of an organ and how it reacts to the external stimuli.

1.3 Main Sources of Cells for Organ-On-chip

One of the most important aspects of the successful development of OOC is the investigation of cell sources. Two factors determine the type of human cells that are used for OOC. The first one is whether there are cells available for this purpose and the second the ability of cells to interact with each other outside of the biological environment [12]. The ideal scenario according to previous surveys is the organ units for OOC models to be isolated from the same kind of cells [12]. Adult primary cells can be found in adult patients and they are suitable for clinical studies in humans. However, this type of cells is limited in number in tissues such as the heart. On the other hand, Pluripotent Stem Cells (PSC) can be produced after reprogramming adult somatic stem cells (human induced pluripotent stem cells) [2]. It is important to mention that hiPSC can be found in any individual. However, the maturation of hiPSC cells beyond a fetal stage requires a great effort. For this reason, the development of an environment which ensures the maturation of these cells is a big challenge [2][13].

1.4 Main Applications of Organ-On-Chip

This section focuses on the main applications of OOC technology including Blood-Brain-Barrier (BBB), liver-on-chip, lung-on-chip and heart-on-chip.

1.4.1 Blood-brain barrier

The Blood-brain barrier acts as a separation of blood from the brain tissue and it is aiming to offer homeostasis by protecting the brain from harmful substances from the blood. For this reason, the investigation of Blood-brain barrier and its functions is crucial for drug development and the advance of research in the biomedical field. A wide spectrum of microfluidic devices that aim to mimic the function of the Blood-brain barrier on a chip has been developed in the last years. All developed models are facilitating the study of cell behavior and interaction as well as the effects of drugs. These new developments of in vitro models indicate that the field of Blood-brain barrier on chip is moving forward [14][15].

One of the most remarkable Blood- brain barrier on-chip models was developed by the research team of Griep et al. who used human cerebral endothelial cells and placed them on the top of a PDMS membrane. Specifically, they achieved to adjust the Barrier function mechanically through shear stress exposure and biochemically by applying stimulation using a tumor necrosis factor "a". Furthermore, the research team incorporated electrodes in order to measure the transendothelial electrical resistance aiming to analyze the barrier tightness (Figure 1.1) [14].

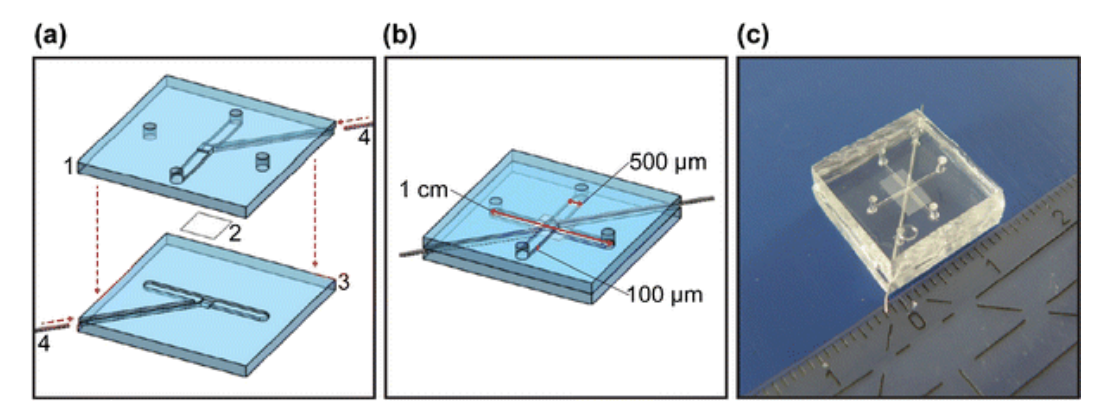


Figure 1.1: Brain on Chip model: (a) 1. top part of the device, 2. Membrane, 3. the bottom part of the Brain on Chip, 4. Pt integrated electrodes and (b) the figure of the assembled device. (c) Illustration of Brain on chip made in PDMS [14].

1.4.2 Liver-on-Chip

The liver is a vital organ of the body because it participates in several functions with the most significant being that of digestion[16]. The main role of the liver in the digestive system is to metabolize substances such as lipids and carbohydrates. The effects of new drugs in the liver are examined during clinical trials. More specifically, it is commonly accepted that one of the major factors which can interrupt the development of new drugs is toxicity and its consequences in the liver [16][17]. The difficulties in the fabrication of microfluidic devices for the study of the liver, stem from the complexity of the organ. The fact that it participates, as it is mentioned before, in several functions in combination with the different types of cells that are responsible, makes the modeling of liver hard [17][16].

Over the last decades, experiments focused on the development of in vitro cultured cells from liver tissue slices or liver cells to study the effects of drugs in the liver. Although these models presented some important advantages over the conventional models (animal testing), they are still unable to fully replace animal testing because limited viability was observed in most of the cases. They also presented the inability to exactly emulate the liver physiology. The advance of technology and science led to the development of new in vitro culture cell models that propose remarkable solutions to the aforementioned problems [17][16]. Most of the liver-on-chip designs used scaffolds for the fabrication of 3D liver structure. The research group of Weng YS et all. developed a new approach avoiding the usage of scaffolds and introducing primary hepatic stem cells for the creation of liver tissue. The proposed design was developed by implementing microfabrication techniques. As it is illustrated in the next figure (Figure 1.2), the PDMS (Polydimethylsiloxane) was used as a substrate where the liver cells were placed. A hydrophilic flow diverter then was used to create a chamber for the culture of liver cells. The chamber on which the cells cultured was hexagonal and the inlets which ensure the insertion of flow were placed at each corner of the chamber. Furthermore, a flow outlet that allows the flow from the portal vein to the central was positioned in the center. The primary goal of the liver-on-chip device was to create a controlled environment that emulates the natural growth of primary liver cells in an organism[17].

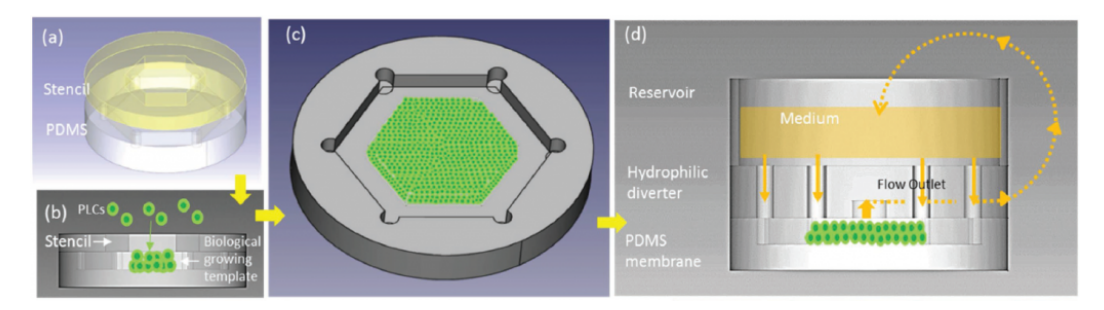


Figure 1.2: Multiple layers of PLCs were deposited on PDMS membrane to form a biological template and hexagonal coutour [17].

1.4.3 Lung-on-Chip

The lung is one of the most vital organs of the body and the main organ in the respiratory system [18]. The normal function of the respiratory system includes several steps. Firstly, the trachea has the responsibility to transport the inhaled air in the lungs via the tubular branches. Continuously, the oxygen is extracted from the air and is inserted into the blood whereas the carbon dioxide follows the opposite direction and it is transferred from the blood to the air through the alveoli. It is important to mention that alveoli is separated from capillaries by a thin membrane made of epithelial cells (alveolar-capillaries barrier) [18].

The primary aim of lung-on-chip devices is to create a controlled microenvironment mimicking both morphological and biological functions of the human respiratory system, to investigate serious diseases and study the effects of new drug treatments [18][19]. The first lung-on-chip device has been developed to emulate human breathing. As it is illustrated in the following figure (Figure 1.3), the lung-on-chip device constitutes of two channels in the opposite direction while a PDMS membrane creates a separation wall between the two channels [18]. The PDMS membrane is covered by an Extracellular Matrix (ECM). On the one side of the PDMS membrane alveolar epithelial cells are placed and on the other side pulmonary endothelial cells. Continuously, the air enters the epithelial part while blood liquid is injected in the endothelial cells[18][19]. The desirable mechanical stretching of the membrane is achieved by the application of a vacuum. This lung-on-chip model is the first successful model of mimicking human breathing and a promising model for the study of drug treatments [18].

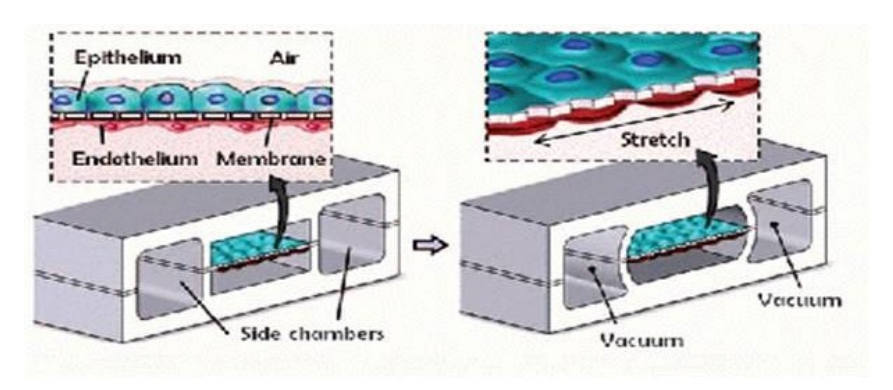


Figure 1.3: Illustration of the lung-on-chip device with a PDMS membrane which separates the two microchannels forming a barrier between alveolar and capillaries. The right figure depicts the applied vacuum to the chambers aiming to introduce the desirable mechanical stretching[18].

1.4.4 Heart-on-Chip

Being a vital organ in the human body, the heart has the responsibility to pump the blood via the vascular system, transferring nutrients to many organs in the human body and extracting wastes from other organs. This way, the heart has a major role in the maintenance of the human body homeostasis [20].

The simulation of heart electrophysiology should be the main priority for the development of reliable and representative heart-on-chip models. Previous surveys have indicated that the growth, maturation and regeneration of cardiac cells depend on several stimuli. Among these stimuli, the properties of the scaffold, the mechanical stimulation and the electrical stimulation have been proven essential elements [7]. Therefore, it is possible to imagine a complex heart-on-chip system that has the ability to apply all mentioned stimuli and to record the response of the cells. In such a platform even, the maturation could be induced and effectively tuned, a parameter that remains a big challenge until nowadays. Using the previous requirements of an "ideal" heart-on-chip the literature can be put into perspective.

Currently, different heart-on-chip models have been created aiming to conduct pharmacological tests. Among them, Radisic et.al incorporated a poly(tetrafluoroethylene)(PTFE) tubing in a bioreactor to facilitate the adherence and elongation of cardiomyocytes[20]. Continuously, in order to provide cardiac bundles with electrical stimulus, the integration of electrodes took place in the platform. After the development of this heart-on-chip model the functionality of the system was tested by using nitric oxide. A significant decline of the beating rate was observed, a detail that reinforces their conviction that this device can be sufficiently used for modeling diseases and pharmacological tests [20].

Another heart-on-chip platform was designed by G. Conant et al., the principal aim of which was to measure the contractility and the action potential propagation [21]. Polymeric thin films were fabricated where the cardiomyocytes cultured. This kind of heart-on-chip device can offer without any doubt remarkable insight regarding the contractility of cardiomyocytes. However, it presents an inability to screen various compounds at the same time.

1.5 Summary

OOC technology has presented remarkable progress during recent years and a wide spectrum of applications such as lung-on-chip, liver-on-chip, blood-brain-barrier and heart-on chip demonstrate its evolution. Testing of drugs, screen toxicity, and research on different diseases are some of the most important fields that take advantage of the evolution of this technology. Despite this, many challenges remain and OOC technology is not widely established in the scientific community and not yet widely accepted by the pharmaceutical industry and by regulators as a *gold standard*. Currently, microelectronics and microfluidic technology have improved in comparison with the past but further advance is required in the near future. In addition, major challenges include a better interpretation of interactions between cells and between cells and the material in an OOC device.

1.6 Engineered Heart Tissue(EHT)

1.6.1 Introduction

The heart is one of the most important organs of the body because it is able to deliver and recycle the blood to other organs through the vascular system. Nowadays, cardiovascular diseases are the most common cause of death worldwide [22]. Over the last decades, many drugs were developed, although the effects of them are ambiguous and a great number of them have not been approved. On the other hand, heart-on-chip models simulate human physiology and the environment of the

cardiovascular system [22]. This way, they are going to provide remarkable insight regarding cardiac diseases, cardio-toxicity testing and personalized medicine as well[22].

In comparison with other cell types, it remains a challenge to produce cardiac cell cultures due to the fact that cardiomyocytes express limited proliferation. The maturation of hiPSC beyond the fetal stage requires a great effort, therefore the creation of proper conditions that facilitate the maturation of these cells is essential [23].

Until nowadays, conventional *in vitro* 2D models have been used in many laboratories for the study of cardiomyocytes. However, these 2-D models have not yet sufficiently simulated the interactions between cardiomyocytes or cardiomyocytes and the matrix, a parameter that limits the study of their function and development. Therefore, currently scientists are making an intense effort to create three dimensional in vitro cardiac models. These 3-D engineered heart models emulate precisely the physiology of the heart and allow the measurement of important properties of the heart such as the contractile force [11].

1.6.2 Advantages over 2-D structures

There is a growing evidence that engineered 3-D tissues have the potential to mimic better the natural environment of the heart in comparison with the 2-D cultures. Some of the most noteworthy advantages of 3-D engineered tissues over the 2-D are the following [23] [24] [25]:

- All the cells in a 3-D tissue can contact the surrounding cells, contrary to the single-layer cell cultures where the cells have little communication.
- The proliferation rate of cells in 3-D engineered tissue is low, something that facilitates long-term studies. At the same time, the usage of pharmacological suppression of activity that is used in 2-D cultures is eliminated
- There is a possibility that the 3-D cell cultures contribute to a better maturation of cardiomyocytes, although this hypothesis should be investigated further.
- Parameters of contractile function such as rate, peak force, and rhythm can be measured more precisely in 3-D engineered heart tissue than in 2-D cell[23][24][25].

1.6.3 EHT as a promising solution

Over the past two decades, EHT has been introduced as a promising way to study the heart tissue in vitro [6]. The first EHT was designed in 1997 aiming to fulfill two goals: The first aim was to produce three-dimensional tissue for organ repair and the second one to model the physiological function of an organ in a more efficient way than two-dimensional cell cultures[6]. Although the first goal seems very optimistic and many challenges should be faced for its implementation, the second one is a more realistic scenario. In the majority of previous experiments, EHT is cultured in a dish that consists of two or more anchoring points and the tissue is formed around them (Figure 1.4). The main role of the anchoring points is to provide support to the tissue and the desirable stretch. In addition, further electrical and mechanical stimulus is provided to cells in order to cause maturation.

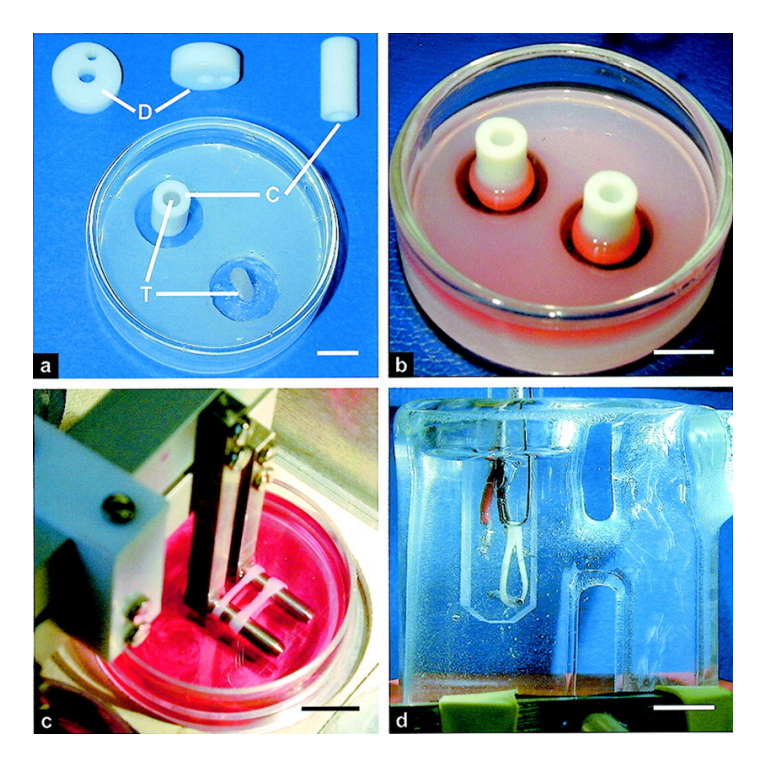
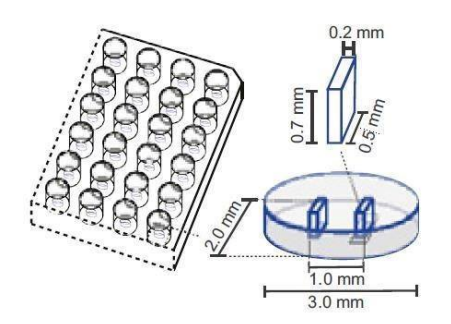


Figure 1.4: Schematic representation of the proposed set up for EHT. Picture (a) illustrates the assembly of a casting mold. Specifically, tubing (T) was attached to the substrate made by glass. Then the disks (D) and the cylinders (C) function as spacers while the casting mold is prepared. Picture (b) depicts the creation of EHT around the cylinders. Picture (c) shows the transfer of EHT in a stretch device which provides the desirable stretch contributing to further development of EHT. Picture (d) shows the EHT in a thermostated organ bath. Scale Bars=10mm [26]

A noteworthy example of EHT was made by the group of Thomas Eschenhagen in UKE Hamburg. Their primary goal was to miniaturize the heart tissue and create multi-well testing. To achieve this goal, they cultured a rat heart tissue around two anchoring points in rectangular molds [27]. In a later study, the same group used human cardiac cells in order to create the heart tissue and they cultured it in the same rectangular molds [27]. The trials of the previous research group were not limited to these experiments, but they continued to improve the engineered heart tissues. More specifically, in the next experiment, they studied the heart hypertrophy by increasing the afterload in the tissue [28]. Two elastic posts were used in order to facilitate the binding of the tissue. The cell culture took place in a 24-well plate. To achieve the increase of the afterload, two metallic bars were used for the strengthening of elastic posts [28].

The research group of J. Hudson developed a 96-well device aiming to screen the conditions of cardiac maturation in an engineered cardiac muscle. The Heart-Dyno device consists of PDMS chambers with two pillars, the primary purpose of which was to ensure the automated formation of dense muscle bundles and at the same time the automated analysis of force contraction avoiding tissue handling (Figure 1.5) [29].



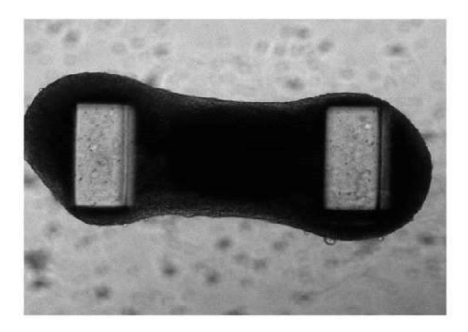


Figure 1.5: In the left figure a general design of Heart-Dyno is provided, and in the right Figure the formation and the culture of cardiac tissue in this device is illustrated [29].

Another noteworthy example of EHT, has been developed recently by the ECTM group in TU Delft. Specifically, three scaled down chips have been fabricated in order to host different number of cells. The fabrication of the EHT platform is based on surface micromachining and elastomer molding techniques. The maximum size of the EHT platform is 3uL and the capacity is up to 47000 cells. The second chip can host up to 31000 cells, and the smallest one is 1uL and the capacity is 16000 cells (Figure 1.6). It is important to highlight that the PDMS pillars have been molded to a silicon wafer that is used for mechanical support of the cardiac tissue growth[30].

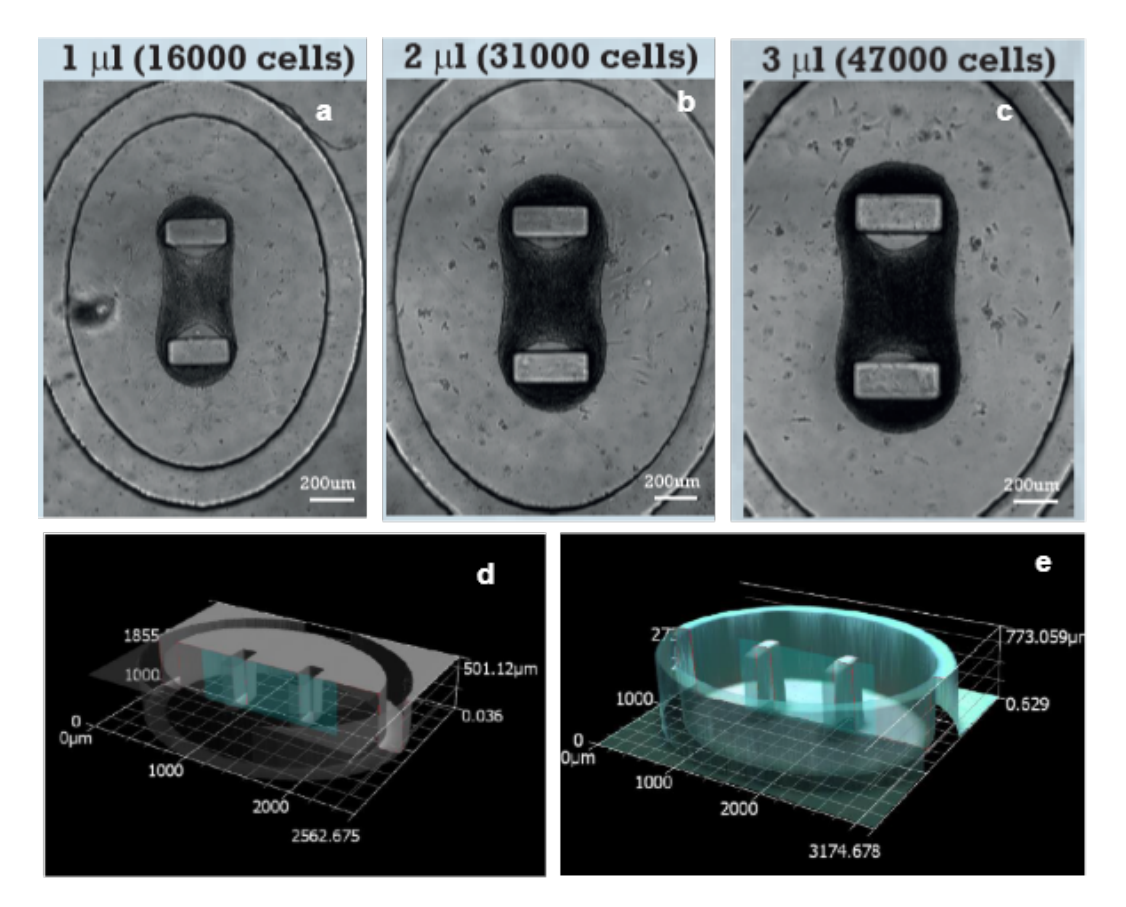


Figure 1.6: Schematic representation of EHT platform developed at ECTM group in TU Delft. Pictures (a),(b),(c), shows the three scale down chips. The first one (a) can fit up to 16000 cells, the second one (b) up to 31.000 cells and the third one (c) up to 47000 cells.(d) illustrates the etched silicon wafer and the (e) illustrates the final PDMS structures of the EHT platform [30].

Despite the benefits an EHT can provide, many challenges must be faced such as the achievement of better alignment and maturation of cardiomyocytes [5]. The maturation and normal function of cardiomyocytes depends on several micro-environmental aspects such as electrical, mechanical, chemical factors and intracellular interactions. The improvement of them in order to create an environment that mimics the native one remains a big challenge [31].

1.7 Importance of Electrical Stimulation in EHT maturation

The progress of OOC technology and the advance of EHT have been highlighted in the previous sections. As it is already mentioned a major challenge that is important to be faced for the evolution of the EHT model is the maturation of the cardiac tissue. The heart is a mechanical pump which responds to mechanical stimuli[32]. Therefore, mechanical stimuli can be essential for heart development. The mechanical stimuli can be separated into three categories: 1) the strain due to heart filling, 2) the hemodynamic loads and 3) the produced force during contraction[32]. These categories of natural mechanical stimuli contribute to the design of in vitro systems that simulate the physiological conditions and can cause maturation to cardiomyocytes. Another parameter that can induce maturation to cardiomyocytes is the change of some properties of ECM such as the stiffness or the alignment of the cells. Mixing also this type of cells with fibroblasts or endothelial cells possibly contributes to a considerable maturation of cardiomyocytes (Figure 1.7)[32]. Among the aforementioned parameters which cause maturation of cardiac cells the electrical stimulation of cardiomyocytes has a principal role in their maturation.

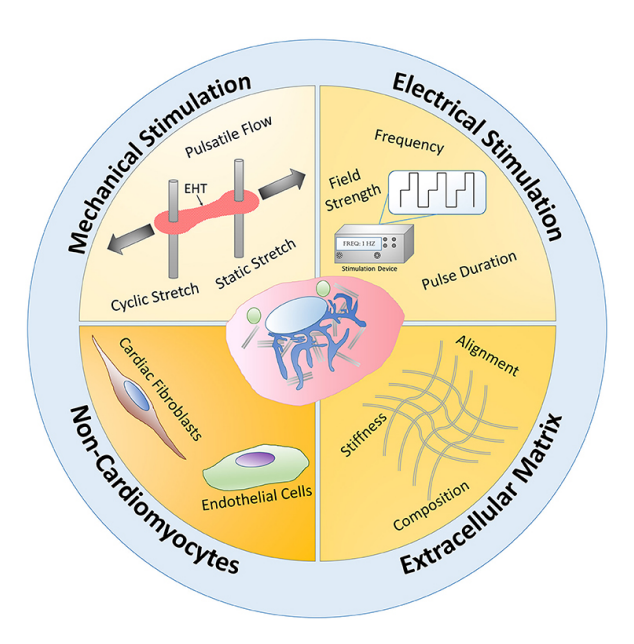


Figure 1.7: Schematic of all the possible methods that cause maturation to cardiomyocytes. The introduction of mechanical stimuli such as cyclic or static stretch, the electric field by using electrical stimulation of cardiomyocytes, the change of extracellular matrix properties and the mix of cardiomyocytes with fibroblasts or endothelial cells are some of the most important factors[32].

1.8 Parameters for Electrical stimulation of Cardiomyocytes

According to previous studies, electrical stimulation plays a significant role in the recreation of the in vivo environment of cardiac tissue but also in the promotion of cardiomyocytes maturation. The importance of electrical stimulation becomes more essential for the cells and tissues that express electrophysiological behavior such as the cardiomyocytes or neurons. For this reason, through the implementation of electrical stimulation in vitro, researchers have achieved a better contractile function, cell-cell communication, maturation and orientation of the tissue, improving the behavior of engineered heart tissue [20] [33]. The efficiency of electrical stimulation depends on several factors, among them is to induce a proper physiological response without causing damage to the surrounding tissue. Therefore, the shape of the applied pulse (Monophasic/Biphasic), electrode materials and the way of charge transfer are crucial to be investigated before the implementation of electrical stimulation. An electrode material can be characterized as proper for stimulation if it is

bio-compatible (elimination of undesirable toxicity or immune responses) with the tissue. As far as the charge transfer is concerned, two mechanisms determine the way of charge transfer, Faradaic and non-Faradaic reactions [34].

1.8.1 Shape of pulse (Biphasic/Monophasic)

The shape of the applied signal to cardiomyocytes constitutes one of the most important parameters which defines the efficiency of electrical stimulation. Electrical stimulation can be a pulse or a continuous wave, and it is transferred either sinusoidally or in square waves. Sometimes, it is monophasic and other times biphasic. The effects of monophasic and biphasic electrical stimulation methods to the tissues have been investigated by many research teams in the past.

Monophasic pulses may lead to tissue damage as a consequence of accumulated charge. This charge accumulation causes irreversible reactions. Therefore, electrical stimulus is preferred to be biphasic[35]. Biphasic electrical stimulation fields presented better results compared to monophasic electrical fields in terms of the excitability of cardiac cells. A parameter that indicates the excitation of cardiac cells is the action potential. Action potential is the molecular basis of electrical activity of cardiac cells[36]. When an action potential occurs there is an unexpected positive shift in the potential of cellular membranes of cardiac cells, called depolarization[36]. This depolarization contributes to the contraction of cardiomyocytes. In biphasic pulses the anodic pulse which injects charge from the electrode into the tissue is followed by cathodic pulse with the same amplitude but an opposite polarity charge. Thus, the charge balance is maintained. Therefore, biphasic pulses generate better action potential excitation since the two pulses (biphasic) act synergistically in order to induce excitation [34] [37].

According to previous electrical stimulation experiments, the most common range of signal amplitude is between 3V and 24V. Although, these values depend also on other parameters of the experiment, such as total duration of experiment. Furthermore, in most of the cases the total pulse duration ranges from 0.1 to 20ms, while the frequency of the stimulation pulse ranges 0.5-5Hz [38]. The following Figure 1.8 demonstrates the basic parameters for functional electrical stimulation in terms of frequency, pulse width, amplitude and total duration.

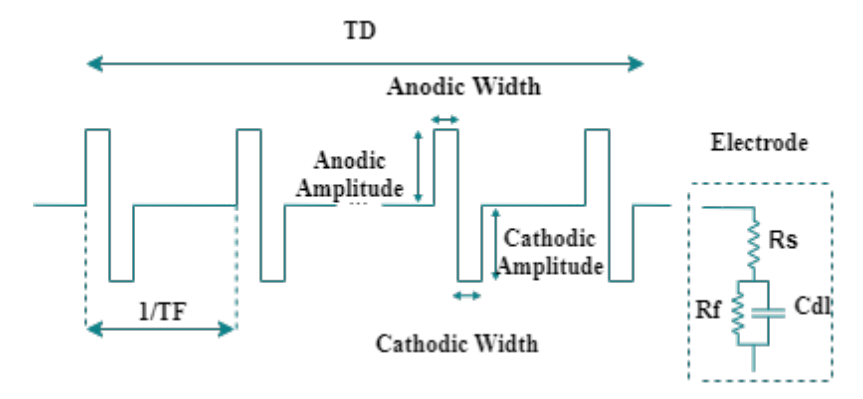


Figure 1.8: Illustration of biphasic pulse generator and the circuity of the electrode. As the figure shows the anodic amplitude of the pulse is followed by a cathodic amplitude of the pulse but in the opposite polarity. The symbol TF represents the train frequency of the pulse and the symbol TD represents the duration of the pulse [38].

1.8.2 Faradaic versus Non Faradaic charge transfer

It is widely known that both Faradaic and Non-Faradaic reactions can occur at an electrode. In electrochemistry field there is a clear distinction between these two mechanisms[39][34]. This distinction

stems from the fact that in Faradaic reactions the charge is transferred far away from the electrode and for this reason, atoms, reactants, and other products are involved and are transferred across the metal-solution interface. As a result of this, electron transfer oxidation or reduction can take place[39][34]. The electrodes which support Faradaic processes are called charge-transferred electrodes. This is directly related to the material of which the electrodes are made of. On the other hand, in the cases when Non-Faradaic processes take place the charge (either electronic or ionic) stays inside or at the electrode. During these processes, no real charge transfer happens across the interface of the electrode. This is because no reduction or oxidation processes take place or when they do they remain inside the electrode. The following picture (Figure 1.9) explains in detail the difference in the mechanism of both processes [39]citetandon2006characterization34.

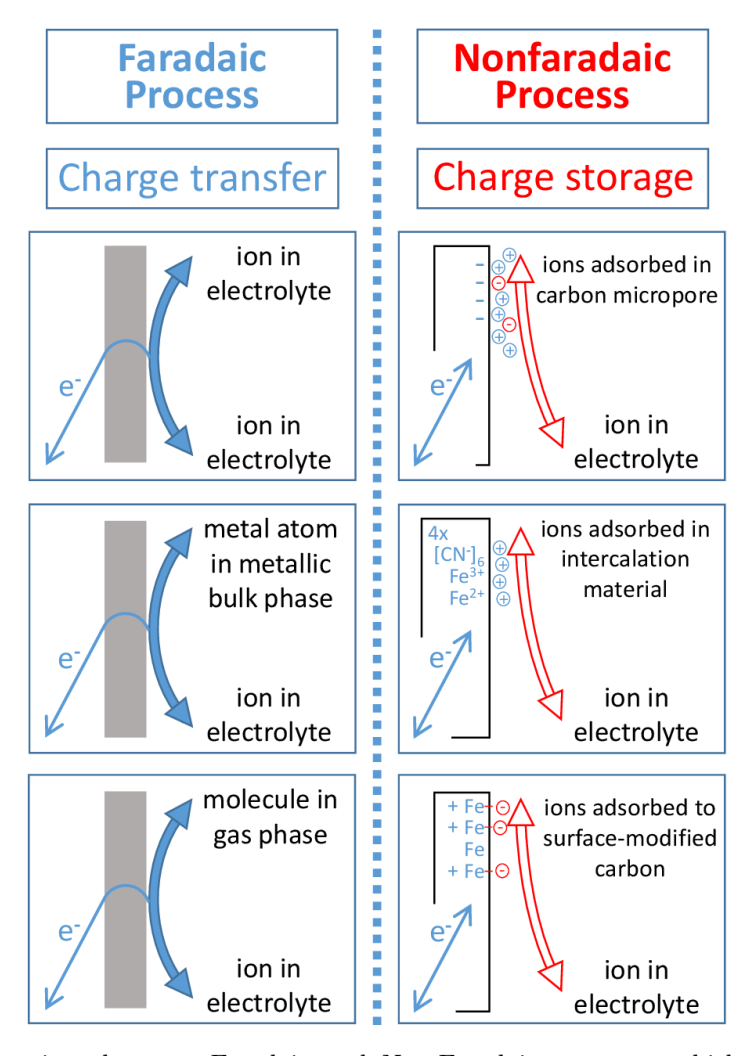


Figure 1.9: Comparison between Faradaic and Non-Faradaic processes which take place at an electrode [39].

1.8.3 Type of electrodes used for electrical stimulation

Ideal Polarized Electrodes: Ideal Polarized Electrodes are the electrodes in which there is no real charge transfer between the electrode- electrolyte model regardless of the value of potential created by the applied to the electrode voltage [39].

Charge Transfer Electrodes: When an electrode is not ideal polarized is called charge transfer electrode. In these electrodes, the processes of oxidation and reduction occur. It is important to highlight that in charge transfer electrodes conduction current flows across the interface of the electrode [39].

1.8.4 Equivalent Circuit model for electrode-electrolyte interface

Integrated electrodes are widely applied to control and stimulate in vitro and in vivo biological systems consisted of electrically active cells for instance neurons or cardiomyocytes[40][41]. It is widely known that the membrane of these cells consists of ion channels that have the ability to transfer ions with the surrounding extracellular matrix (ECM). This way, they produce a difference in ionic concentration[40]. Thus, the electrical potential of the intra-cellular matrix is changed. As a result of these, chemical and electrical processes electrical signals are generated [42][43]. These electrical signals can be detected with integrated electrodes[44][45][41]. Specifically, The electrode acts as charge transfer interface between cardiac cells and a read-out system (Figure 1.10).

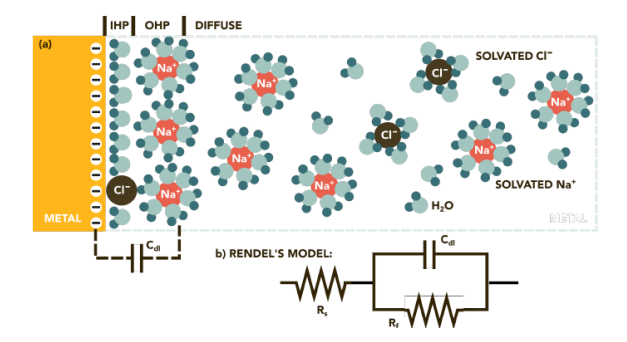


Figure 1.10: Rendel's model as a representation of the electrode-electrolyte interface which is created by inserting an electrode in contact with cells[40]

1.9 Goal of the Thesis and Research Statement

1.9.1 Goal of the thesis

The principal goal of the thesis is to develop an electrical stimulation set up which ensures the stimulation of cardiomyocytes in an EHT platform. This proposed set up includes the design and fabrication of a pulse generator circuit and the fabrication of integrated electrodes in an existing EHT platform. After the previous comparison of electrical stimulation methods (monophasic or biphasic rectangular pulses), the selected method for electrical stimulation and consequently excitation of cardiac cells is biphasic rectangular pulse. The envisioned set up will consist also of multiple EHT platforms (total of 16) integrated in a read-out interface. Particularly, the pulse generator circuit will be connected with read-out interface which hosts multiple EHT platforms with integrated TiN electrodes. The EHT platform which was developed at the ECTM group consists of two pillars

where the cardiac tissue is formed. Perpendicular to these pillars and on the bottom of PDMS, TiN electrodes will be placed to create a uniform electric field during the electrical stimulation process. The range of frequencies that are going to be implemented for excitation of cardiac cells according to literature study and after a discussion with biologists from LUMC is 0.5-4HZ. The period of pulse activation (duty cycle) will be also adjustable and will follow the aforementioned protocols (1-25ms). A connection of this envisioned system with a PC through USB will facilitate the real-time monitoring of electrical stimulation parameters.

1.9.2 Research Statement

Design and Fabricate of an Electrical Stimulation Set up for Electrical stimulation of Cardiomyocytes in an EHT platform.

The research questions which are going to be answered in the following chapters are:

- Which is the amount of current passing through the electrodes in order to provide electrical stimulation but also prevent any possible damage of the cells?
- Which is the best method of electrical stimulation of cardiomyocytes (Voltage Controlled or Current Controlled stimulation?)
- What kind of electronic components must be integrated in the pulse generator circuit in order to provide biphasic rectangular pulses?
- What kind of adjustments must be done in the pulse generator circuit so to provide electrical stimuli not only to a single but to multiple EHT platforms.
- Which is the most efficient design of the read-out interface for multiple electrode chips in order to fit also as a bottom in a 96-well plate?

1.10 Thesis Outline

Chapter 1: The first chapter is the current introduction chapter.

Chapter 2 includes a review of previous electrical stimulation set up systems (Integrated electrodes and hardware designs of electrical stimulators).

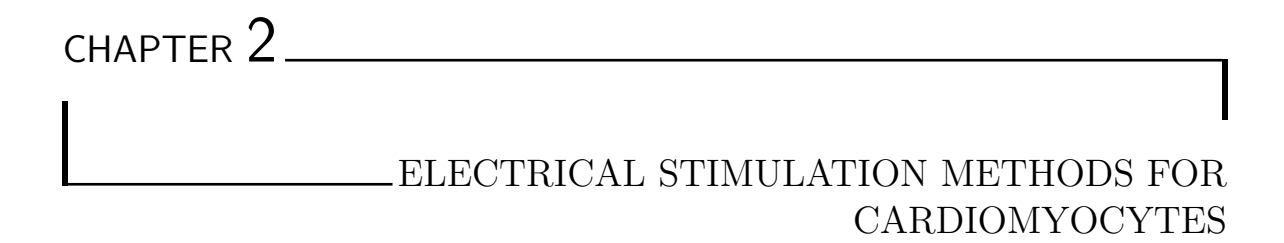
Chapter 3 consists of the General Design of the Pulse Generator Circuit including the design of the power supply system, the design of the pulse generator unit, and the design of a driver unit which drives the biphasic pulse to 16-EHT platforms. Also an advanced version of the stimulator in order to support voltage controlled current source stimulation is provided, In this chapter, the design and the schematics of the driver unit is presented but also the design of the current measurement circuit which is going to measure the current passes through the electrodes

Chapter 4 presents the performance of the proposed system after testing all the integrated components and measuring the output signal. All the testing procedures are explained in detail while a discussion for future improvement of system performance and specifications is followed.

Chapter 5 includes a detailed description of the applied microfabrication processes for the fabrication of TiN electrodes in the EHT platform.

Chapter 6 presents a general discussion regarding the proposed electrical stimulator and challenges during the design and fabrication. Also a discussion regarding the electrodes fabrication is provided.

Chapter 7 is the chapter of the thesis in which important conclusions and future recommendations are presented.



This chapter is focused on the methods for the achievement of efficient electrical stimulation of cardiac cells. A wide spectrum of electrical stimulation methods have been developed in the past such as the use of external pacing electrodes in order to "train" the tissue, the fabrication of electrodes which induce a uniform electrical stimulus around the cardiac tissue (carbon or platinum electrodes), the microfabrication of integrated electrodes on a chip (MEA), the fabrication of interdigitated array and the use of nanotechnologies. A presentation of the entire electrical stimulation set up which has been used in previous studies is also provided. Among the aforementioned electrical stimulation methods, more emphasis will be given in the microfabrication of integrated electrodes on a chip. This chapter at the beginning highlights the importance of electrical stimulation for cardiomyocytes maturation, continues with an overview of previous electrical stimulation methods and design of pulse generator systems and concludes with an overview of signal parameters.

2.1 Methods for electrical stimulation of 2D cell cultures and design of stimulator systems

Microelectrode arrays are used nowadays in order to record cell activity or to stimulate cells in 2D cultures. They have the potential to provide local stimulation and micro-scale precision. Using lithographic microfabrication techniques, the electrodes for the recording and stimulation of electrical signals are deposited on substrates [46]. The electrodes in MEA can be fabricated from different materials such as TiN [46], graphene, gold [47]. The electric field is applied over one or more microelectrodes and not across the entire cardiac tissue. Currently, new microfabrication techniques for microelectrode deposition on substrates have been developed. However, the use of MEA is limited to the study of planar tissues (2D cell cultures). In most of the previous experiments the MEA electrodes are arranged in a symmetrical way across the surface. The chip (Figure 2.1) with the integrated electrodes is glued and wire-bonded on a PCB (Printed Circuit Board). The primary goal of the MEA electrodes is to generate local point-source stimulation while only the peripheral cells are subjected to local field current [47].

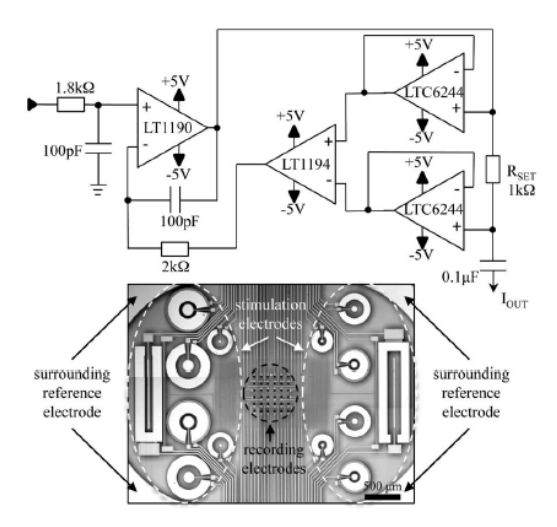


Figure 2.1: Schematic representation of MEA chip for 2D cell culture. The MEA chip is glued and wire-bonded to the PCB. The electronic circuit which provides electrical stimulation to MEA chip is also presented.[47]

Different stimulation techniques are applied in MEA electrodes in order to achieve a functional electrical stimulation for cardiomyocytes maturation. The research group of L. Giovangradi who developed the previously illustrated MEA for 2D cell cultures (Figure 2.1) based the electrical stimulation of cells in high frequency during the experiment on the electrical stimulus imposed on one or multiple electrodes. Stimulation signals were produced by a signal generator and then provided to a custom-made voltage-controlled current source in order to give current stimulation to cardiac cells. An operational amplifier was used for current sense (LT1194) which takes as inputs the current from the two op amp (LTC6244) giving feedback to the LT1190 for accurate control of the current signal. During this experiment the researchers applied low voltages in high-frequencies concluding that for a long- term electrical stimulation, high frequencies and low voltages can enhance the safety and the maturation of the cells significantly [48].

Other research teams focused on both recording and stimulation of cardiomyocytes using recording MEA and stimulation electrodes on the same platform. In this case, advanced stimulation circuits designed in order to provide biphasic controlled pulses to cardiac cells. A micro-controller was used as the principal component of the circuit controlling a Digital-to-Analog-Converter(DAC) to produce biphasic pulses in various voltages, frequencies and width of pulses. The stimulator designed by the research group produces also four channels of pulses that ground the electrodes by using a low-value resistor and a switch applying a low charge injection. The proposed system generates biphasic pulses with 2.5V or 5V amplitude. The supplied current from the current source reaches to 10mA (Figure 2.2)[49].

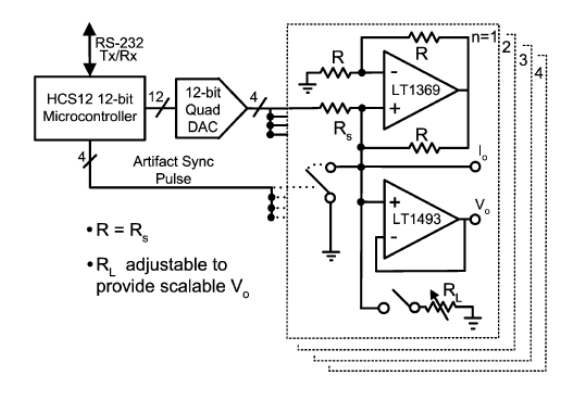


Figure 2.2: Demonstration of electrical stimulation for MEA[49].

The research team of Kujala et al proposed as a solution a container for six MEAs with integrated electrodes and cells located on MEA dishes. A more general description of the electrical stimulation set up is illustrated in the following picture (Figure 2.3). The electrodes are made by stainless steel (10mm wide stainless-steel electrodes, 5mm apart). The major advantage that this MEA set up offers is that it allows a long-term electrical stimulation of multiple cell cultures. The strength of the electric field that is created with the aforementioned set up is up to 5V/cm while the frequency of the pulse ranges from 1HZ to 40Hz. An operational amplifier is used in order to amplify the signal produced by a National Instruments USB-6008 Data Acquisition (DAQ) device controlled by a PC. In addition, the fully programmable environment ensures the control of the electrical stimulation method [50]. One of the most important results steming from this experiment but also from previous studies was that the higher the strength of the electric field created by the stimulation set up, the easier the cells could achieve the depolarization threshold and contract in response to the stimulus (Figure 2.3) [50][51].

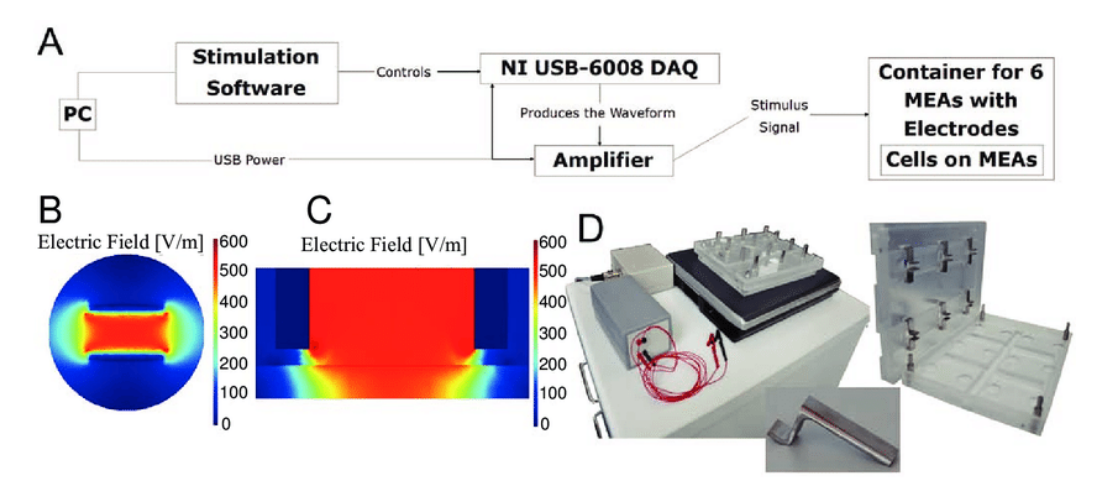


Figure 2.3: (A) Demonstration of the general set up of the electrical stimulation system (Block Diagram). (B), (C) An illustration of the electric field during the electrical stimulation (D) In detail illustration of container for six MEAS with cells culture on them [50].

2.2 Methods for electrical stimulation of 3D cardiac tissues

2.2.1 Training the cardiac tissue by using electromechanical stimulation

In the past, many research groups gave more emphasis on miniaturization and improvement of maturation of cardiac tissue by "training" the tissue with a combination of electrical and mechanical stimulation. Specifically, it has been shown that mechanical and electrical stimulation at frequencies similar to normal heart rate results in significant maturation of engineered heart tissue [52]. The research team of Vunjak-Novakovic et al investigated the regimens which contribute to heart hypertrophy. In particular, they tried to find the most efficient way to support the tissue and thus, they optimized two anchoring points around which the tissue formed [53][54]. The anchoring points located in little chambers made of PDMS. The little chambers located on the top of PDMS channels, the main purpose of which was to cause actuation. This way, they achieved to apply mechanical stimulation to the tissue providing significant insight that it induces maturation to the cardiac tissue. Before the application of the mechanical stimulus, electrical stimulus applied to the tissue aiming to "train" the tissue by using pacing electrodes [53]. In another study, the group of professor F.G Godier-Furnement examined the role of electrical and mechanical stimulation to the EHTs. They applied the electrical stimulation field at different frequencies (0-6 Hz) for five days. Simultaneously with the creation of the electric field around the cardiac tissue, they strained on flexible poles aiming to create auxotonic contractions. The results from their experiments have shown that the electromechanical stimulation of mammalian engineered heart tissue, contributes to the functional maturation of the tissue [54].

2.2.2 Current Techniques: Bioreactors

Recently, the electrical stimulation of cardiac cells became reality by using sophisticated bioreactor systems consisted of multiple stainless steel electrodes located 5mm apart in each dish. Previous studies indicated that direct contact of the electrodes with the tissue presented an obvious effect on contractile function of the cells. Although, in this experiment the electrodes were not attached with the cells avoiding any possible structural damage. Thus, the electrodes were located nearby to an edge during culture, and then the whole stimulation system was removed for physiological measurements. Biphasic rectangular pulses of +-2.5 volt and 3Hz of frequency, were applied to cardiac cells. LEDs were integrated in the platform in order to indicate in which well the pulse is delivered each moment. The current was balanced and controlled by using 1k resistor and 1 capacitor. The results of this experiment provided a significant insight regarding the improvement of electrophysiological properties of cardiac cells (Figure 2.4)[55].

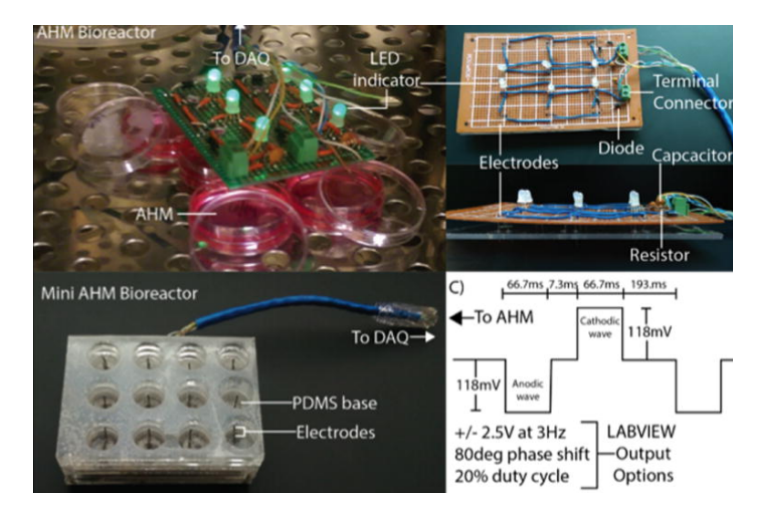


Figure 2.4: (A) Electrical stimulation of cardiac tissue using the proposed bioreactor. B) Mini bioreactor with electrodes and PDMS base for gene expression tests. C) The result from electrical stimulation with biphasic square pulse measured with an oscilloscope [55].

2.2.3 Current Techniques: Fabrication of 3D electrodes

Apart from the aforementioned techniques for electrical stimulation of cells, currently new methods have been developed such as the development of 3D electrodes array. More specifically, a novel platform of interdigitated platinum electrodes was fabricated by the research team of S. Ahadian in order to stimulate engineered muscle tissues. It is important to highlight that for the testing of the functionality of this platform, skeletal muscle cells were used. Although, the proposed platform can be used for other types of cells or tissues such as the cardiac cells [56]. The benefits that the aforementioned set up provided, was the creation of an electric field above and perpendicular to the electrode structures. In the proposed set up, the electrodes were located on the substrate and were able to create a homogeneous electric field requiring a small amount of energy. In addition, this technology offers flexibility in terms of electrodes properties and design [56]. The proposed platform was used for the stimulation of 3D arrays of engineered muscle tissue as it is shown in the following picture (Figure 2.5). According to the research team, it can also be used for different types of cell structures and tissues.

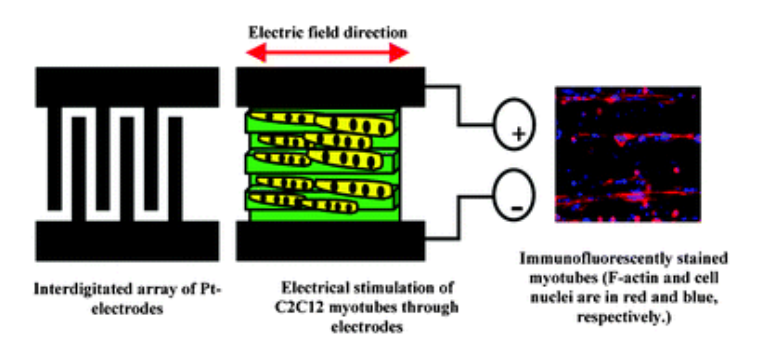


Figure 2.5: Fabrication of the interdigitated array of Pt electrodes and application of electric field stimulation of C2C12 myotubes [39]. The interdigitated array of Pt- electrodes used for the stimulation of 3D arrays of engineered muscle tissue, made by a hydrogel called gelatin methacrylate (GelMA). GelMA hydrogel consists of gelatin modified with methacrylic anhydride. This hydrogel is very useful for tissue engineering applications[56].

2.2.4 3D pillar electrode for 3D cardiac tissues

With the advance of technology and microfabrication process, new methods came to the light such as the fabrication of 3D pillar electrode for culturing and growing 3D cardiac tissues. With the development of such a device, the researchers aim to achieve electrical pacing and controlling of 3D cardiac tissues. The electrodes made by Pt-PDMS using microfabrication techniques. The protocol that was followed for the electrical stimulation was biphasic rectangular pulses with a frequency of 1Hz and 0.1 mA current. It is worth mentioning that the pillar electrode facilitates the formation of 3D cardiac tissue around it without the using of any ECM hydrogel. In the following schematic (Figure 2.6) the design of the electrode pillar is presented and insight regarding the electrical stimulation parameters is provided[57].

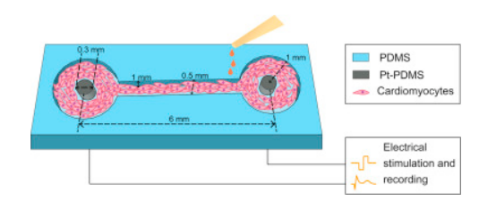


Figure 2.6: Illustration of 3D pillar electrode for 3D cardiac tissues [57].

2.2.5 Summary

This section has presented the most important electrical stimulation methods in 2D and 3D cardiac cell cultures. Before the analysis of the principal and advanced electrical stimulation methods, the most important parameters for a functional electrical stimulation are highlighted. The chapter then continues with the analysis of electrical stimulation methods for 2D cell cultures. Microelectrode arrays (MEA) made by different materials such as stainless steel, TiN or graphene, have been developed providing a more precise model of signal recording and stimulation of cardiomyocytes. A connection of MEA with fully programmable stimulators and the development of user-friendly interfaces will provide better results in the electrical stimulation of cardiomyocytes using this technology in the future. Besides, the presentation of the electrode materials and designs, a brief explanation of the hardware part of electrical stimulator set ups is provided. As far as the stimulation of 3D cardiac tissue is concerned, the progress of technology and engineering contributed to the transition from simple methods of electrical stimulation of EHT such as external pacing electrodes or bioreactors to more advanced methods such as interdigitated electrodes arrays or 3D pillar electrodes.

2.3 Hardware designs of Electrical Stimulators

2.3.1 Introduction

Electrical stimulation is a method that has different applications ranging from rehabilitation treatment for people who are suffering from spinal cord injury to excitation of cardiomyocytes in an EHT platform in order to cause proper tissue maturation. Electrical stimulators are devices that have been used to provide voltage or current pulses of proper intensity to the biological tissue, applied via electrodes [58] [37] [59]. Different hardware designs have been implemented to produce the biphasic pulse. Some of the most common techniques are provided and discussed in the following section. Even if the mentioned electrical stimulator systems, developed for different applications than ours, the main hardware design principles used for the biphasic pulse generation remain the same. Two mechanisms can ensure an efficient electrical stimulation, and are the most widely used by the scientific community: voltage-controlled electrical stimulation (which includes the voltage controlled voltage source (VCVS) and voltage control current source stimulation) and the current controlled electrical stimulation. The main modules of which an electrical stimulator consists of, are the power supply, the pulse generation unit, and the modulator unit. Usually, the pulse generation unit includes oscillator units or microcontrollers that produce low power signals with adjustable frequency, width, and amplitude [58] [37][59]. Then, the second module is the modulator which modulates the incoming from the pulse generation unit signal in order to make the biphasic pulse. The biphasic pulse in most of the cases is generated by using either the H-Bridge method or more simple and easier to control by using a series of op-amp amplifiers. Many times, an output signal amplification is required to reach the desired (high) amplitude (either voltage or current).

2.3.2 Voltage-Controlled Voltage Source(VCVS) vs Current Controlled (CCS)

In voltage-controlled voltage source stimulation, the voltage remains stable during the stimulation but the current changes when the load presents small changes during the experiment. This method which is used for the development of cardiac pacemakers, provides high power efficiency due to the fact that it lacks current injection control into the tissue[60][59][61]. On the other hand, current-controlled stimulation provides a safer way of electrical stimulation in comparison with voltage-controlled because the user can have better control of the current injection to the tissue. Although, this type of stimulation has worse power efficiency compared to voltage controlled.

Whether the applied method of stimulation is voltage or current controlled, the hardware design of the unit which generates the biphasic pulse remains the same. One of the most well-known methods of producing biphasic pulse is the H-bridge. Another way is the use of a microcontroller and an operational amplifier. Both of the methods are explained and a comparison study is conducted to choose the best and most well-controlled method of biphasic pulse generation.

2.3.3 H-Bridge for Biphasic pulse Generation

An H-bridge circuit implementation includes four switches (Sl-S4) and two current sources. It is a way of producing biphasic pulses precisely. The four switches act synergistically to achieve biphasic stimulation. According to what is illustrated in the following figure (Figure 2.7) in the first state, the switches are off to ensure that no current flows through the load at the beginning. In the second state, the S1 and S4 are switched on, whereas the S2 and S3 are switched off. In this scenario, the current flows from S1 switch of H-Bridge to S4, providing one phase of stimulation(the anodic pulse). In the third state, the opposite concept takes place. The S2 and S3 are switched on, whereas the S1 and the S4 are switched off. The current flows from S2 to S4 creating the second phase of stimulation (cathodic phase). The described circuit design has integrated also a voltage controlled current source the main aim of which is to maintain the current stable even if the impedance alters during the

experiment. The research team of Khosravani et al. (2011) [62]also developed an H-bridge circuit to produce biphasic current over load. The switching of the transistors used in the proposed system was achieved by a microcontroller. Although, no details provided it regarding the performance of the circuit.

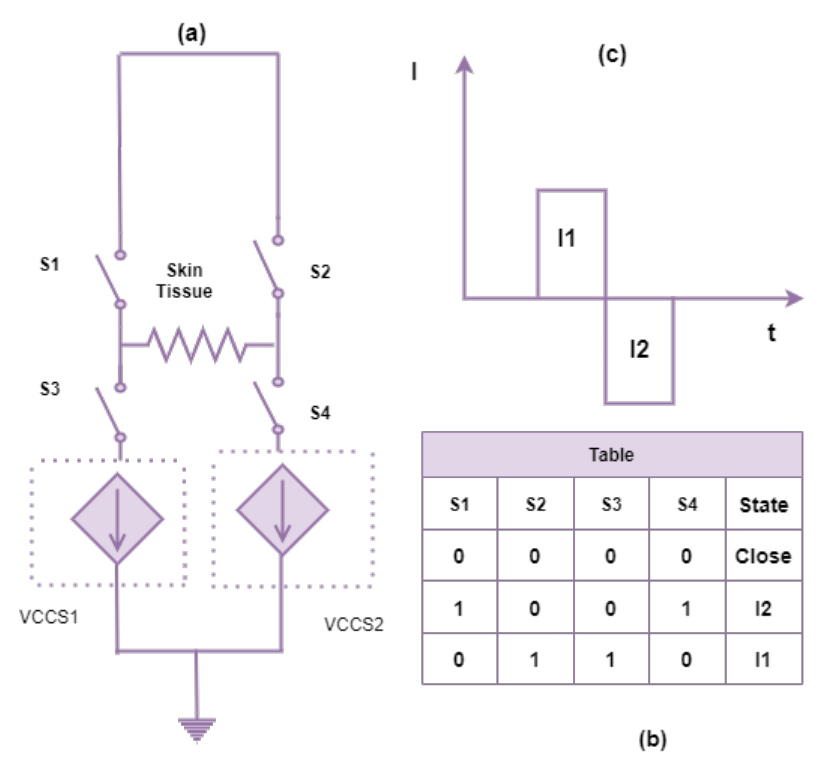


Figure 2.7: (a)Schematic representation of H-Bridge method for generating biphasic pulse. (b)The relation among S1-S4 in order to produce the pulse. (c) Illustration of biphasic balanced current pulse [62][63].

2.4 Operational Amplifier for biphasic pulse generation

Previous studies have shown that using an operational amplifier controlled by a microcontroller which sends monophasic pulses of standard amplitude and frequency, it is feasible to generate rectangular biphasic pulses[64]. More specifically, Elyahoodayan et al., developed an electrical stimulator for neural applications based on a microcontroller which was programmed to generate PWM in a specified range of frequencies and an operational amplifier was integrated in order to convert a PWM in a negative pulse. In the next step an inverter amplifier was used in order to invert the signal to a positive pulse. A similar technique was used also in the past by the research team of Shendkar et al, but for different application as this electronic stimulator was designed and developed for producing ankle dorsiflexion in patients with foot drop problems (Figure 2.8) [65].

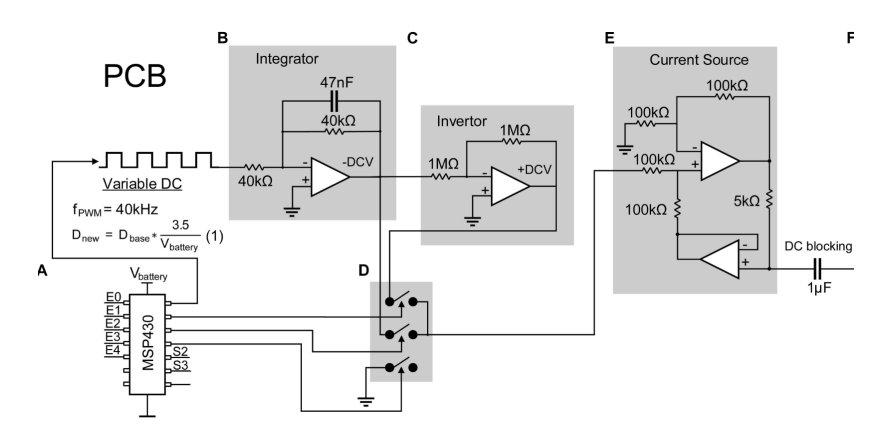


Figure 2.8: Depiction of a constant current biphasic stimulator for neural applications. It consists of a microcontroller (MSP430) which produces a PWM at a very high frequency (up to 40 kHz). The electronic circuit consists also of a second amplifier which generates negative DC voltage, (C) an inverter amplifier that produces a positive DC voltage, (D) multiple analog switches and (E) a converter which converts the voltage source to current source [64].

2.5 Voltage Source to Current Source Conversion

According to the previous discussion regarding the electrical stimulator circuit designs for cardiac cell stimulation (Introduction), they are based on either voltage source or current source stimulation. The majority of circuit designs that implement current source stimulation, use a voltage source in the beginning to produce a voltage biphasic pulse, and then in the last step the voltage source is converted to current source. This way, the applied current to the tissue remains stable even if the load changes during the experiment. Different techniques have been implemented for the achievement of this conversion. Among them, the two most popular hardware techniques are the Wilson current mirror and the Howland Converter. As far as the Wilson Current Mirror technique is concerned, it is a three-terminal circuit that gets an input current at the input terminal and produces a "mirrored" current source or sinks output at the output terminal. Actually, the mirrored current is an accurate copy of the input current. Another way of voltage to current source conversion is named the Howland Converter or Howland Charge Pump Circuit [66]. This technique is based on the use of an operational amplifier and a bridge of precise resistors and it is going to be analyzed in the next sub-section.

2.5.1 Wilson Current Mirror Technique

Wilson Current Mirror is an improved version of simple current mirror technique used for generating a current source. It is implemented in many pulse generator's designs to provide output stable current which is independent of the load (Figure 2.9).

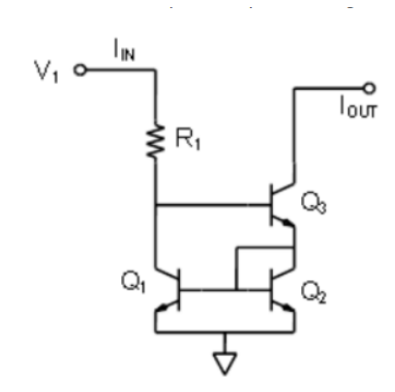


Figure 2.9: Illustration of Wilson current mirror technique: The current in the output is equal to the input current [67].

If it is assumed that all transistors have the same current gain β and Q1 and Q2 are matched, their collector currents are equal. Therefore, IC1 = IC2 (=IC) and IB1 = IB2 (=IB).

In this case the base current B3 is driven by:

$$IB3 = \frac{IC3}{\beta} \tag{2.1}$$

. The emmiter of Q3 current

$$IE3 = \frac{\beta + 1}{\beta}IC3 \tag{2.2}$$

IE3 = IC2 + IB1 + IB2.

Substituting for IC2, IB1 and IB2, IE3 = IC + 2IB, so

$$IE3 = (1 + \frac{2}{\beta})IC \tag{2.3}$$

Substituting for IE3,

$$\frac{\beta+1}{\beta}IC3 = (1+\frac{2}{\beta})IC \tag{2.4}$$

, rearranging

$$IC = \left(\frac{\beta+1}{\beta+2}\right)IC3\tag{2.5}$$

The current through R1 is given by, IR1 = IC1 + IB3

But, IC1 = IC2 = IC

Substituting for IC and since $IC3 = \frac{IB3}{\beta}$ we get,

$$IR1 = \left(\frac{\beta+1}{\beta+2}\right)IC3 + \frac{IC3}{\beta} \tag{2.6}$$

Therefore,

$$IR1 = \left(\frac{\beta+1}{\beta+2} + \frac{1}{\beta}\right)IC3\tag{2.7}$$

Finally,

$$IC3 = \frac{IR1}{1 + \frac{2}{\beta(\beta + 2)}}\tag{2.8}$$

But because $\frac{2}{\beta(\beta+2)}$ is much smaller than 1, $IC3 \approx IR1$

And the output current (assuming the base-emitter voltage of all transistors to be 0.7 V) is calculated as,

$$IC3 \approx IR1 = \frac{V1 - VBE2 - VBE3}{R1} \tag{2.9}$$

The research group of M. Yochum et.all [67] designed the following topology (Figure 2.10) using two Wilson current mirrors to achieve a biphasic current pulse. More specifically, they used one operational amplifier (OPA) as a buffer, main purpose of which was to create a zero input current. After using this operational amplifier, the transistor Q1 and the resistance control the current I1 which is then copied in the load by implementing Wilson current mirror technique. $I1 = \frac{V}{R1}$

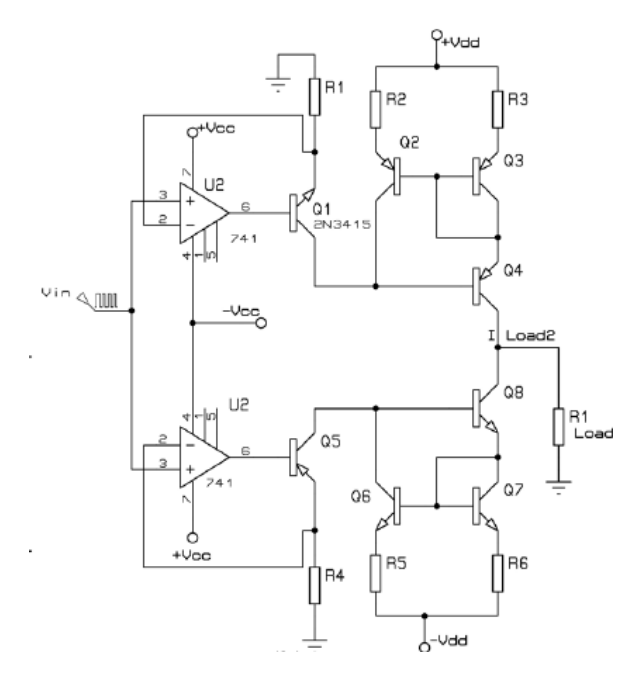


Figure 2.10: Two current mirror as a technique to produce biphasic current pulses for electrical stimulation [67].

2.5.2 Voltage to Current Converter

The research team of F. Brunetti ,implemented a different way of producing output current in biphasic pulses for robotic applications. This method is based on a voltage-to-current converter. This converter consists of an operational amplifier and a bridge of high-precision resistances. The advantage of this method is that due to the amplifier specifications the rising and falling time of the pulse is fast in comparison with other methods and also the amplifier gain that is created is stable. The following Figure 2.11 explains the design of the voltage to current converter they used [68]. The current in this case is related to the programmed voltage through the following equation as long as R1=R2=R3=R4a+R4b $Iout=\frac{V1}{R4b}$

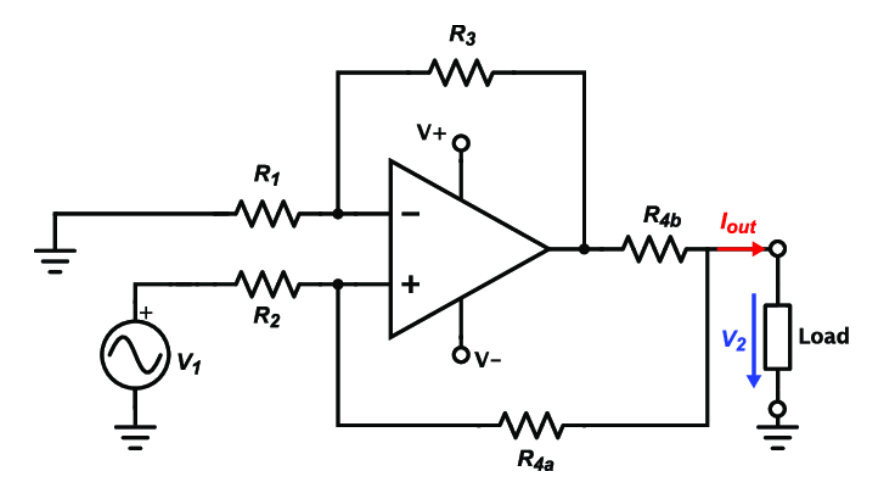


Figure 2.11: Circuit design of voltage to current converter implemented in electrical stimulator for robotic system [67]

The Howland converter is able to offer high output impedance implementing low complexity, avoiding the use of any transistors or switches for this purpose. One disadvantage that maybe this method creates is that the accuracy depends on the resistors tolerance and the attributes of the operational amplifier.

2.6 Hardware designs conclusions

In most of the aforementioned hardware designs either voltage or current controlled, the way of biphasic pulse generation is similar. H-bridges are a more complicated way of producing biphasic pulses because an accurate and well-controlled monitor of the signals sent from the microcontroller to the MOSFET is required. For this reason an advanced microcontroller must be used. From the pulse quality point of view, H-bridges generates rectangular pulses independent on pulse duration [62] [63]. The use of operational amplifier and a microcontroller for biphasic pulse generation can be characterized a less complicated and better-controlled method of generating pulses. The advantage of this method in comparison with the H-Bridge method is that the pulses are easily created and the switching time of pulses is always the same due to the function of the differential operational amplifier. The quality of the pulse also is similar to the quality of the pulse which is produced by using the H-bridge method. The most widely known techniques for voltage source to current source conversion is the Wilson Current Mirror Technique and the Howland Converter. The first one is a transistor-based technique where the current on one side of the transistor is copied to the other and as a result of this, the current remains stable and independent of the load [67]. The second one, can be developed by using an amplifier and a bridge of resistors. An important consideration that should be taken into account in this case, is to select resistors with high precision to achieve the desired balance in the system and keep the current stable despite of the impedance changes. After all, the selected method of biphasic pulse generation is the use of a microcontroller which generates well-defined monophasic pulses and a series of operational amplifiers for the conversion of previous pulses to a biphasic rectangular pulse.



3.1 Introduction

In this chapter, the design of an electrical generator device for producing perfect rectangular biphasic pulses using a voltage source is presented. The principle aim of the EHT stimulator is to provide rectangular biphasic pulses for the electrical stimulation of cardiomyocytes in an EHT platform. One of the main characteristics of this device is that it allows the user to regulate the range of the voltage values applied to the tissue(up to 15V), by using a potentiometer. Furthermore, through a user-friendly interface, the control of frequency, duty cycle, and the selection of specific for stimulation channel is feasible. A current measurement circuit is also integrated into the device allowing the user to observe the amount of current that passes through the electrodes and regulate accordingly the voltage to the desired levels establishing the device as a voltage controlled biphasic pulse generator. As mentioned in previous chapters, the amount of current that causes excitation of cardiomyocytes without damaging the tissue and leading to death is up to 10-15mA. Taking into consideration this important parameter the system designed in a way that keeps the amount of current to a safe level (up to 10mA) preventing potential damage of cardiomyocytes. Since the future aim of this system is to be used for electrical stimulation of 16 EHT platforms with integrated electrode chips, the architecture of the pulse generator circuit supports sixteen different channels for the electrical stimulation of cardiomyocytes.

3.2 Important Parameters for the circuit design

3.2.1 Equivalent circuit of electrode and cardiac cells interface

Equivalent circuit models have been widely used to model the electrical properties and the impedance of the interface between the electrode and the electrolyte. Previous studies in early 1899 Warburg revealed that the interface between the electrode and the electrolyte could be fully described by a polarization resistance in series with a polarization capacitor [69]. More specifically, the well known Randles' model which is illustrated in the following Figure 3.1 consists of a capacitance called double layer capacitance in parallel with the electrode's resistance. This electrode's resistance is in series with the electrolyte resistance, in our case the cardiac cells[70].

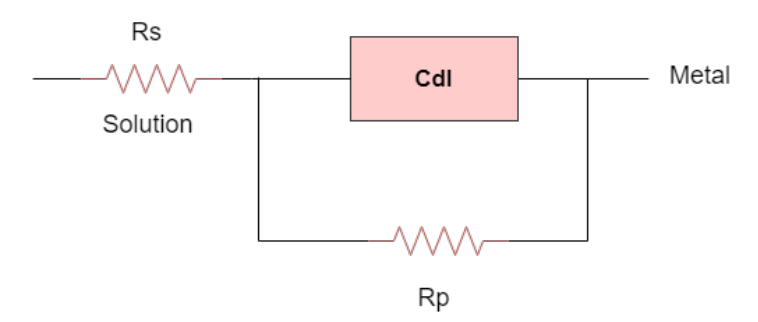


Figure 3.1: Randell's circuit for modelling the load of the pulse generator circuit[70].

Implementing this model to specify the load of the electrical stimulator, individual calculations took place in order to find out the values of the electrode resistance, solution resistance (cardiac cells). Since the electrical stimulator system was designed before the completion of electrodes and their characterization of them, a theoretical calculation of electrodes resistance gave a good sense of the resistance. The impedance of the TiN electrode is going to be tested later by conducting EIS (Electrochemical Impedance spectroscopy in a range of 1Hz to 1KHz). Since the resistivity of the TiN electrode is known from previous studies 1.1^* 10^{-7} Ω m and the dimensions of the electrode (Cross sectional Area and Length) is known as proper masks with the corresponding dimensions was previously designed by M.Dostanic, the value of TiN electrode resistance can be obtained (Figure 3.2).

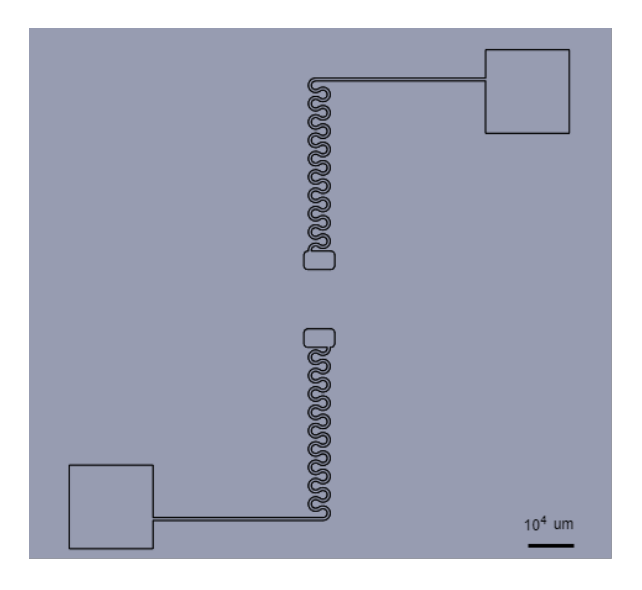


Figure 3.2: TiN electrodes shape and contact pads illustration CAD model

The total length of the electrode's interconnects was designed to be 3.46mm while the cross sectional area of each electrode is 50mm. The TiN electrode resistance can be calculated from the following formula:

$$Rp = p\frac{L}{4} \tag{3.1}$$

By substituting p=1.1*10⁻⁷ Ω m, L=3.46*10⁻³m and A=50*10⁻⁶m,

$$Rp = 7mOhm (3.2)$$

The resistance of the cardiac cells according to previous studies ranging between 300-400 Ohm[71]. The double-layer capacitance which is created between the electrode and the electrolyte is going to be specified after making Electrochemical Impedance Spectroscopy measurements for the electrodes. The literature study alongside the aforementioned calculations provides a good sense of the cardiac cells load. However, the designed electrical stimulator can provide current up to 10mA, even in higher values of loads than that. The simulations and the experiments that were conducted can verify the previous argument[72][70].

3.3 System's specifications

The designed EHT stimulator delivers short pulses in the range of 0.25ms, at very low frequencies of 1-5Hz. The user is able to change the value of the frequency by steps of 0.1Hz according to the experimental conditions and the needs of the experiment. The maximum desired current must not exceed approximately the 12mA. The specifications of the system are briefly presented in the following Table 3.1:

Table 3.1: Specifications of Pulse Generator Circuit

Type of Pulse	Biphasic Rectangular Charge-Balanced
Voltage	up to $24V(\pm 12V)$
Current Limitation	up to 12mA
Frequency Range	1-5Hz (step 0.1Hz)
Duty Cycle	0-25ms(step 0.1)
Channels	16

Taking into consideration these requirements the pulse generator circuit was designed using firstly LT-spice simulation tool to simulate the possible solution of generating the biphasic pulse and the KiCad software tool to develop the schematics and the Printed Circuit Board(PCB). In the following figure, the general block diagram of the EHT pulse generator is presented. As it is shown the pulse generator schematic is divided into six units (Figure 3.3).

- (i) The user interface
- (ii) The Micro-controller Unit
- (iii) The main waveform generation unit
- (iv) The circuit which measures the current and keeps it to safe levels
- (v) The demultiplexing unit which drives the current to 16-electrode chips (Figure 3.3).

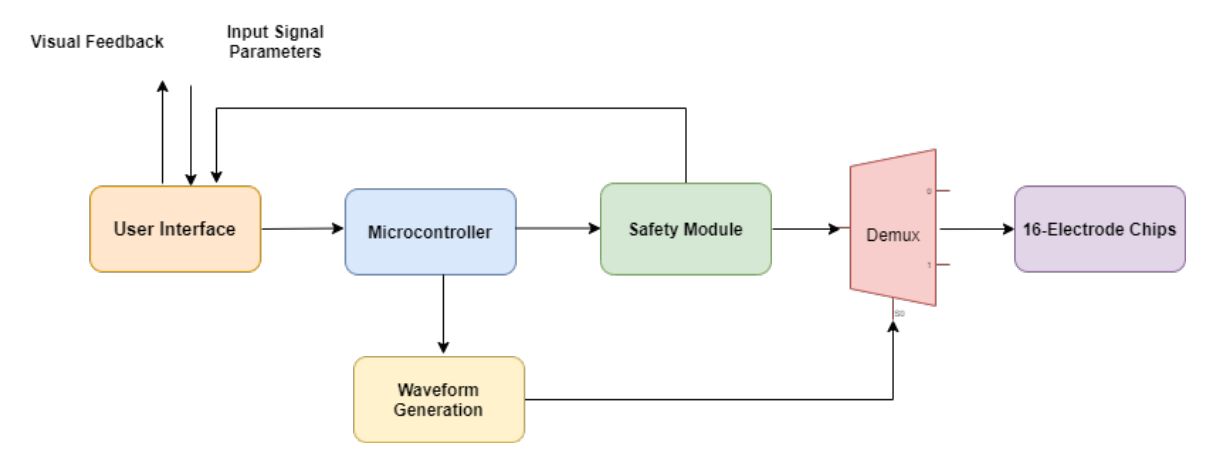


Figure 3.3: Block diagram of Power Supply system of the pulse generator circuit.

3.4 Design of Power Supply System

The range of the operational voltage of the EHT pulse generator is low (up to 12Volts). Therefore, the selected power supply unit of the system based on the use of batteries of 15Volts or an external charger of 15V is also recommended. The primary function of the power supply system consisted of two converters, is to provide voltage to all the electronic components of the EHT pulse generator. In the next Figure 3.4, a block diagram of the designed power supply unit is provided.

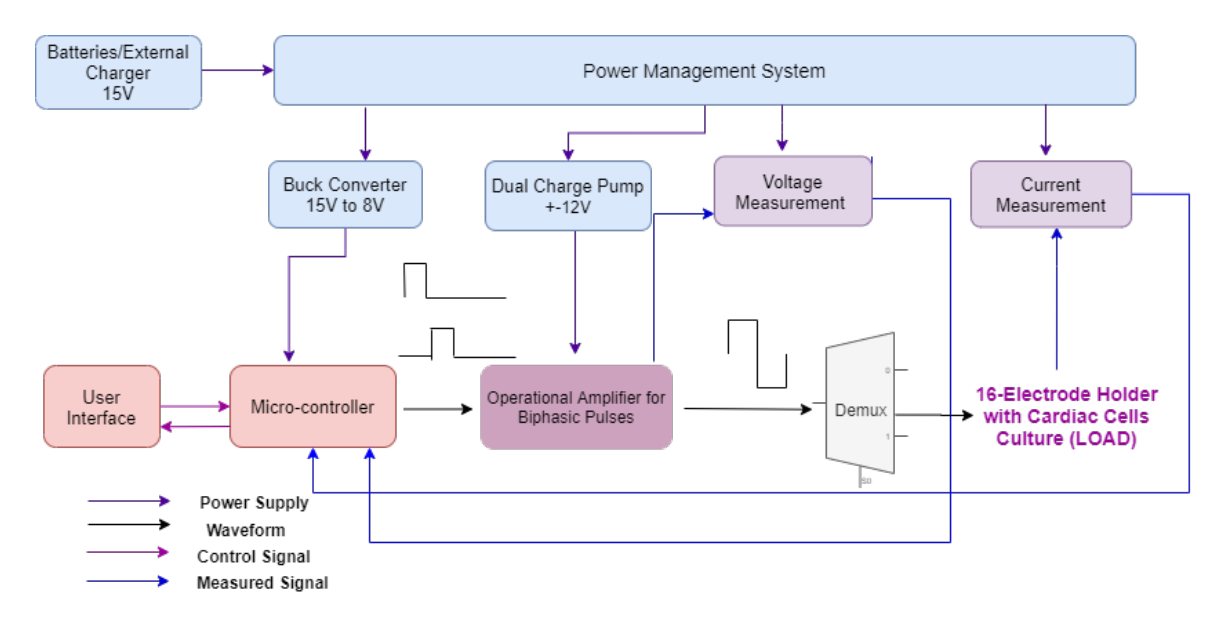


Figure 3.4: Block diagram of Complete Electrical Stimulator for EHT platform. The Power management System which supplies power all sub-units is illustrated together with the main unit of biphasic pulse generation.

3.4.1 Description of Charge Pump Converter

The first converter is a low noise dual supply inverting charge pump (LTC3260EMSE). It consists of an inverting charge pump with both linear positive and negative regulators (LDO+, LDO-). Linear regulators (positive or negative) operate as voltage dividers. In particular, the internal resistance is varied to maintain a constant output voltage. These regulators that are also integrated in the charge pump chip provide a very stable output with low ripple and noise.

The principle function of this converter is to convert the 15V of battery supply to +12V and -12V in order to supply voltage to the op-Amp amplifiers, which are used to generate biphasic pulses. The selected charge pump can operate in a wide range of 4.5V to 35V while the output current of this converter can reach up to 100mA.

The charge pump presents two modes of operation, the burst mode and the low noise constant frequency mode. In Burst Mode output voltage of the charge pump converter operates to 0.94VIN, and the LTC3260 quiescent current is only 100 μA , while both LDO regulators are on. On the other hand, in constant frequency mode, the charge pump generates an output equal to VIN and operates at a standard 500kHz or between 50kHz to 500kHz which can be achieved using an external resistor on the RT pin. At this point, it is important to highlight that at lower frequency levels the open-loop output resistance of the charge pump converter is higher and thus, the charge pump offers a lower average output current. In the cases when the RT pin is directly grounded, the part operates at a constant frequency of 500kHz so the output current is higher. For this reason, in our case, the RT was not grounded directly but through a resistance of 200k [73].

The (Figure 3.5) refers to the internal design and the pin functions of the chip, while (Figure 3.6) demonstrates the values of the selected capacitors and resistors integrated in the circuitLTC3260EMSEPBF.

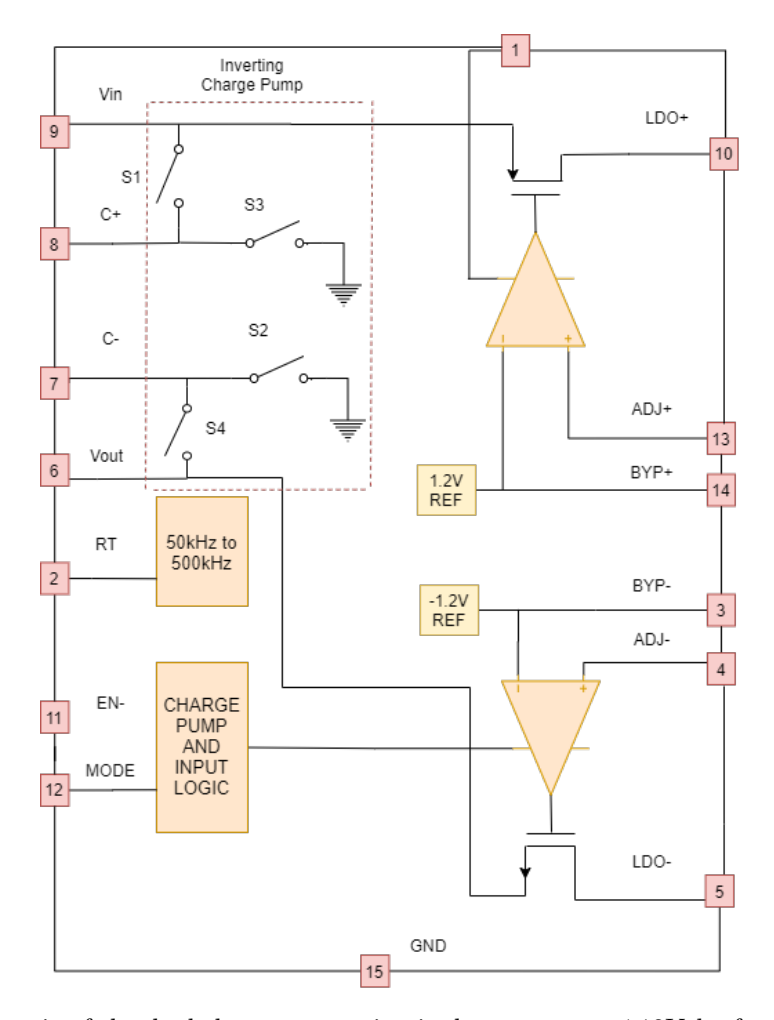


Figure 3.5: Schematic of the dual charge pump circuit that generates ± 12 Volts for the power supply of amplifiers[73].

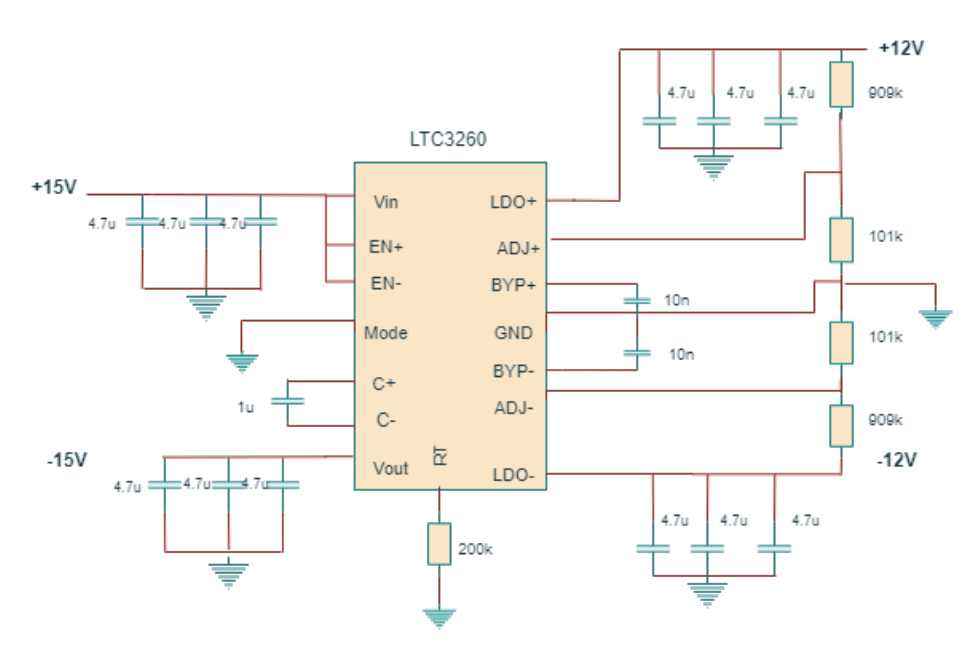


Figure 3.6: Schematic of the dual charge pump circuit that generates ± 12 Volts for the power supply of amplifiers[73]

The output of the positive and negative regulators (LDO), can be adjusted to the desired voltage level(+-12V) by using a voltage resistor divider in the output. In detail, the positive Linear Dropout Regulator (LDO+), which is illustrated in the schematic, is powered from the VIN pin and drives the LDO+ output pin to a voltage adjusted by the resistor divider connected between the LDO+, ADJ+ and GND pins. For stability reasons in the circuit design, three ceramic capacitors are integrated into the LDO+ output. It is also worth mentioning that the LDO+ is enabled or disabled using the EN+ logic input pin. The equation that is used in order to calculate the values of the resistor's dividers that provide the desired voltage of +12V is the following: [73]

$$V_{LDO+} = V_{REF} \frac{R_6}{R_7} + 1 (3.3)$$

Respectively, the output of the negative regulator LDO- can be adjusted using resistor dividers in the same way as it was analyzed before, and according to the equation:

$$V_{LDO-} = V_{REF} \frac{R_8}{R_9} + 1 (3.4)$$

Since the

$$V_{REF} = 1.2V \tag{3.5}$$

according to the datasheet and:

$$V_{LDO+} = 12V \tag{3.6}$$

By dividing the (3.3) by (3.4), the values of the resistor dividers are obtained.

$$R7 = 101k, R6 = 909k \tag{3.7}$$

3.4.2 Description of Buck Converter

The designed power supply system consists also of a DC-DC step-down converter (buck converter) that is the main source of power supply for the microcontroller (Figure 3.7). The buck converter steps down the voltage (while stepping up current) from its input (supply) to its output (load).

The basic operation of the buck converter has the current in an inductor controlled by two switches (usually a transistor and a diode) The selected buck converter has two integrated n-channel MOSFETs one for the high side and one for the low side. In some cases, the low side MOSFET can be replaced by a diode but in the selected buck converter a low side MOSFET has been chosen as it prevents the system from high losses[74].

The conceptual model of the step- down converter is understood better in terms of the correlation between the current and voltage of the inductor. In more detail when the switch is open (off-state), the current passing through the circuit is zero. The time when the switch is closed for the first time (on-state), the current starts to rise, and the inductor generates an opposing voltage as a response to the current that changes. This voltage drop counteracts the voltage of the source and therefore reduces the net voltage across the load. Over time, the ratio in which the current changes, decreases, while the voltage across the inductor also decreases, causing an increase in the voltage at the load. That time, the inductor stores the energy in as a magnetic field [74].

In the case when the switch is opened while the current is still changing, a voltage drop across the inductor is presented, in order the net voltage at the load to be less than the input voltage source. The time when the switch is opened again (off-state), the voltage source will be removed from the circuit, and the current will decrease. The decreasing current generates a voltage drop across the inductor (opposite to the drop at on-state). In this case, the inductor becomes a Current Source. The stored energy in the inductor facilitates the current flow via the load. The "increase" in average current is responsible for the reduction in voltage. When the circuit is off, the inductor discharges its stored energy into the rest of the circuit. In the special scenario when the switch is closed again before the inductor fully discharges (on-state), the voltage at the load will always be greater than zero[74]. The selected buck converter chip TPS54335-2A, can take as an input a voltage that ranges from 4-28V and steps it down to 8V. The voltage in the output can be adjusted to the requirements of our system using a voltage divider.

$$R_6 = R_5 \frac{V_{REF}}{V_{OUT} - V_{REF}} \tag{3.8}$$

In our case, the desired voltage in output is equal to 8V and the V reference according to the datasheet of the device is 0.8V. This way, by replacing these values in the above equation and assuming that the R5=100k, the value of R6=11.1k

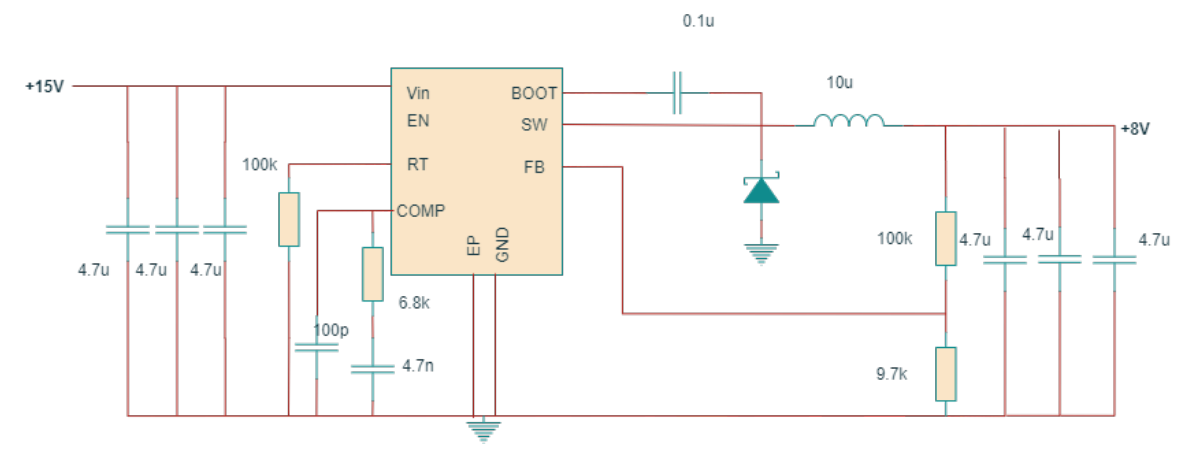


Figure 3.7: Schematic diagram of Buck Converter which supplies with voltage the microcontroller [74].

Calculation of Minimum Value of the output inductor

The most significant component that must be selected for the output filter is the output inductor (L). The following calculations support the value of the inductor used in the presented design:

$$L_{MIN} = \frac{V_{out} * (V_{in} - V_{out})}{V_{in} * K_{IND} * I_{out} * f_{sw}}$$
(3.9)

By substituting in the aforementioned equation the desired Vin=15V and Vout=8V the value of the inductor is obtained. Thus, for the design, a close standard value of 10 μ was selected for the inductor.

In addition, in order to ensure that the selected inductor will be functional, the RMS current (the amount which the current changes through switching) and the saturation current must be calculated according to the following equations.

$$I_{L(RMS)} = \sqrt{I_{out}^2 + \frac{1}{12} * (\frac{V_{out} * (V_{in} - V_{out})}{V_{in} * L_{out} * f_{sw} * 0.8})^2}$$
(3.10)

Making the proper calculations the value of the RMS current is:

$$I_{L(RMS)} = 3.02A (3.11)$$

Calculation of Peak inductor current

$$I_{L(PK)} = I_{OUT} + \frac{V_{out} * (V_{in} - V_{out})}{1.6 * V_{in} * L_{out} * f_{sw}}$$
(3.12)

Thus $I_{L(PK)} = 3.607A$. The inductor must meet these requirements for the ripple and peak current. Since the selected inductor has RMS current equal to 4A and saturation current equal to 5.5A, it meets the calculated requirements.

3.5 Uni-phasic to Bi-phasic pulse converter system

After designing the power supply system according to the requirements of our system, the next and the principal goal of the thesis is to create a unit that generates biphasic rectangular pulses. The most efficient and cost effective way of biphasic pulse generation was selected. This includes the use of a microcontroller and an operational amplifier to create perfect rectangular biphasic pulses from a voltage source.

3.5.1 Analysis of Selected Method

In the previous section, the most well-known methods of biphasic pulse generation were compared and analyzed. After this, the selected method for biphasic pulse generation is the use of in series op-amp and a microcontroller which is programmed to produce well-defined PWM waveforms as an input to the operational amplifier. This method of generating biphasic rectangular pulses is inspired by a previous design of a pulse generator circuit for electrical stimulation of human skin. This idea was elaborated and adjusted to the requirements and the needs of our pulse generator for the electrical stimulation of cardiomyocytes [65]. In addition, new circuit designs were invented in order to support the needs of our circuit. More specifically, the proposed design includes measurement circuits for voltage and current measurement that are applied to cardiomyocytes. In addition, the final signal is de-multiplexed in 16-in total electrode chips. For this reason, the system was designed in a way to be compatible with a second PCB (Printed Circuit Board) which hosts 16- electrode chips. Furthermore, the designed circuit supports a safety system that measures the current passes through the cells and when this current exceeds the desired threshold (up to 10mA) the electrical stimulator stops producing biphasic pulses, protecting this way the stimulated cells. A low-cost and user-friendly microcontroller(ATMEGA328)can be used in order to generate two monophasic pulses(PWM) of 5V. These two monophasic pulses are going to be the input in a differential amplifier (opa196), the main purpose of which is to convert these pulses to a biphasic pulse with an amplitude of $\pm 12V$ (Figure 3.8).

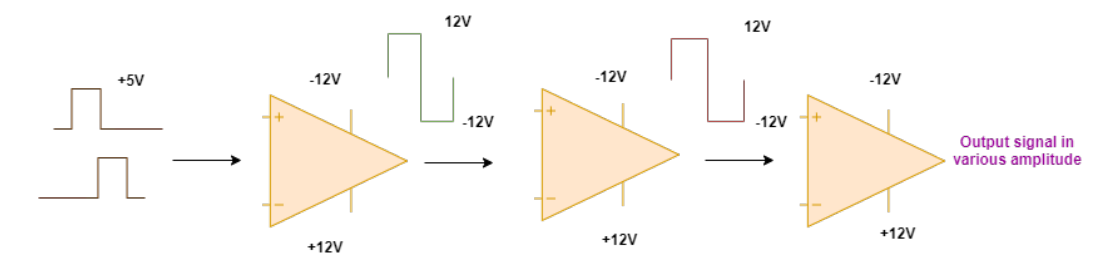


Figure 3.8: Schematic representation of the proposed method for biphasic pulse generation.

Another similar way of pulse generation based on the use of an advanced microcontroller and an operational amplifier. In this case, the digital to analog converter of a microcontroller or an external digital to analog converter generates multiple analog signals. These analog signals are sent then to the input of an operational amplifier to create the biphasic pulse. This way biphasic pulses in different

voltage ranges are created. This method was also simulated in the LTSpice software tool. As far as the quality of the produced biphasic pulse is concerned, it is identical to the proposed method. This method is considered more expensive and more complex than the proposed because in the first one a low-cost microcontroller such as ATMEGA328 can be used. Also, ATMEGA328 which is integrated into Arduino Nano has more user-friendly programming environment and user interface. For this reason, the second method was rejected and the focus is on using an Arduino Nano microcontroller to create two PWM with specific characteristics. However, the LTSpice simulations of the second method are also provided in the Appendix.

3.6 MCU unit and PWM generation

Pulse Width Modulation (PWM) controls analog signals with the digital outputs of a microcontroller. In this technique, the use of Digital-to-Analog conversion is not a requirement because the noise effects are eliminated by keeping the signal digital. In the aforementioned technique, the energy is distributed through pulses (in series) in comparison with an analog signal which varies.

Digital control is applied to create a square wave, a signal that presents two modes ON and OFF. In our system design, an Arduino microcontroller was used (ATMEGA 328 processor) which generates pulse voltages up to 5V. By programming the corresponding outputs (D9 and D10) to generate PWM in specific frequencies the on-off pattern between 0Volts and 5Volts is observable. The time interval in which the pulse is ON is called pulse width. In the PWM technique, the frequency that is used is standard but the duty cycle changes and can be easily adjusted by programming the microcontroller unit. The following picture (Figure 3.9) illustrated the Duty cycle concept of PWM.

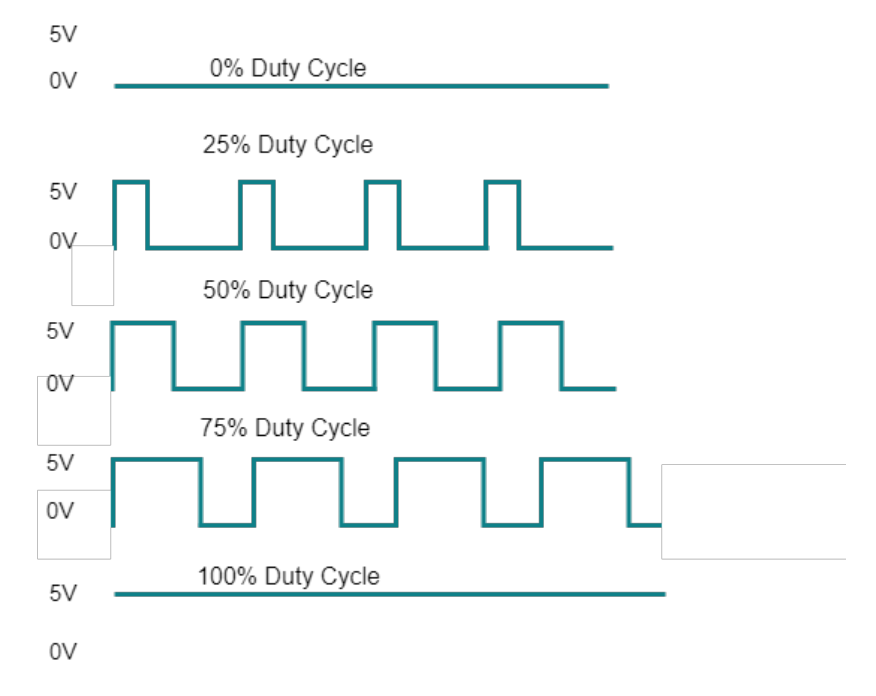


Figure 3.9: PWM waveforms for different values of Duty Cycle. For 0 Duty cycle the PWM signal is off, for 50 Duty cycle half of the signal is OFF and half of the signal is ON, 75 Duty Cycle 75 is ON and 25 is OFF and 100 Duty cycle means that the PWM is ON. [75]

The ATmega328P consists of three timers Timer 0, Timer 1, and Timer 2. Each of them presents two compare registers that monitor the width of PWM for the timer's two outputs according to the following way. If the timer is equal to the compare register value, a toggle is observed in the corresponding output. The outputs of each timer may have exactly the same frequency, but the duty cycle varies[76].

The timer clock is generated by a prescaler. In particular, the clock of the system is divided by a prescaler such as 1, 8, 64, 256, or 1024. The Atmega328 has a system clock of 16MHz and the timer clock frequency will be the system clock frequency divided by the prescaler factor. Due to the fact that the application of electrical stimulator includes biphasic pulses in very low frequency 1-10Hz a large prescaler should be used (1024). The timer which supports so high value of prescaler is timer1 and the output pins are D9 and D10. Thus, these output pins were programmed with the timer interrupt method to provide monophasic pulses up to 5V with a 180 phase difference between. Timers can be configured in different modes [77][76].

The mode that was used in order to create the monophasic pulse in low frequencies was the CTC mode. CTC mode means, Clear timer on compare match. When the timer counter reaches the compare match register, the timer will be cleared. At this point, the timer generates an interrupt when there is a match with the compare register.

In the following paragraph, the concept of interrupt is explained because this method was implemented in the microcontroller to generate two PWM with 180 degrees phase shift, in very low frequencies.

In the microcontroller, the program is running instruction by instruction. An interrupt occurs externally and stops the instructions of the program to be executed while it runs a specific interrupt service routine (ISR). When the ISR has been completed, the program continues to execute the next instruction [76].

After the ISR has been finished, the running program is continued with the next instruction. Interrupts are generally enabled/disabled with the function interrupts() / noInterrupts(). By default in the Arduino firmware interrupts are enabled. Interrupt masks are enabled / disabled by setting / clearing bits in the Interrupt mask register (TIMSKx)[76].(see the code in C++ at the end of the chapter).

Through the proposed design of the electrical stimulator the user will be able also to change the duty cycle of the biphasic pulse. The duty cycle of a biphasic pulse as it was explained also previously, is defined as the percentage of which the pulse is activated (ON-state, anodic and cathodic activation) over the period of the pulse. Thus, the microcontoller was programmed to calculate the duty cycle in the following way: the frequency of the pulse was divided by 100 and by using a counter and a variable which takes various values depending on the desired duty cycle the duty cycle is calculated and implemented on the pulse (see full code in Appendix, and testing part). The next Figure 3.9 presents a small part of the code which shows the CTC mode, the timers that were used for the specific low frequencies and the way that the interrupts were activated.

```
11_9_20_final §
  DDRB |= (1<< PB1);
                                  //D9 pin of microcontroller is set as output (PWM1 is generated from D9)
  DDRB |= (1<< PB2);
                                 //D10 pin of microcontroller is set as output (PWM2 is generated from D10)
//Initialization of registers for CTC mode and Timer1
  TCCR1B=0;
  TCCR0A=0;
  TCCR0B=0;
  TCNT1=0;
   TCCR1B = _BV(WGM12)|_BV(CS12)|_BV(CS10); // CTC mode & 1024 prescaler
// Set the desired Frequency
  Serial.print("Select frequency of stimulation");
  delay(5);
  f=1.0; // Choose a desired frequecly in the range of 0.5-5Hz and set it to this variable f
  OCR1A = (16000000/(f*1024)-1)/100;
//Enabling the interrupts for Timer1 (Dont touch this )
    {\tt TIMSK1} |= (1 << OCIE1A); // Enable the interrupts of OCR1A
    sei():
```

Figure 3.10: Control the clock frequency of the microcontroller to achieve low frequencies in the range of $0.5\text{-}5\mathrm{Hz}$

3.6.1 Opamp for biphasic pulse generation

Due to the fact that the input of the differential amplifier is two independent rectangular monophasic pulses of 5V, the circuit design that corresponds to the needs of our system is the following (Figure 3.11):

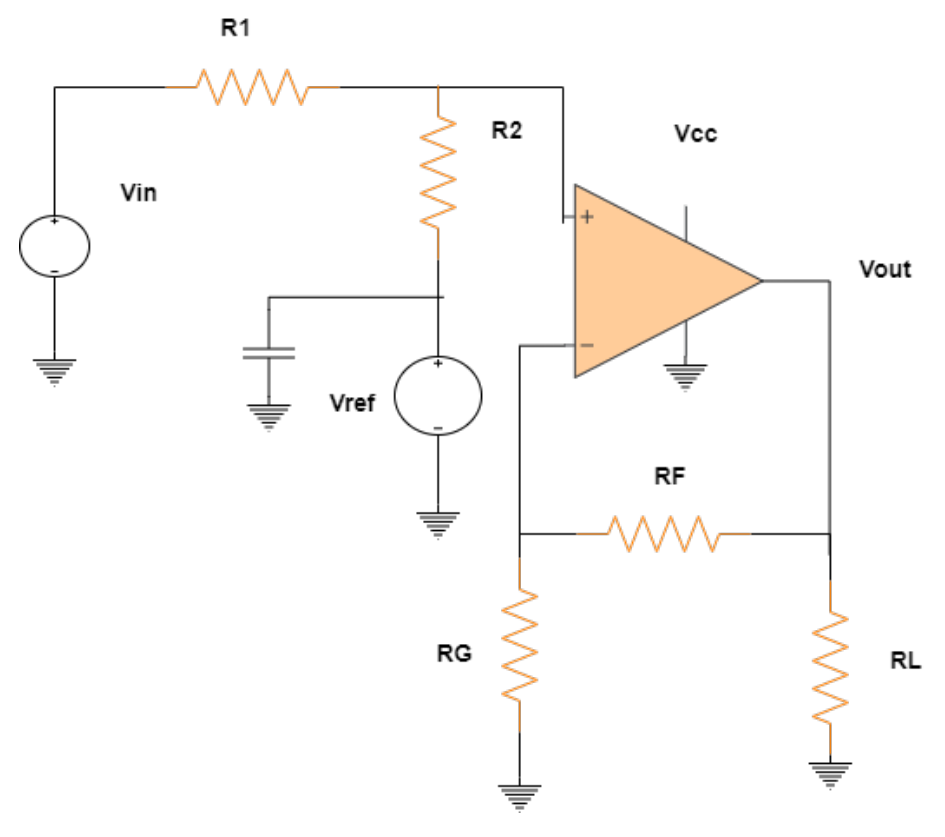


Figure 3.11: Schematic design of the amplifier circuit that will use in our case.

$$Vout = mVin + b \tag{3.13}$$

$$m = \frac{R_2}{R_1 + R_2} \frac{R_F + R_G}{R_G} \tag{3.14}$$

$$b = Vref \frac{R_1}{R_1 + R_2} \frac{R_F + R_G}{R_G} \tag{3.15}$$

Using the aforementioned equations it is observable that in the cases when VREF=Vin=5V, then Vout=0 and thus we can observe a zero pulse in the output. On the other hand in cases when VREF=5V and Vin=0V then in the output we can observe a pulse of +12V after amplification. In the end, in cases when VREF=0V and Vin=5V a negative value of -12V is observed in the output. Solving the previous equations the values of resistors were calculated to be: RF=120K, RG=29.1k, R1=24.3k, R2=100k

The second in series op-Amp amplifier is used as a buffer amplifier. Its purpose is to improve the stability and consistency of the generated by the first amplifier signal. More specifically, a unity gain buffer amplifier is developed using an opamp in a negative feedback demonstration. As it is shown in the Figure 3.12, the output is connected to its inverting input while the signal source is connected to the non-inverting input. Although its voltage gain is equivalent to one or unity, it presents high input

impedance and low output impedance. It is used to avoid loading of the signal source. The buffer op-amp can adjust its voltage in the output equal to the voltage in the input. Due to the fact that the voltage in the output follows the voltage in the input the circuit in other words called op-amp voltage follower.

The third in series amplifier is an inverter amplifier. Its purpose is to invert the signal in the input of the amplifier keeping the same value of amplitude. In parallel with this amplifier, a potentiometer is placed. The potentiometer has the ability to regulate the voltage range. Thus, the user is able to select the desired output voltage for the stimulation.

In the following section the results from EHT pulse generator circuit simulations in LTSpice are presented (Figure 3.13, 3.14, 3.15).

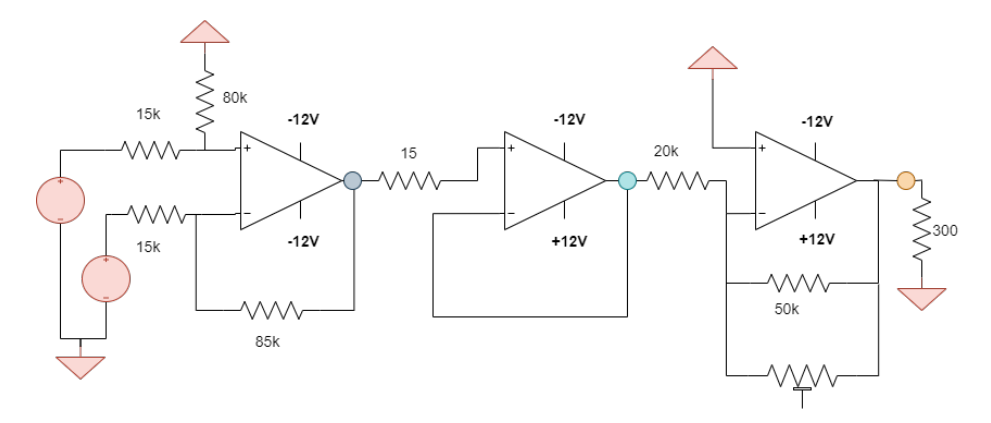


Figure 3.12: Circuit design for the simulations in LTSpice software tool.

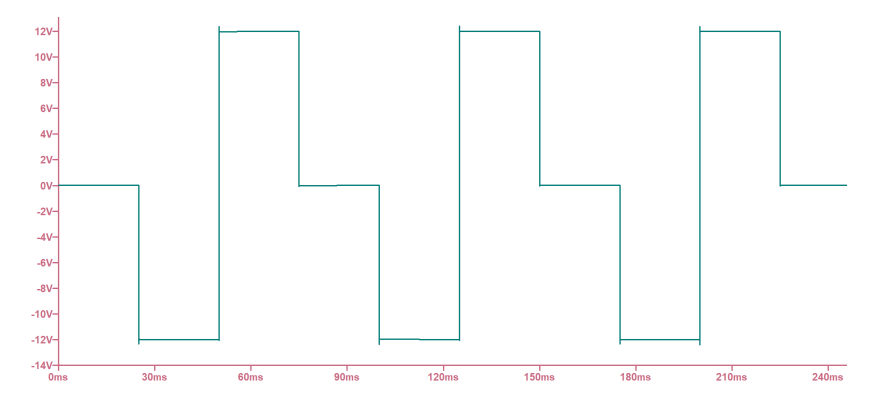


Figure 3.13: Output from the simulation of the first amplifier which takes as an input two biphasic pulses with an amplitude of 5V and converts them to $\pm 12V$ biphasic pulse.

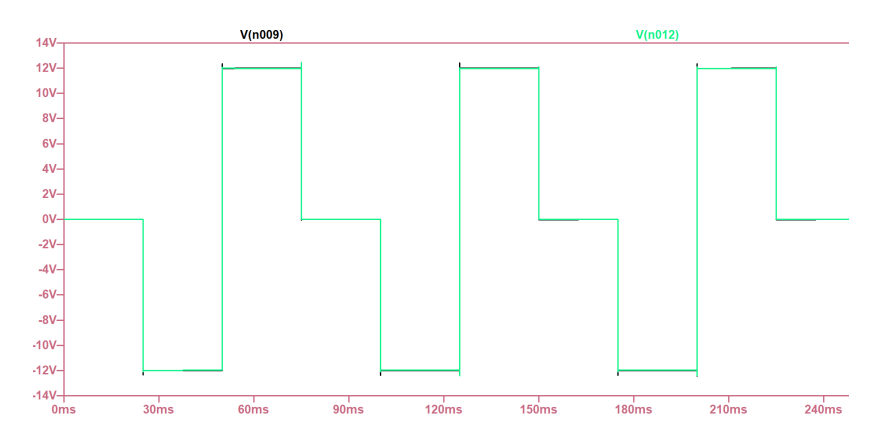


Figure 3.14: Output from the simulation of the second in series amplifier (buffer amplifier) which purpose is to improve the quality and consistency of the signal. The black line in the signal indicates the difference in comparison with the first signal.

By rotating the potentiomer and consequently change the resistor value we can achieve a wide range of voltage amplitudes from 0-12V. The following Figure 3.15 presents a biphasic output signal of 6V, obtained by the simulations in LTSpice.

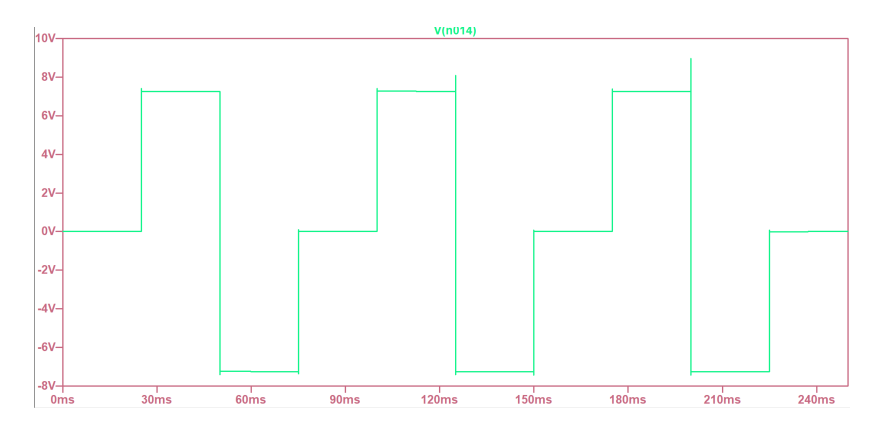


Figure 3.15: Output from the simulation of the third amplifier in parallel of which a potentiometer was placed.

3.7 Demultiplexing the rectangular biphasic signal to the output

As mentioned before, the proposed electronic circuit consists of a driver unit. The driver unit is the unit that drives the rectangular pulses stemming from the amplifiers, to the desired electrode chip through the use of Demultiplexers. A demultiplexer is a circuit consisting of a single input and multiple outputs. In other words, a demultiplexer converts a serial data signal at the the input to a parallel data at its output lines. By applying a control signal the input can be directed to the output. More specifically, a demultiplexer of 2m outputs has m select lines (control bits), used to select the output line in which the input signal will be directed.

In our case, due to the fact that the whole set up was designed for a 16-well plate of EHT (16 chips with two electrodes each, perpendicular to the pillars) two demultiplexers 1:8 was used to fulfill the needs of our system. The selected demultiplexers have 8 outputs. Each of the 8 outputs is connected to one of the two electrodes of the EHT platform, while the second electrode of the EHT platform is grounded. This way, we can achieve the creation of an electric field above and perpendicular to the pillars of the EHT platform. In the following paragraph the exact mechanism of a 1-8 Demultiplexing unit is going to be analyzed.

The selected demultiplexers for the designed electronic circuit are the ADG1408 monolithic iCMOS analog multiplexers/demultiplexers comprising eight different channels[78]. The 3-bit address lines A0, A1,A2 determine the input to one of the eight outputs. It is worth mentioning that this type of switches can be used as multiplexers and as demultiplexers due to the fact that the inputs can be also used as outputs and reversely. In addition, the most important characteristic is that this electronic component can be powered from a dual power supply establishing it suitable for our application (Biphasic rectangular pulses). According to what is mentioned before, two demultiplexers will be used in order to drive the biphasic rectangular pulse to sixteen in total electrode chips. The following schematic design (Figure 3.16) explains all the pin-out connections between the demultiplexers and the microcontroller which monitors the operation of the demultiplexers by programming the unit properly [78].

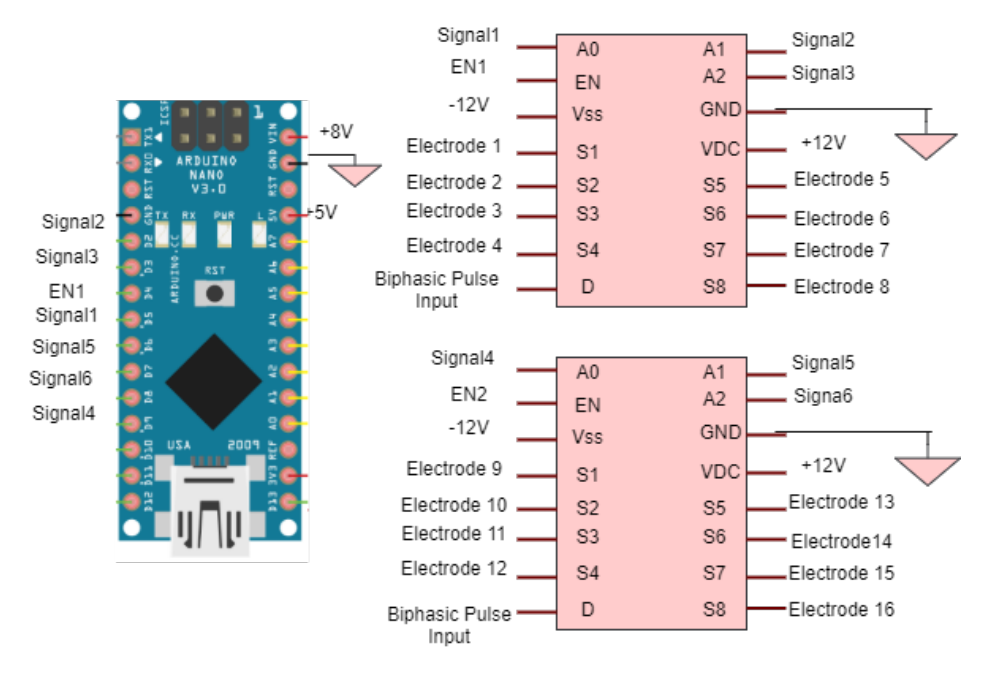


Figure 3.16: Conceptualized schematic of microcontroller and demultiplexing unit

3.8 Measuring the current through the electrodes

One of the most important characteristics of this system is the potentiality to measure the value of the current that passes through the electrodes. This is a major advantage for the experimental set up, allowing the user to adjust the voltage according to the value of the current that passes through the electrodes. This scenario was implemented by using a precise current sense amplifier.

The most common method is to perform an indirect measurement by measuring the voltage across a precision resistor and using Ohms law to measure the current across the resistor. According to Ohms law in an electrical circuit, the current passes through a conductor between two points is directly proportional to the potential difference across the two points and inversely proportional to the resistance between them. The most common sensing element used to detect current flow is a low value, precision resistor(shunt resistor) placed in the current path. This resistor develops a voltage across, proportional to the current passing through it. Because the shunt resistor should not affect the current flow significantly, it is quite small in the order of mOhm. As a consequence, the voltage developed across the shunt resistor is also quite small, and often requires amplification before being connected by an ADC[79]. For this reason, it is important to use an amplifier that amplifies the very small voltage across to the resistor and then an ADC from the microcontroller to convert the amplified voltage into a digital representation.

Taking into consideration the basic function of a current-sense amplifiers which was analyzed previously, and taken as granted that the ADC of the microcontroller can measure voltages up to 5V and cannot measure negative values, a voltage reference must be created. Due to the fact that the signal that is sent from the amplifier to the microcontroller will be up to 5V and the amplifier gain is 100, a voltage reference of approximately 2.75V must be developed. According to the following equation Vout=mVin +b, when the Vin will be 12V, the amplifier will sent to microcontroller 5V. When the Vin will be 0V the amplifier will send 2.5V and when it is 0v will send 2.75V. A zener diode was used in order to create a voltage reference. The breakdown region of the selected zener diode is at 2.75V.

In the following Figure 3.17, the schematic of the current measurement circuit is illustrated designed with KiCaD software tool.

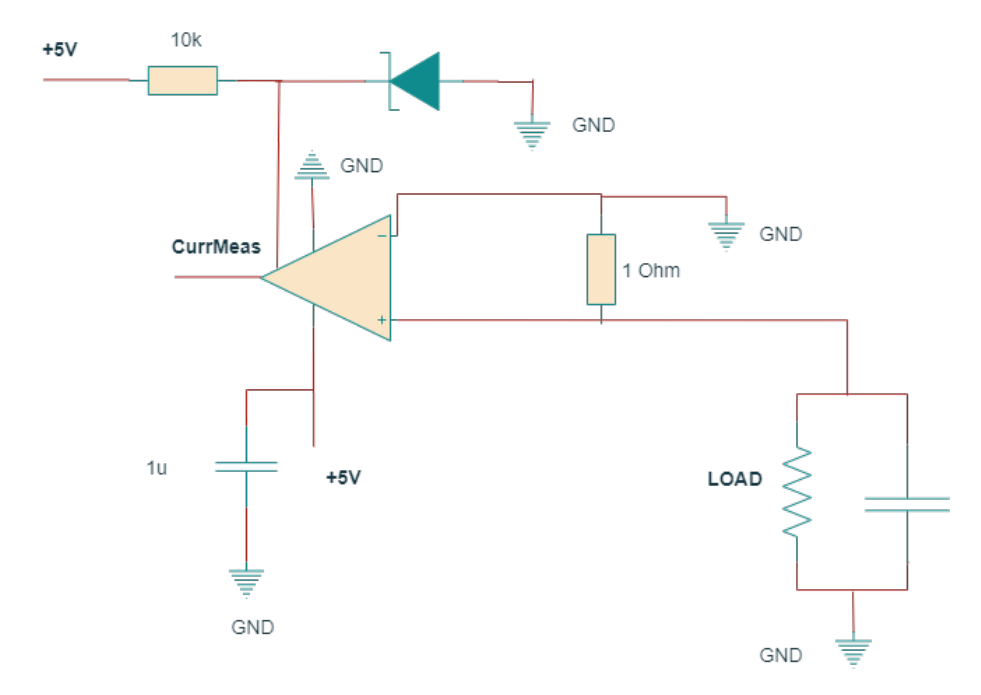


Figure 3.17: Schematic of circuit which measures the amount of current passing through the connected electrodes

3.9 Circuit for Measuring the applied voltage amplitude

Apart from the current measurement capabilities of the system, the designed pulse generator circuit measures also the applied voltage to cardiomyocytes. This is a principal specification of an experimental set up allowing the user to measure and observe the voltage amplitude precisely without the using of an external device such as a multimeter or an oscilloscope. This way, the parameters of electrical stimulation can be adjusted to the desired levels in a more automated way.

The voltage measurement will be achieved by using the Arduino (ATMEGA) microcontroller. In previous chapter, it was explained that the selected microcontroller is able to measure a voltage signal up to 5V. The input voltage amplitude in the amplifier will be up to 12V. Due to the fact that it is a biphasic pulse, it includes also negative values up to -12V. Thus, the idea behind the designing of the electronic voltage measurement circuit, is to use an operational amplifier and calculate its gain according to the following concept (Figure 3.18). When the value of the voltage input signal is 15V, the operational amplifier will convert it to 5V according to the following calculations (a value that can be measured by the microcontroller). Accordingly, when the value of voltage is 0V, the amplifier will amplify it to 2.75V(which is a voltage reference made by using a zener diode). Due to the fact that the microcontroller is able to calculate voltages in the range of 0V to 5V, the proposed idea is an accurate way to measure the amplitude of the signal applied to cardiomyocytes.

VREF V+ RL
VIN RG

In the next paragraph all the calculations for specifying the desired gain of the amplifier are presented.

Figure 3.18: Schematic design of the circuit for measuring the applied voltage.

RF

In following calculations it is assumed that Vin=12V, Vout=5V in the first case and Vin=0V, Vout=2.5V in the second case. The gain and the offset of the amplifier were calculated m=0.16 and b=2.5. According to the following equations and substituting the m and b, the value of R1,R2,RG and RF can be calculated.

$$m = \frac{R_2}{R_1 + R_2} * \frac{R_f + R_G}{R_G} \tag{3.16}$$

VOUT

$$b = V_{ref} \frac{R_1}{R_1 + R_2} * \frac{R_f + R_G}{R_G}$$
 (3.17)

R1 = 10k, R2 = 2k, RF = 1.6k, RG = 8k The entire schematic diagram of the electrical stimulator is presented in the appendix.

3.10 Current Source Electrical Stimulation

So far, voltage-controlled or current-controlled electrical stimulation methods are the most widely used by the scientific community in order to achieve functional electrical stimulation and excitation to cardiomyocytes. As it was analyzed previously during the voltage-controlled stimulation the voltage remains stable and the current changes according to the change of load. In this case, a constant voltage is offered through the system regardless of the electrode impedance[80]. The previous design of the pulse generator offers voltage-controlled electrical stimulation. On the other hand, an-other method of electrical stimulation named voltage-controlled current source adjusts the current to adapt the changes in impedance of the tissue-electrode interface[80]. In this scenario, we can have better control of the current that passes through the tissue. According to previous research in this field, there are cases in which the impedance of electrode-tissue interface changes during the experiment. In these cases, it is highly recommended to keep the applied current to the tissue stable.

The effectiveness of electrical stimulation in cardiomyocytes depends also on the electrode's material. In particular, an electrode is characterized as ideal for stimulation when it delivers a high amount of charge preventing potential irreversible electrochemical reactions such as corrosion of the metal

or toxic chemical products produced by the stimulation process. In our experiments, Titanium Nitride (TiN) was used as an electrode material. TiN has several advantages, among them and the most significant is the capacitive charge injection mechanism that follows during the electrical stimulation. The capacitive mechanism of charge transfer includes charging or discharging of the electrode double layer. Specifically, the charge injected from the electrode attracts or repels ions coming from the tissue. This way, pulses from ion current are created. Actually, there is no real charge transfer across the electrode and the electrolyte interface[81]. This mechanism is considered an ideal method of electrical stimulation because by charging and discharging the double layer capacitance, electrochemical reactions are eliminated. Previous studies have shown that TiN as material presents a more stable behavior when charge-balanced stimulation is applied to it. As a result of this, a second mode of charge-balanced biphasic pulses will be integrated into the existing electrical stimulator circuit. Including these two modes of electrical stimulation (biphasic pulses with voltage source and biphasic pulses with current source stimulation) the user will be in a position to compare the results of stimulation and follow the most efficient and stable method regarding the electrode's material and the properties of cardiac tissue [81].

For this reason, the designed electrical stimulator circuit was further advanced to provide both voltage source and current source stimulation, introducing the charged-balancing technique in the system. The update of the presented design will allow biologists to switch between voltage source and current source stimulation and make comparisons between them determining the best way of electrical stimulation and excitation of cardiac cells.

3.11 Voltage to Current Source Stimulation

3.11.1 Current Source

The current source of the electrical stimulator should be able to generate a constant current to cardiomyocytes. The injected current should be constant and independent of the load impedance in order to create better control of the electrical stimulation[82]. As it is shown in the next Figure 3.19, a current source offers an output impedance (Rout) that influences the precision of the current delivered to the load (RLoad). More specifically, the current that is delivered to the load (ILoad) depends on both impedance of the current source and the load impedance[82]. During the electrical stimulation the load impedance is something dynamic that changes during the experiment. Thus, it is difficult to predict accurately the value and for this reason, it is important to maximize the output impedance of the designed system.

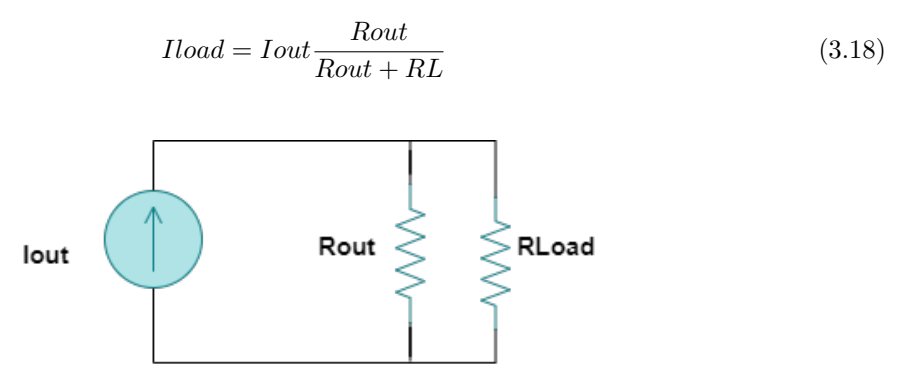


Figure 3.19: A practical current source

The selected method of charged-balanced electrical stimulation is based on a voltage-to current converter, called Howland charged pump circuit. The Howland current pump is a widely known bio-electrical circuit, which is implemented in order to transfer accurate electrical currents. Bio-electrical

current sources transfer a specific amount of energy to excite and stimulate biological volume conductors [83]. Until nowadays, various current source topologies have been applied in bioelectrical studies. However, the Howland source remains the most well-known since it can be developed simply by using an operational amplifier and a bridge of precise resistors. The tolerance of resistors is an important parameter because the absence of good tolerance can lead to an imbalance between transfer function in positive and negative input [83][84][85]. Previous research in this field has shown that the Howland presents similar performance and results to other more complex and advanced current sources.

For the implementation of this idea, different parameters must be considered to ensure the accuracy of this method. First, a good operational amplifier must be selected. The slew rate of the amplifier needs to be high enough in order to allow for fast setting time of the output current. It would be also important that the operational amplifier draws relatively low current in order to minimize the power consumption of the system. As far as the resistors that are going to be used to create the bridge, they must have very good tolerances because possible mismatches of the resistors could lead to inaccuracies in the output current. For this reason resistors with tolerance 0.05% for this circuit design. In the following Figure 3.20, the hardware circuit of Howland Current Pump is demonstrated to provide full explanation regarding the basic circuit operation.

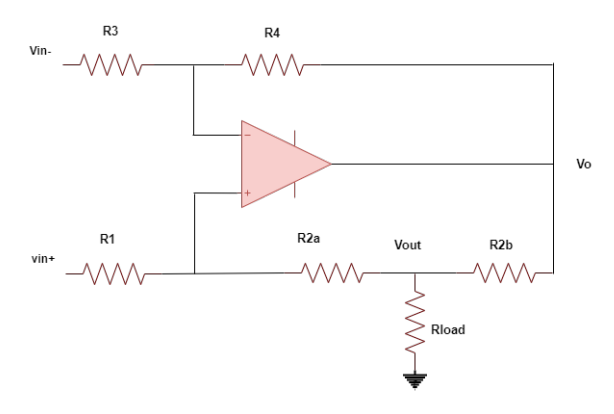


Figure 3.20: The Improved Howland Current Pump Method for current controlled stimulation [83] [84] [85].

The Howland is unique method of voltage-to- current converter because it has both positive and negative feedback paths. The feedback paths are balanced when the resistors are matched according to

$$\frac{R4}{R3} = \frac{R2a + R2b}{R1} \tag{3.19}$$

When there is a good balance of bridge resistors a voltage controlled current source stimulation is achieved. The balancing of the method was ensured by integrating very sensitive resistors 0.05 or less tolerance. In this case, the gain is set by R13, modified by the ratio of R14/R15 (which is typically 1/1). [85]

The selected operational amplifier for this circuit design is the OPA462. The selected amplifier has a high slew rate of $32\mathrm{V}/\mu$. The typical supply current that draws this amplifier is 3.2mA while the maximum is 3.5mA. It would be good that the power consumption of this device is at low levels. Although, the power supply of the proposed electrical stimulator can be replaced by an external charger instead of batteries making this consideration a second priority of the circuit design. The circuit model for the simulation of the voltage to current source converter is provided in the next figure. In order to investigate the efficiency of the proposed converter, three different values of load were used for the simulations in LTSpice (Rload=300 Ω , 500 Ω , 1 k Ω). The next Figure 3.21 shows the circuit design of Howland converter while the Figure 3.22 shows the output signal from LTSpice simulations.

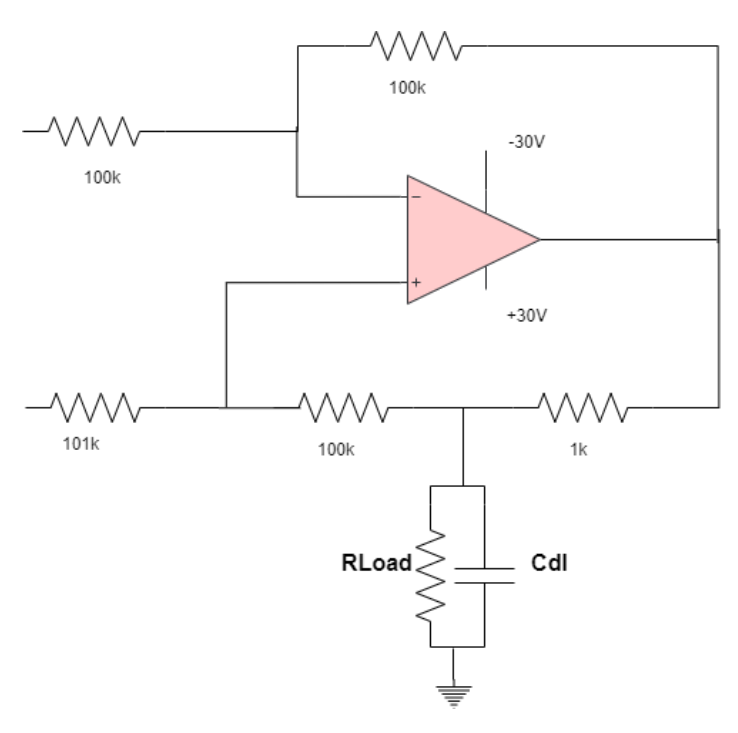


Figure 3.21: Howland circuit with the used values of resistors. The Rload of this circuit tested for different values $(300\Omega, 500\Omega, 1k\Omega)$.

In the following figure, the simulation result of the voltage-controlled current source electronic circuit for different values of output load is provided. The output was exactly the same for the three different values of resistors and the current remained stable at 7mA. By rotating the potentiometer the current can be increased or decreased.

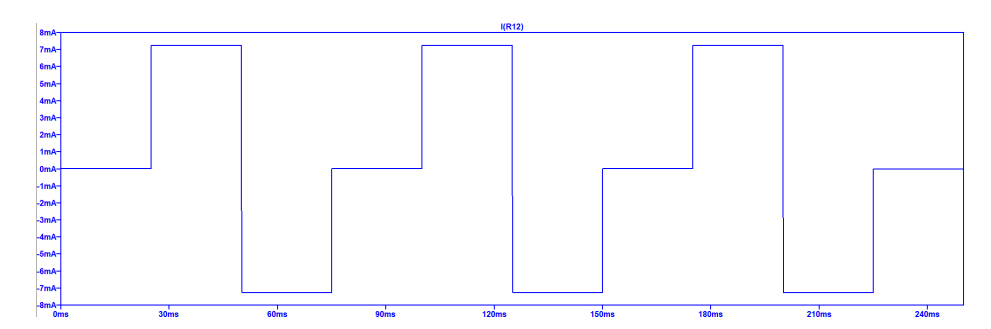


Figure 3.22: The Improved Howland Current Pump Method for Voltage Controlled Charge-Balanced method. The current remains stable at 7mA and independent of the load.

At this stage it is important to highlight that in order the electrical stimulator to support this system advance (Howland converter), some changes in the power supply system were considered essential. More specifically, in the previous method, batteries up to 15V or an external charger can be used as a power supply unit. Then using the proper converters (Buck converter and dual charge pump) the power was distributed to all of the electronic components of the system. In this case, the converter of the circuit must be supplied with voltages up to 30V according to the previous calculation analysis. The power supply of the operational amplifier should be at least double of the Vout of the load in order to keep the current stable even if the load in the output changes. Since, the systems was designed to provide up to 15V (negative and positive rails) the power supply of amplifier should be at least double of this value. The next Figure 3.23, demonstrates the changes in the power supply system in order to support the voltage to current source converter (Howland Converter) while the Figure 3.24 presents the 3-D CAD model of the designed PCB.

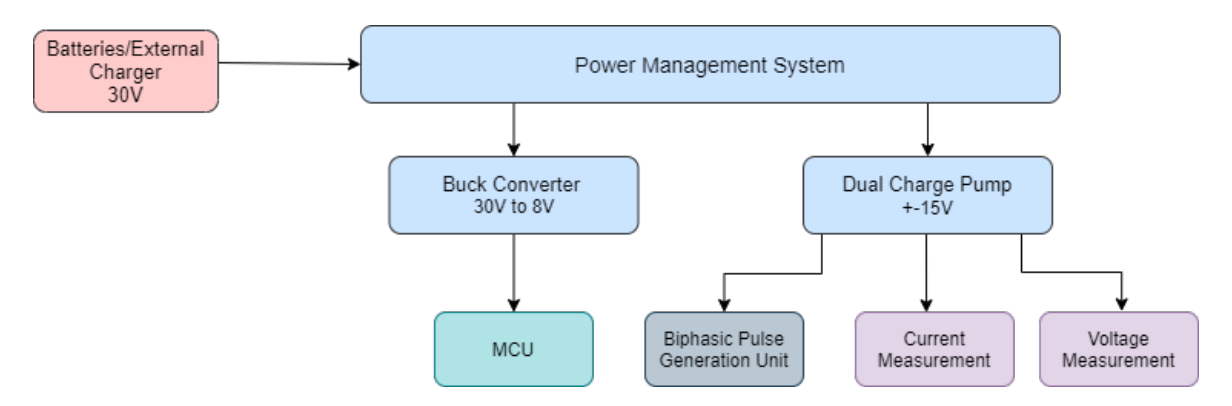


Figure 3.23: The updated power supply system consists of an external charger (30V) and a power management system. The power management system includes a buck converter which supplies the microcontroller and a dual charge pump converter which supplies the biphasic generation unit and the measurement circuits.

After the changes to the power supply system the new PCB was designed and the 3D version of the KiCad model is provided.

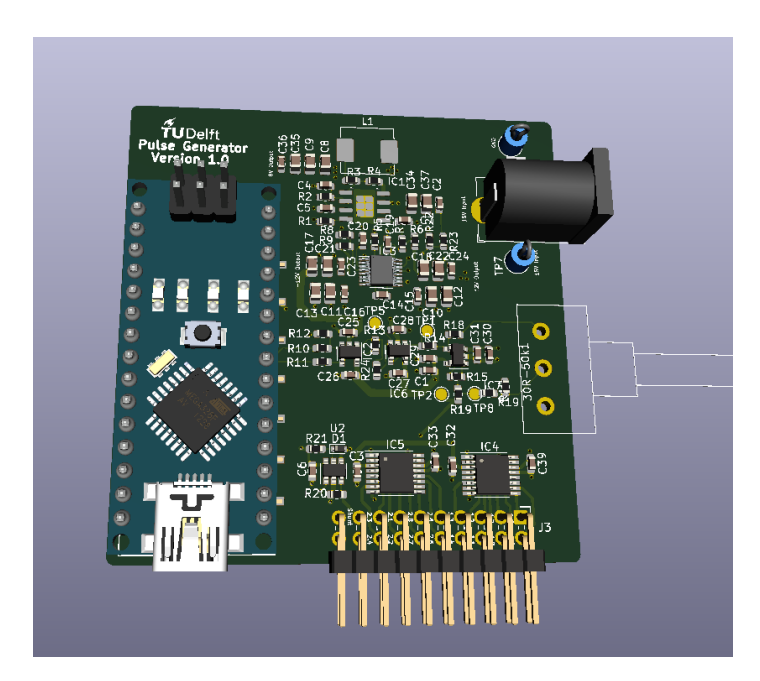


Figure 3.24: 3D CAD Model of Pulse Generator Circuit for Electrical Stimulation of Cardiomyocytes in an EHT platform.

3.12 Design of a PCB for 16- integrated electrode chips

The next goal of the thesis includes the design and fabrication of a read-out interface for the TiN electrode chips. The Printed Circuit Board (PCB) where the chips will be integrated, is going to be the bottom of a 96-Well plate which is used by biologists for experimental purposes. Firstly, a PCB was developed only for one electrode chip (Figure 3.25) and then a 16-PCB holder designed (Figure 3.26) in a way to fit in the dimensions of the 96-well plate. The electrode chips will be diced in dimensions of 1cm by 1cm. The diameter of each well plate is 6mm while the center of one well plate will be 12mm far from the center of the next one. The PCB holder will fit 4 rows of 4 electrode chips with the aforementioned distances. For this purpose, a 2-layer PCB was designed while the width of

the track lines that create the interconnects between the pads and the connector is 0.3mm. The pads were placed close to the side the pads electrode chips are located at. This facilitates the wire-bonding between the pads of the PCB and the electrode pads. The following figure demonstrates the design of the electrode holder firstly for a single electrode chip and then the design for 16-electrode chips.

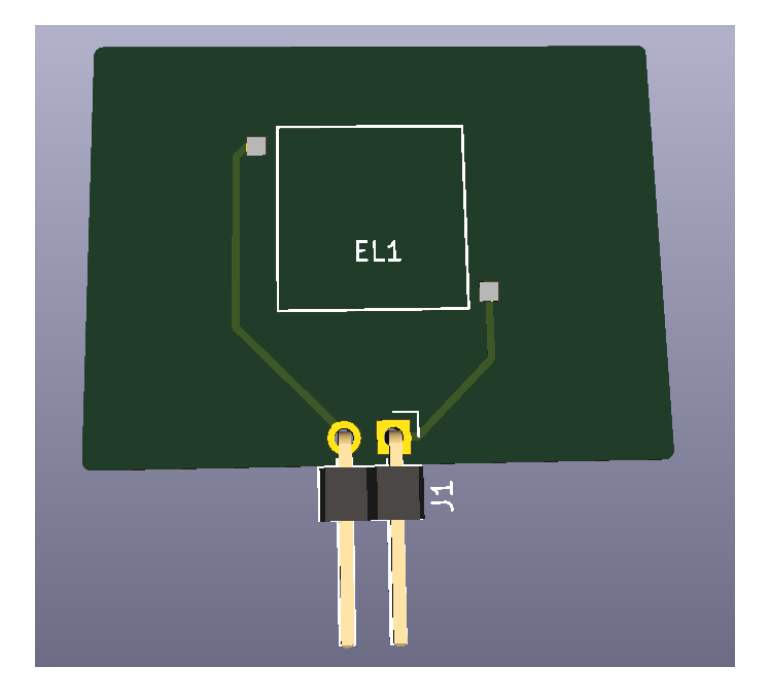


Figure 3.25: 3D CAD model of PCB holder for one electrode chip.

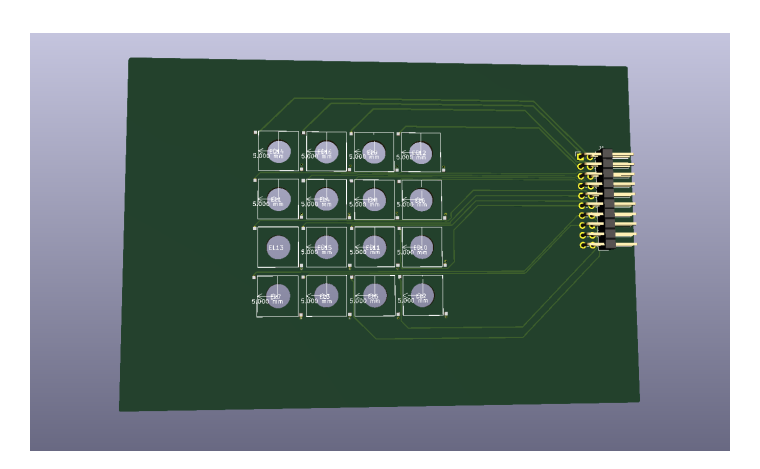


Figure 3.26: 3D model of PCB holder for 16-electrode chips. The 6mm holes in the PCB enable the transparency and observation of the cardiac cell cultures during the experiments.

The next Figure 3.27 demonstrates the 3D model of the holder which hosts a total of 16-electrode chips. The bottom of the holder structure is the designed by me printed circuit board. The rest 3D model was designed by M. Dostanic. The proposed holder allows the culture of cardiac cells inside an incubator and its connection with the proposed electrical stimulator. Thus, the electrical stimulation set up is completed and we are only one step far from the actual electrical stimulation of cardiomyocytes in the EHTs platform.

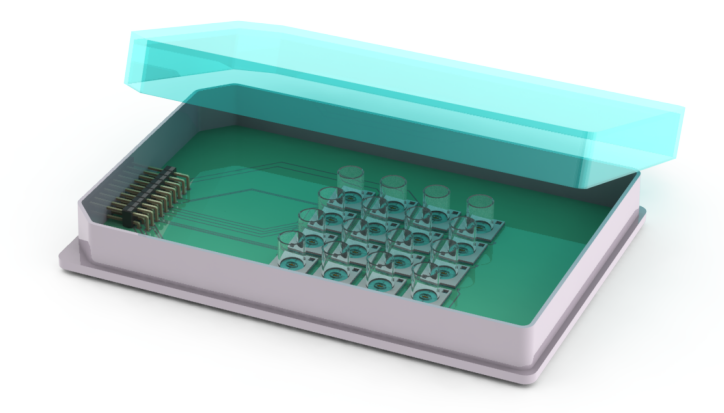


Figure 3.27: 3D model of holder structure for 16-electrode chips. The bottom of the holder was designed in KiCad (see Figure 3.26). Then this PCB was integrated with the entire case for the EHT platforms and was designed in Solidworks by M. Dostanic.

3.13 Conclusions

In this chapter, the full design and the development of electrical stimulator were provided. The electronic circuit design techniques and methods were explained in detail, combined with the simulations and the actual circuit design in the Kicad Software tool. The advanced version of the proposed stimulator includes two modes: voltage-controlled voltage source and voltage controlled current source stimulation giving the user the flexibility to switch between modes and explore the best results in terms of electrical stimulators. Current and voltage measurement circuits were integrated ensuring the notification of the user for the values of applied voltage and current to cardiomyocytes. Furthermore, the user-friendly interface of this device allowing the user (biologists) to easily interact with the stimulator through a serial monitor, inserting the desired stimulation parameters (channel of stimulation, frequency, duty cycle) and initializing the procedure, was developed. The voltage amplitude is controlled manually by rotating the potentiometer. Switching between two modes (voltage-controlled voltage source and voltage-controlled current source) is feasible through changing the corresponding switches. Since the highest allowed amount of current to cardiomyocytes that provides excitation without causing any kind of damage is up to 12mA, a protection circuit that detects the over-current and stop the stimulation was introduced.



4.1 Description of Measurement set up

To verify the functionality of the system and its performance, several measurements were conducted. Before assembling the individual parts on the PCB, two output pins of the MCU unit (Arduino Nano) were programmed and tested properly to generate monophasic pulses with 180 degrees phase shift, in low frequencies (0-5Hz). That was simply tested in a separate breadboard by connecting one LED in the output pin of the microcontroller. This produces a monophasic pulse with an amplitude of 5V. Optical observation of the LEDs (ON-OFF state) in the corresponding outputs, as well as a measurement of the PWM with an oscilloscope, verified the accuracy of the PWM programming in terms of amplitude and frequency (Figure 4.1). The way of MCU programming was previously explained (Chapter 3) and the code is provided in the Appendix.

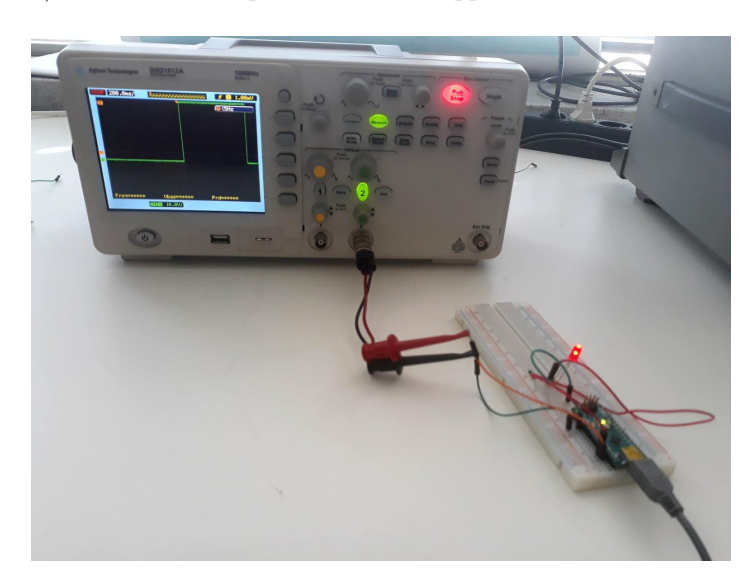


Figure 4.1: Simple set up for testing the microcontroller output using a digital oscilloscope.

The next step includes the assembly of all electronic components in the PCB unit. After completing the soldering procedure, the PCB was optically observed for potential short circuits between two different pins or pins and a pad, which are maybe caused during the soldering procedure. In cases when a short circuit was detected, a repetition of soldering took place. Due to the fact that sometimes it is difficult to optically detect a short circuit, a multi-meter was used and was set it in the corresponding output to recognize potential circuits.

The fabricated version of the PCB (version1 and version2) can be seen in the following picture (Figure 4.2, 4.3). The fabricated circuit is a 4 layer PCB. Analog and digital tracks were routed in such a way that they did not cross each other. Good ground connections were designed for the return currents of signal paths to reduce possible interference between signals.

Although the PCB is power supplied by batteries up to 15V (for the first version) or by a charger up to 30V in the second version, all measurements were performed by an external supply of 30V. The measurement set up is illustrated in the following figure (Figure 4.2). It is important to highlight that all the measurements were conducted by using different values of pure resistive load for a better sense of system performance.

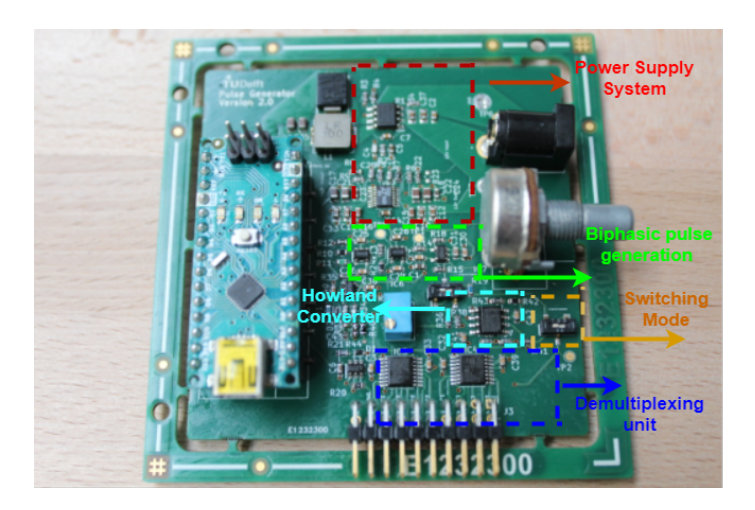


Figure 4.2: Fabricated version of PCB.



Figure 4.3: Entire measurement set up which includes the power supply of 30V, an oscilloscope, a multimeter and the testing PCB.

4.2 Testing procedure of the Power Supply circuit

At the beginning of the testing procedure, a power supply unit of 15V DC was connected to the test points of the PCB in order to control the Voltage and the current that passes in the system efficiently. After connected the power supply, a multi-meter was connected to the output of each of the power converters in order to measure the output voltage. The output of the buck converter was tested. Indeed, the output of the designed circuit generates 8V to supply the microcontroller.

The same procedure applied for testing the second converter (Dual Charge Pump Converter), to demonstrate its performance. The output of the Charge Pump Converter was designed in a way to generate positive and negative 15V to power supply the operational amplifiers. Also, it produces -30V in order to power supply the voltage to the current converter in the current-controlled mode of the stimulator. The output voltages of the charge pump converter are in full agreement with the expected values verifying the accuracy of the designed power supply system.

4.3 Testing Procedure of the Biphasic Pulse generation unit

The signal in the output of the first operational amplifier and in the second in series operational amplifier was observed through oscilloscope to verify that reaches the desired threshold $(\pm 15\text{V})$ for the second version of PCB. In the following illustration (Figure 4.4), the output voltages of the first operational amplifier are provided for the two versions of PCB.

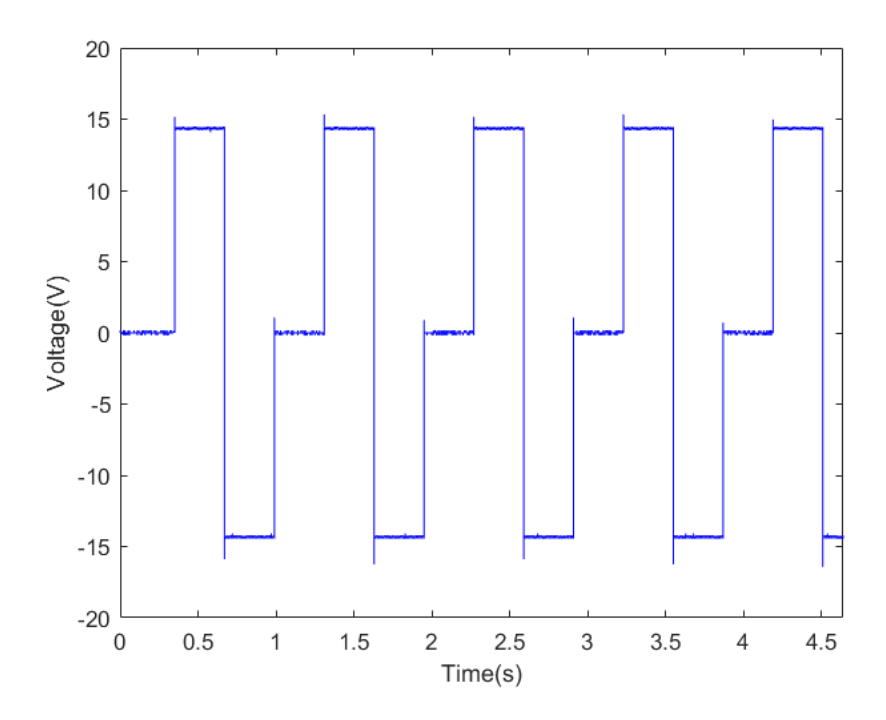


Figure 4.4: The output of the first amplifier which creates the threshold of ± 15 Volts. The biphasic pulse reaches up to 14.8V and the period of the signal is T=1sec.

4.3.1 Testing the functionality of the potentiometer

In parallel with the last amplifier, a potentiometer was placed to provide full control of the signal voltage amplitude from 0 to 15V. The output of the last amplifier was tested by connecting an oscilloscope in the test point of the last amplifier and moving the rotated knob to achieve different voltage amplitudes in the range of 0V to ± 15 V. The following picture (Figure 4.5) presents the different voltage amplitudes in the output of the amplifier.

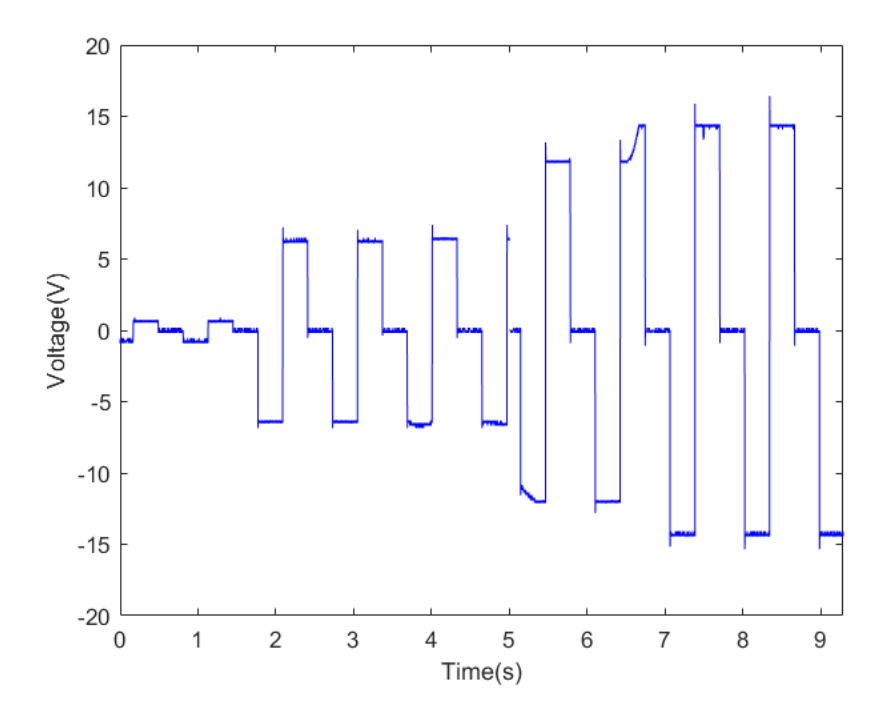


Figure 4.5: The pulse generator circuit for EHT electrical stimulation purposes has the ability to alter the voltage amplitude by simply rotating a knob to be adjusted in the experiment needs. The Figure illustrates various voltage amplitudes (0.7V, 6.31V, 14.26V, 14.8V).

The presented electrical stimulator can provide very low voltage signals, even close to zero, but also higher voltages in a wide range of -15V to +15V. The knob of the potentiometer should be gently rotated to achieve better precision in voltage values.

4.4 The proposed circuit design can provide a wide spectrum of frequencies

The pulse generator circuit was designed and programmed in a way that gives the user the ability to change the channel of the simulation and the desired frequency. Through a user interface a serial communication between the micro-controller and the circuit is achieved. In the serial monitor of the Arduino microcontroller app, a message is prompted to the user to select the channel of the electrical stimulation and the desired frequency of stimulation. The next figure (Figure 4.6) shows a range of different stimulation frequencies.

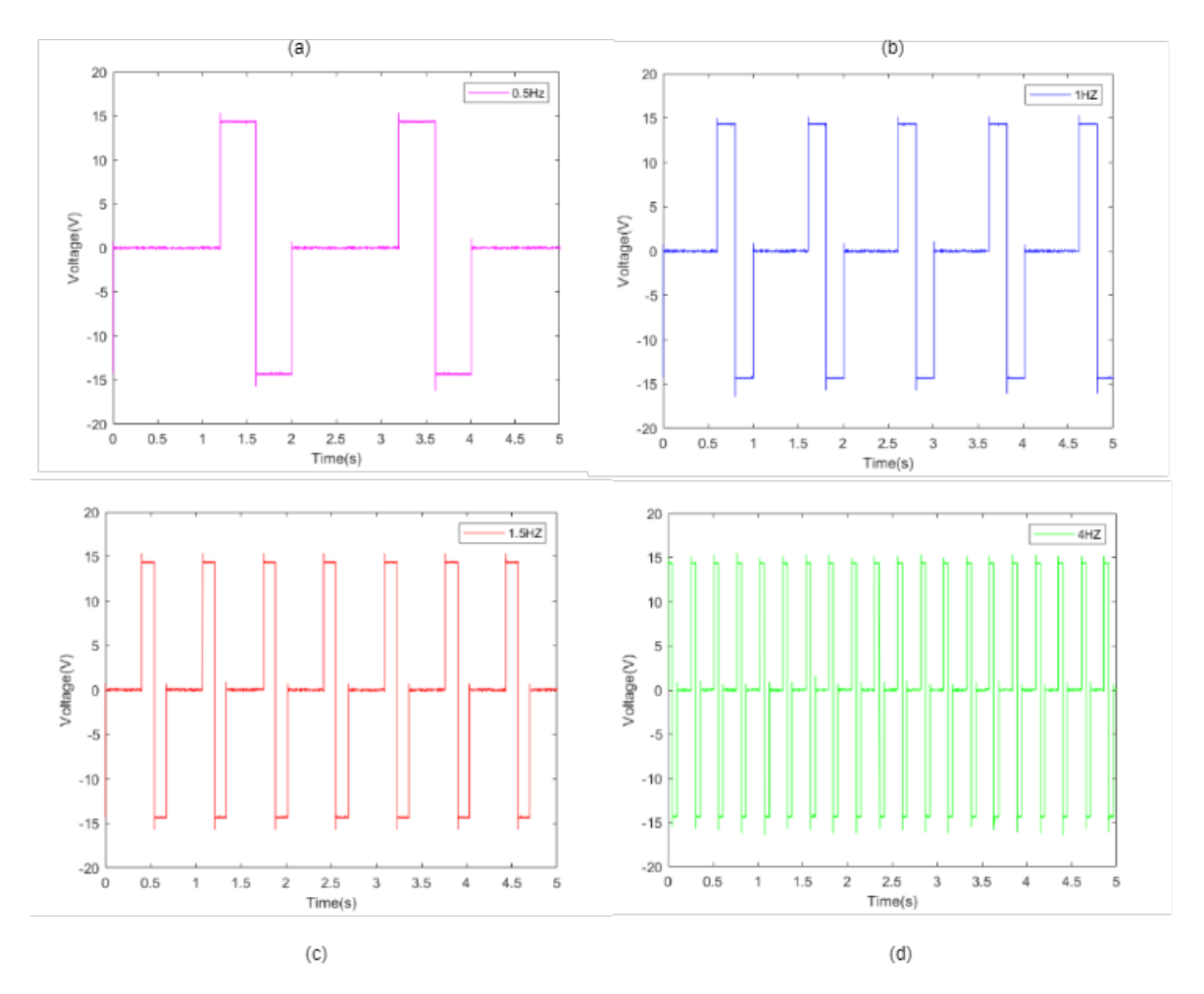


Figure 4.6: The design electrical stimulator provides biphasic pulses in various frequencies in the range of 0.3-4Hz. The results from the measurements verify the precision in the achievement of low frequencies. The user can change the frequency by step of 0.1Hz. (a) 0.5Hz, (b) 1hZ, (C) 1.5HZ, (d) 4HZ

4.5 Testing and Measurement of Duty Cycle

The duty cycle is considered an important parameter for efficient electrical stimulation of cardiomyocytes as it defines the time of the pulse activation during a period. In our case duty cycle is defined as the ratio of pulse width (anodic or cathodic), over the entire period specified by the user. Through a user interface biologists can change the duty cycle of the pulse according to the needs of the experiment. That system was tested by inserting 4 different values of the duty cycle as a parameter to the program and measuring the corresponding output signal using an oscilloscope. The following figure (Figure 4.7) presents the biphasic rectangular pulse for 2.5%, 5%, 10%, and 40% duty cycle. The microcontroller was programmed in C++ programming language and the code is presented in the Appendix.

 $DutyCycle = \frac{PW}{T}$ PW: pulse width (of anodic or cathodic), and T: period. For example for Duty cycle 5% means that the signal is 5% in anodic phase, 5% in cathodic phase and 90% is OFF (inactive).

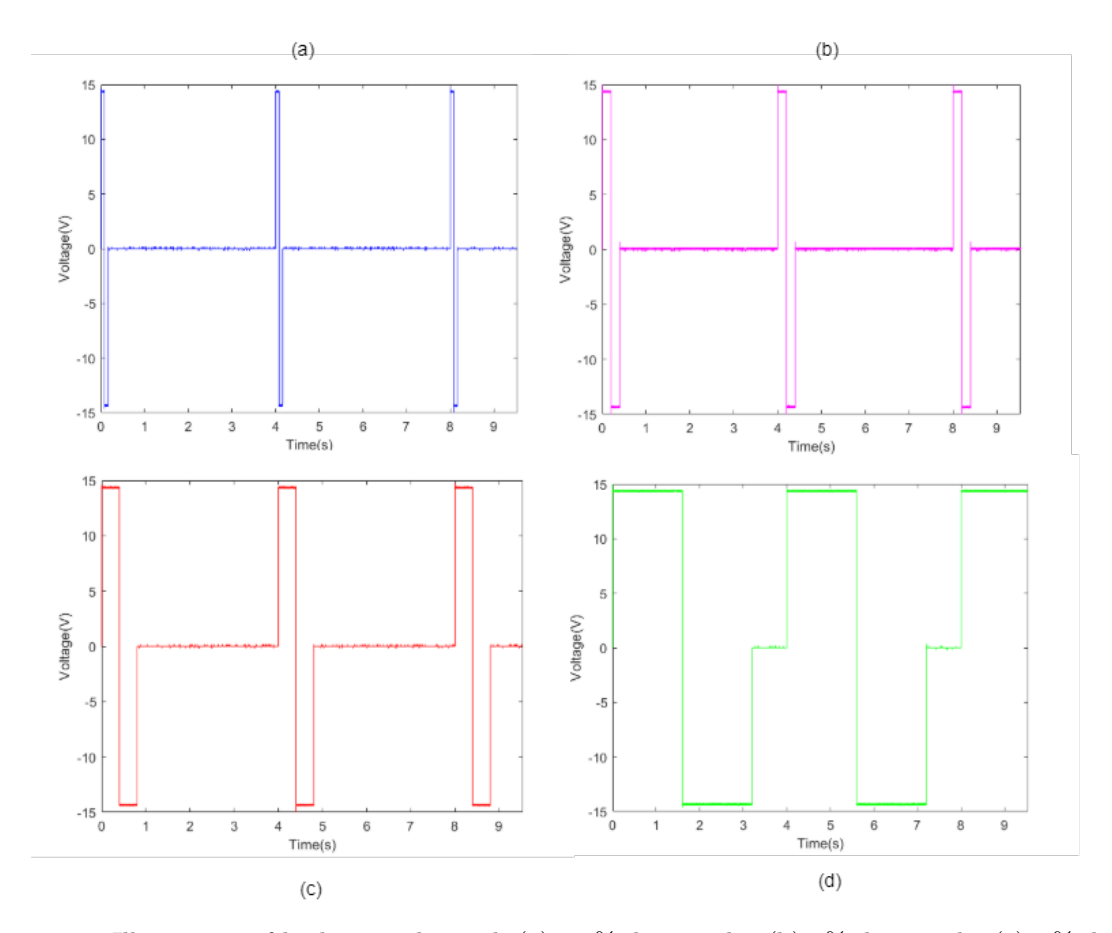


Figure 4.7: Illustration of biphasic pulse with (a) 2.5% duty cycle. (b) 5% duty cycle, (c) 10% duty cycle and (d) 40% duty cycle

4.5.1 Measurement and verification of current measurement circuit

The accuracy of the current measurement circuit must be investigated since it is highly important for a well-controlled electrical stimulation of the cells. To test the current circuit and its accuracy a load of 1 k Ω and then a load of 2k Ω was connected to the output connector of the pulse generator circuit. Different values of voltages (8V and 8.68V) were applied to the load. Using an oscilloscope the signal was measured in two different points. Firstly, the voltage in the load was measured and secondly in the A7 pin of the microcontroller which reads the signal from the output of the current sense amplifier. At this point, it is important to remind the reader that the current measurement circuit consists of a current sense amplifier and a shunt resistor (Low- value resistor). The signal is sent to an ADC of the microcontroller for reading. Due to the fact that the pins of this microcontroller can read a signal up to 5V, this current sense operational amplifier functions in the following way. When the input in the amplifier signal is 15V it converts it to 5V and the signal is sent to the ADC of the microcontroller for reading. By programming the microcontroller properly the voltage signal is translated to the current signal. In cases when the input in the operational amplifier signal is 0V, a signal of 2.5V is sent to microcontroller. The 2.75V (Voltage Reference) was created by using a zener diode. In the following Figure 4.8, two pulses are illustrated. The pulse that is presented with a blue line, represents the voltage in the load. The pulse which is presented with the red line, represents the pulse as it was measured from the microcontroller. According to theoretical calculations for $1k\Omega$ Load and VLoad=8V, the current that passes through the shunt resistor is calculated:

$$I = 0.008A \tag{4.1}$$

Because the shunt resistor is 1 Ω the voltage in the shunt resistor it, is 8mV. Thus, normally the A7 pin of the microcontroller which measures the current must show:

$$Vout = 100 \times 0.008 + 2.75 = 3.47V \tag{4.2}$$

As it is observed in the following graph Figure 4.8 the real value that the system measured for the current was 0.008A, which is exactly the same with the expected value something that reveals the precision of the circuit design.

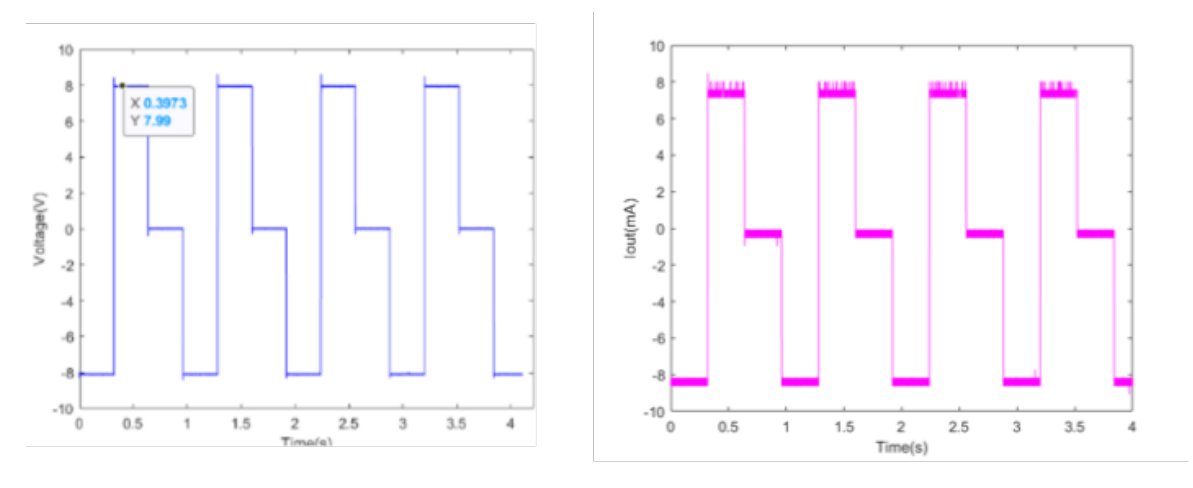


Figure 4.8: The blue graph represents the Voltage Input to the current sense amplifier and the red graph represents the measured signal in the ADC output of the microcontroller

The same procedure was followed for a different value of input voltage and different value of load in the output, to reinforce the argument for the high accuracy of the current measurement circuit. Specifically, in this experiment a load of 2 k Ω was used and a voltage input of 9.5V (Figure 4.9). For 2 k Ω load, Vin=9.5V and Rshunt=1 Ohm

$$I = 0.0047A \tag{4.3}$$

Thus, if the system is accurate the A7 pin of microcontroller must measure:

$$Vout = 100 \times 0.0047 + 2.75 = 3.184V \tag{4.4}$$

As it is illustrated in the following figure the measured signal is 4.7 mA something that ensures the accuracy of the circuit design.

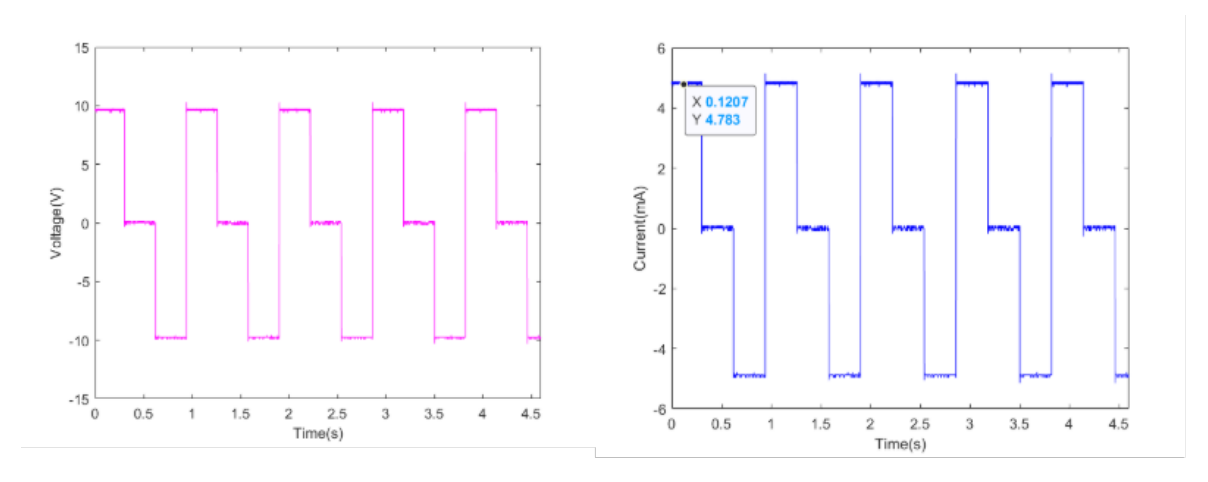


Figure 4.9: The (a) graph illustrates the voltage input to the current measurement circuit while the graph b represents the measured current in the pin A7 of the microcontroller. The measured value was 4.3 mA something that verifies the accuracy of the measurement circuit.

4.6 Measurement and verification of voltage Measurement Circuit

In this subsection the testing and measurements for the voltage measurement circuit were conducted for both modes, firstly for the voltage-controlled mode and then for the current-controlled mode.

4.6.1 Voltage Controlled Mode

The designed circuit for measuring the voltage based on an operational amplifier. In the Design of the Electrical Stimulation chapter, the gain of the operational amplifier was calculated at m=0.16 and the offset b=2.5V. Although, when actual experiments were conducted the actual circuit presented different behavior. One reason possibly was the zener diode that was used in order to create the voltage reference (at 2.5V) in combination with the voltage divider circuit in the input of the operational amplifier. Thus, during the experiments the values of the resistors that create the gain of the amplifier and the values of the resistors in the voltage divider replaced by much higher values in order to create an ideal circuit. Given the new values of resistors, the gain of the amplifier (m) was calculated again. The gain and the offset of this circuit were calculated to be m=0.104 and b=3.39 respectively. In the following Figure 4.10, Figure 4.11 the simulation of the circuit in LTSpice is presented, designed circuit and output signal respectively, and next the results from the actual experiments are provided.

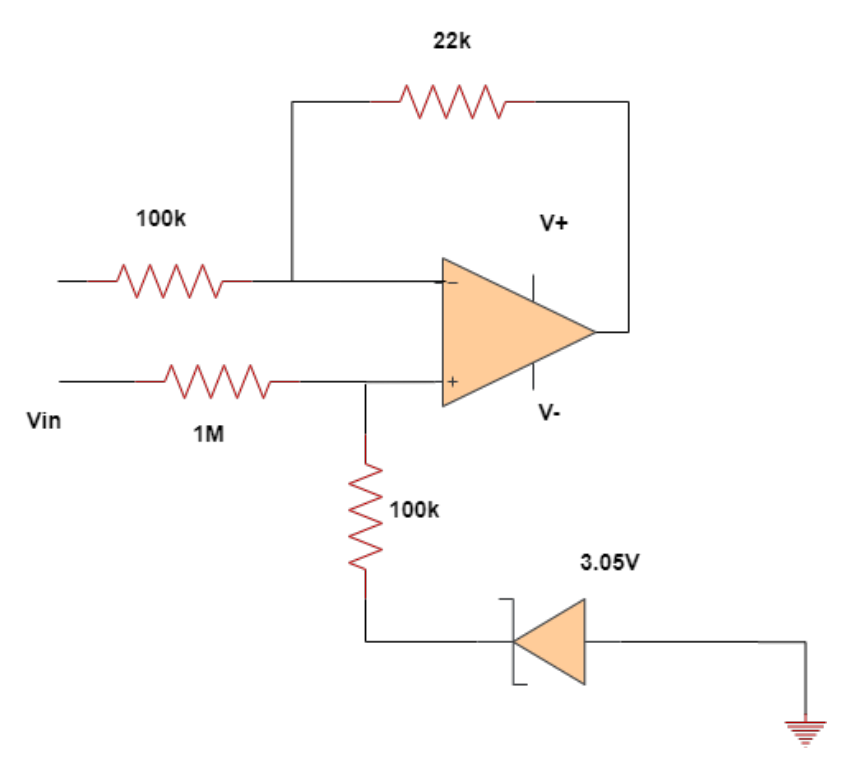


Figure 4.10: This schematic demonstrates the new values of the loads. The gain and the offset of the voltage measurement circuit were calculated according to these values.

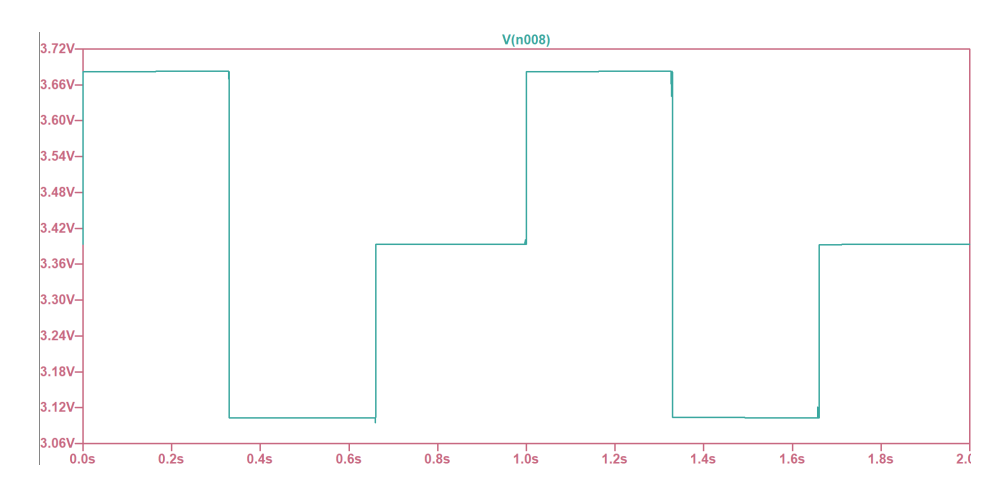


Figure 4.11: Results from simulation circuit behavior in LTSpice.

As it is illustrated in the following Figure 4.12 the voltage measured using an oscilloscope in two points. First, the signal was measured in the blue node and secondly, in the grey node which is the output of the voltage measurement circuit. Then theoretical calculations were performed in order to ensure the validity of the measured value. The oscilloscope was placed at the blue point (Figure 4.12) and the Vblue was measured at 6V. Thus, the voltage at yellow point using voltage divider will be

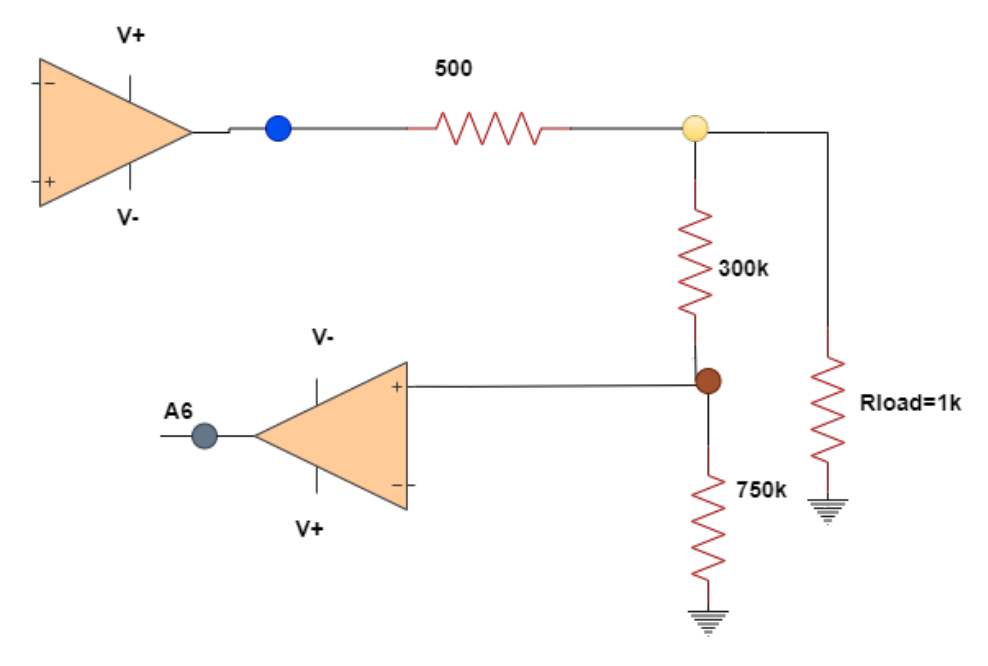


Figure 4.12: The blue dot and the grey dot represent the points where the signal was measured. The A6 label indicated the output of the amplifier which is sent to A6 pin of the microcontroller to measure the voltage.

The next Figure 4.13 demonstrates the voltage that was applied in the blue node (blue line) and the output signal as it was measured from the microcontroller (red line). It is obvious that the measured voltage for 1 k Ω load and Vblue=6V, was 3.704V.

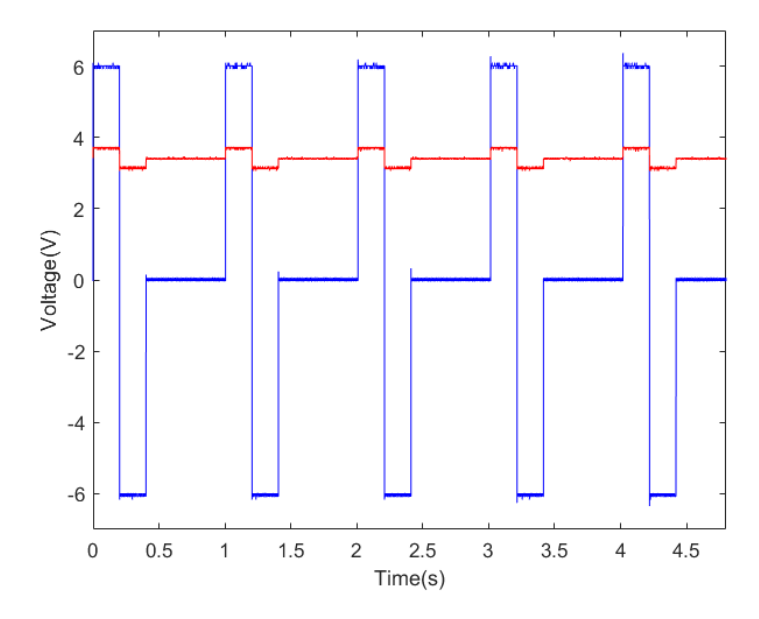


Figure 4.13: The blue line represents the applied voltage in the blue dot while the red line represents the measured voltage by the microcontroller.

$$Vyellow = \frac{500}{1500} \times 6 = 2V \tag{4.5}$$

Using a second voltage divider the voltage in the brown point will be

$$Vbrown = \frac{1050}{750} \times 2 = 2.8V \tag{4.6}$$

Thus the voltage input to the amplifier which measures the voltage according to the calculations must be 2.8V. The voltage output(VA6) must be

$$VA6 = m * Vbrown + b \tag{4.7}$$

$$VA6 = 0.104 \times 2.8 + 3.39 = 3.64 \tag{4.8}$$

The measured value of applied voltage as it is shown to the graph (Figure 4.13) is 3.704V which is very close the the actual value.

The same testing procedure was performed for the same load but now with a different voltage input. In this case the oscilloscope placed again at blue point and Vblue=10V. Then it was placed at the output of the amplifier (A6) and the measured signal was VA6=3.86V (Figure 4.14).

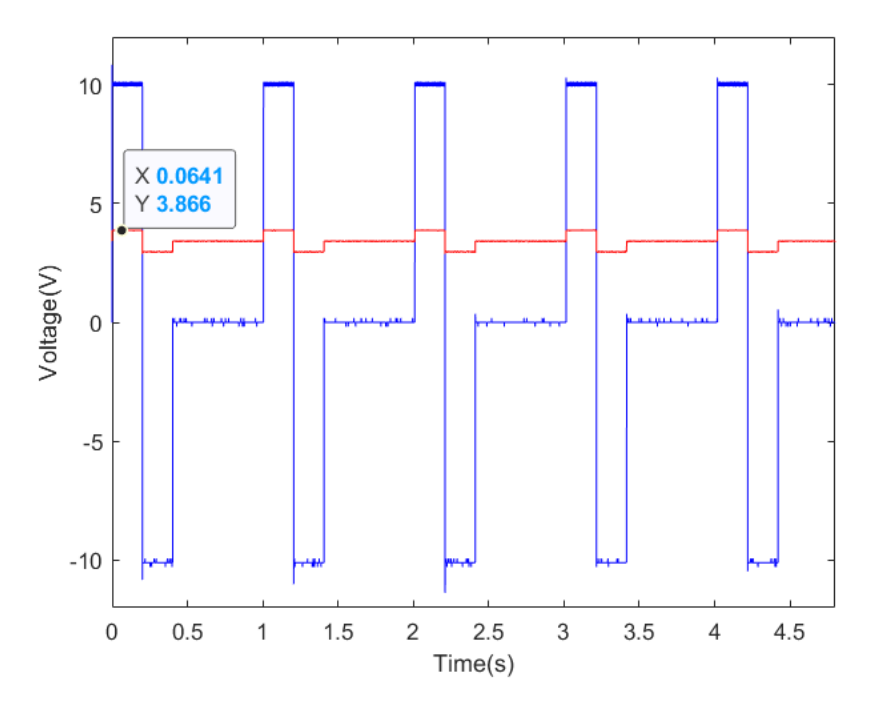


Figure 4.14: The blue line represents the applied voltage in the blue node while the red line represents the measured voltage by the microcontroller(VA6).

Implementing voltage divider for the yellow node (Figure 4.12).

$$Vyellow = Vblue \times (\frac{500}{1500}) \tag{4.9}$$

$$Vyellow = 10 \times (\frac{500}{1500}) = 3.33V \tag{4.10}$$

Implementing again voltage divider for the brown node:

$$Vbrown = Vyellow \times (\frac{1050}{750}) \tag{4.11}$$

$$Vbrown = 3.33 \times (\frac{1050}{750}) = 4.61V \tag{4.12}$$

Vbrown = 4.61V and thus

$$VA6 = 0.104 \times 4.61 + 3.35 = 3.83V \tag{4.13}$$

This calculated value is exactly the same with the measured value using the oscilloscope. Thus, the precision of designed circuit is verified.

4.6.2 Current Controlled Mode

For the testing of the voltage measurement circuit in current source mode the switch of the device was turned to the corresponding mode. A purely resistive load of 1 k Ω was connected to the output of the circuit. The signal was measured at testpoint2(TP2) and in the output of the operational amplifier (A6) (Figure 4.15).

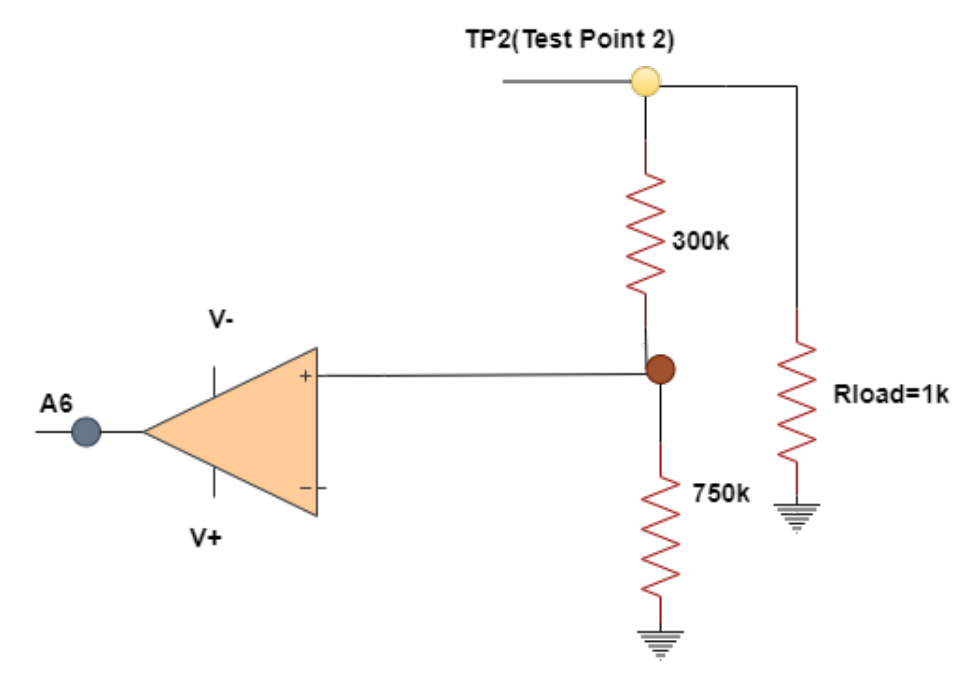


Figure 4.15: The voltage was measured in the yellow node of the circuit and in the brown node (A6)

The next picture illustrates the voltage amplitude as it was measured in the two indicated nodes (Figure 4.16).

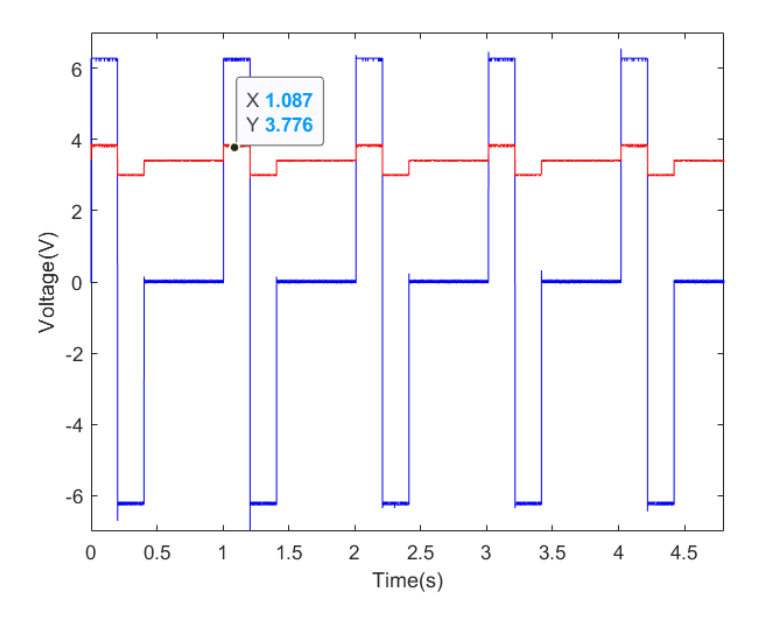


Figure 4.16: The blue line represents the voltage amplitude at the yellow node, while the red line represents the voltage in the grey node(A6)

To demonstrate the precision of the circuit in current-controlled mode, theoretical calculations took place. Since the measured value at TP2 is VTP2=6.16V, the value at the brown node can be calculated by implementing a voltage divider. Thus,

$$Vbrown = \frac{750}{1050} \times 6.16 = 4.41V \tag{4.14}$$

$$VA6 = 0.104 \times 4.41 + 3.39 = 3.84V \tag{4.15}$$

A quick observation in the graph reveals that the voltage output is 3.77V. That means that there is a very small error between the real and estimated value. The error can be calculated according to the formula:

$$error = \frac{measured - estimated}{estimated}\%$$
 (4.16)

$$error = \frac{3.84 - 3.77}{3.8} = 1.8\% \tag{4.17}$$

The same testing procedure for a different value of load in particular 500 Ω was implemented, and now a different value of voltage (3.301V)was applied in the TP2 node. The output graphs are presented in the following figure (Figure 4.17, 4.18).

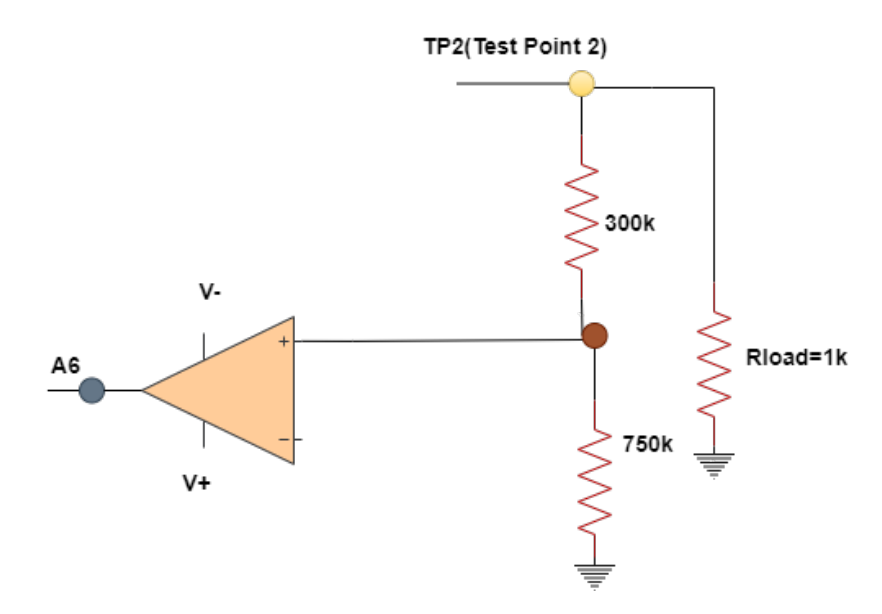


Figure 4.17: TP2: Applied Voltage A6: Measured Voltage

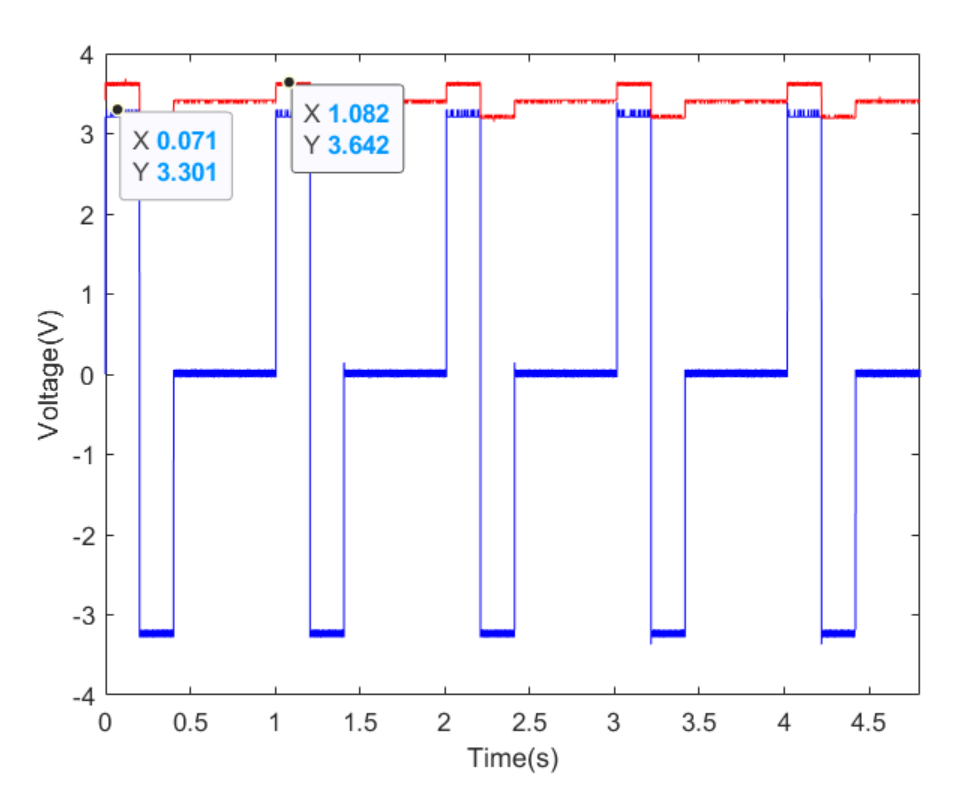


Figure 4.18: Voltage measurement graph: The blue line represents the voltage amplitude as it was measured at the yellow node (TP2), while the red line represents the voltage in the grey node A6 (the pin of microcontroller that measured the voltage)

Since the measured value at TP2 is VTP2=3.301V, the value at the brown node can be calculated by implementing voltage divider. Thus,

$$Vbrown = \frac{750}{1050} \times 3.301 = 2.35V \tag{4.18}$$

$$VA6 = 0.104 \times 2.35 + 3.39 = 3.63V \tag{4.19}$$

According to the graph illustration the measured voltage was 3.641V, a value that is very close to the estimated voltage 3.63V. The design circuit for voltage measurement justifies the requirements.

4.7 Testing of Howland Converter Circuit

The Howland Converter circuit was tested by using different values of pure resistor loads (220 Ω , 500 Omega, 1 k Ω) and investigating the output of the Howland converter and the output of the current measurement circuit which reveals the current passes through the load. If the value of the current remains stable independently of the load change during the time, the Howland converter performs accurately. The signal in the output of the operational amplifier of the Howland converter circuit was also checked through the oscilloscope (Figure 4.19). The next table shows the the different values of loads that were used, the voltage amplitude in the output of the Howland converter and the voltage amplitude in the output of the microcontroller which measures the current. Obviously, the current remains stable while the load in the output of the circuit changes.

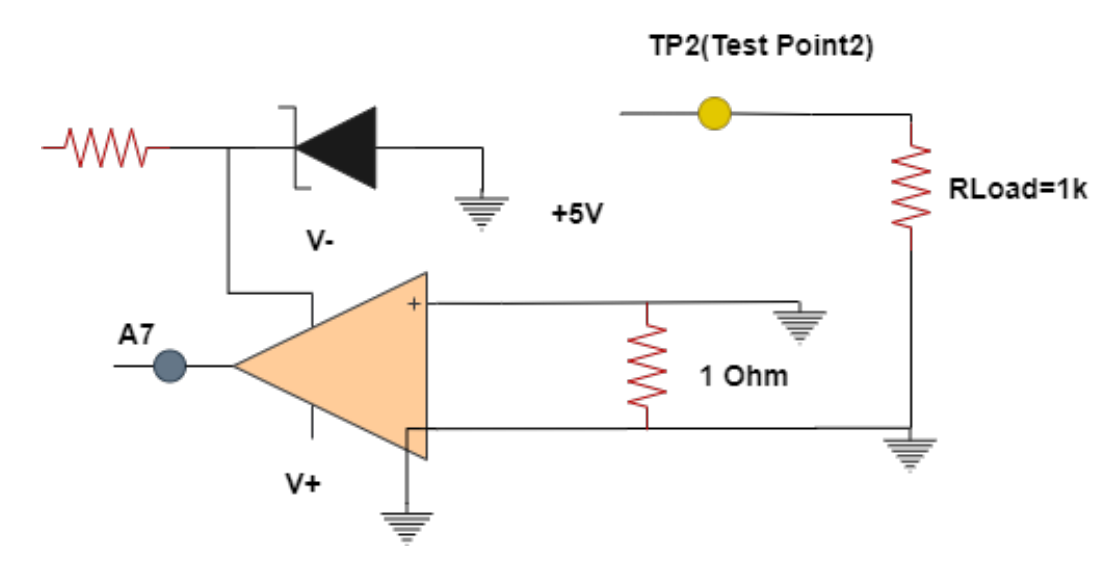


Figure 4.19: Illustration of the circuit and the test points where the oscilloscope measures the signal.

In the first Figure 4.20, the voltages applied in the three different values of loads are illustrated. In the second one, the reader can see the voltage that measures the A7 output of the microcontroller. It is obvious that for different values of load (220 Ω , 500 Ω and 1 k Ω), this value and consequently the current through the load remains stable (Table 4.1).

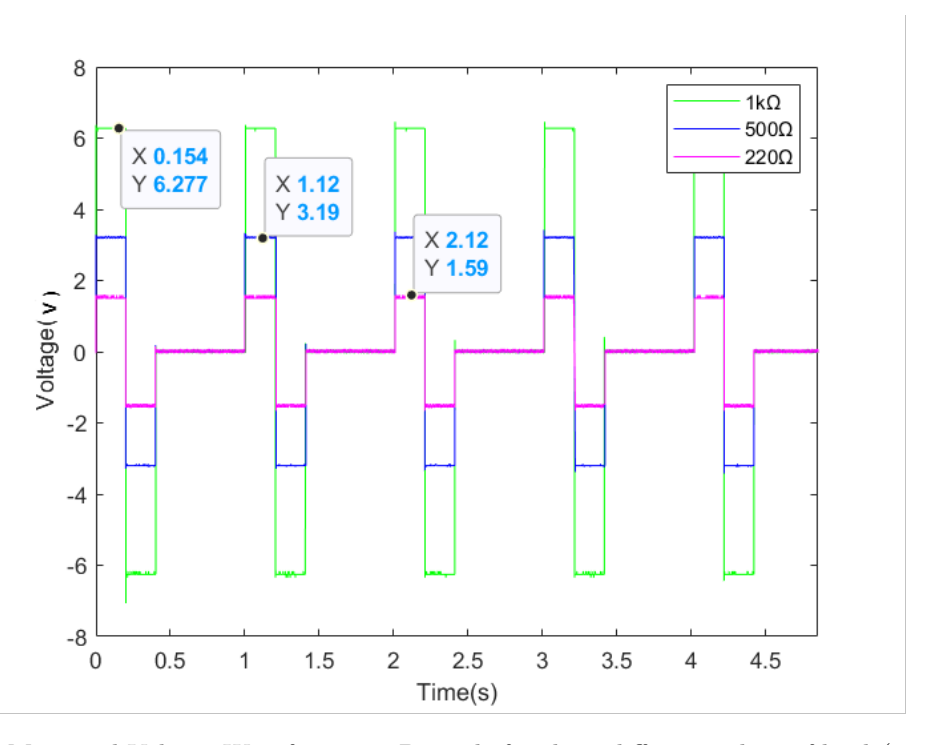


Figure 4.20: Measured Voltage Waveform at TP2 node for three different values of loads (220 $\Omega,\,500$ Ω and 1 kΩ).

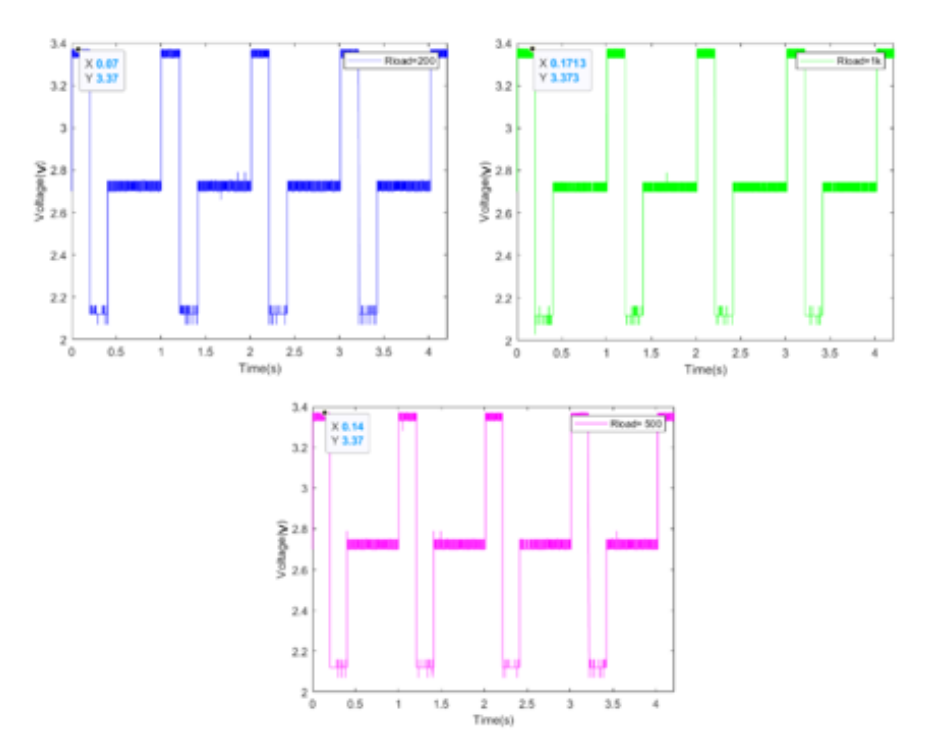


Figure 4.21: Stability of the output current, independent of the load changing, verifying the accuracy of Howland converter.

Table 4.1: Tested load values and Values of the output current after the voltage-to-current converter

Load	VTP2	A7
$ 220\Omega 500\Omega 1k\Omega $	6.277V 3.193V 1.49V	3.373V 3.373V 3.373V

4.8 Conclusion

The results from the measurements of the designed electrical stimulation circuit reveal that all the system requirements are fulfilled successfully. The measurement circuits (Voltage and Current) operate with high precision, improving the efficiency of electrical stimulation by providing accurate feedback to the user. The voltage-to-current converter operates with high precision thanks to the good balancing of resistor's tolerance and to the characteristics of the operational amplifier.



5.1 Introduction

This chapter, consists of a detailed description of the process that was implemented to fabricate TiN integrated electrodes in an EHT platform. The EHT platform which was designed by M.Dostanic, was fabricated again using micro-machining techniques at the EKL cleanroom and was further advanced by integrating the TiN electrodes which provide electrical stimulation to cardiomyocytes for their proper maturation. The polymer that was used for the fabrication of the platform was PDMS. The first part of the following section explains the reasons for the selection of PDMS as a polymer and TiN as electrode material. Afterwards, the applied method for the fabrication of the platform is described step by step. At the end of this chapter, the procedure of the electrode's integration is provided.

5.2 PDMS on Silicon

Polydimethylsiloxane (PDMS) is a well-known polymeric organosilicon compound used in various biomedical applications and also for the development of microfluidic devices due to its worth mentioning characteristics[86]. Among them, the elastomeric properties, the fact that it facilitates the molding in tiny structures and the low manufacturing cost, are the most important[86]. Furthermore, PDMS is a transparent material that allows the control of cells cultured in PDMS structures. The monitor of these cells is feasible with the use of standard optical microscopes[40]. Apart from the advantages that PDMS presents, it also has some limitations. These limitations are connected with the lithographical processes and the deposition of PDMS on other materials or the deposition of other materials (metals) on PDMS. PDMS unfortunalty presents swelling and a high thermal coefficient of expansion, therefore soft-lithographic techniques are considered a better solution for further processing[40][9].

5.3 TiN as a material for electrodes fabrication

The integrated electrodes and the electrical interconnects of the EHT platform are made of titanium nitride (TiN). TiN is a capacitive material, meaning that it follows the capacitive mechanism of charge transfer when charge injection takes place (chapter 1)[87]. This capacitive material has been used in the past in several biomedical applications with electrodes [87]: The advantages of this material stem from

several factors. Among them is that when TiN is sputtered, it has a porous geometry, something that establishes a low impedance in the electrode-electrolyte model. In addition to that, the patterning of TiN is not a complicated process due to the fact that it occurs using standard lithographic processing and dry etching. Previous studies have shown that TiN presents good bio-compatibility with cells and also good mechanical and chemical properties establishing it a stable material [88][87][89].

5.4 Microfabrication of the EHT platform

5.4.1 Introduction

The EHT platform was developed by scaling down the Heart-Dyno system invented by the group of J. Hudson. The main reason for scaling down this system is to conduct experiments and measurements in various sizes of cardiac tissues and also to observe the contractile force of the tissue when the size of the cardiac tissue changes. The EHT platform was fabricated using micro-fabrication techniques in the cleanroom and it consists of two pillars around which the cardiac tissue is formed. The EHT platform was fabricated according to a developed flowchart as a starting point and then it was further developed by integrating TiN electrodes. The microfabrication of the designed EHT platforms took place in the EKL cleanroom at TU Delft, in the department of Microelectronics.

5.4.2 Manufacturing process of EHT platform

The miniaturized EHT platform was fabricated on a wafer using silicon-based micromachining and polymer molding. As it was analyzed in the introduction part, the EHT platform is an anisometrically downscaled version of HeartDyno. More specifically, the process started with 1mm thick double-side polished Si wafers. The main concept of the process is to develop mold in Si wafers and fabricate three different dimensions of anisometrically scaled pillars. For the fabrication of the mold, Si wafers will be etched, by using a hard mask made of the SiO2 layer.

Before the detail description of the fabrication process the full flowchart diagram is illustrated to provide an optical sense of the process (Figure 5.1).

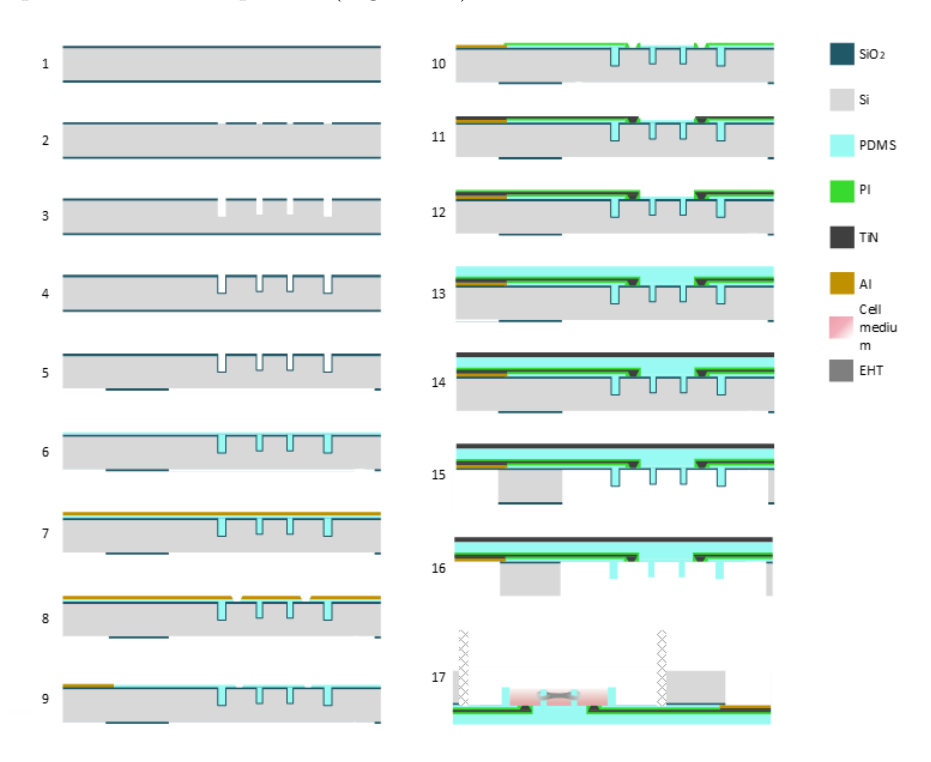


Figure 5.1: Sketch of the flowchart for TiN electrodes integration in EHT platform

The fabrication process started with the creation of alignment marks. This step is not illustrated in the flowchart. This is the first and most important step because multiple masks were going to be used for the entire procedure and all of them must be aligned with the zero layer to ensure the placement of the structures in the proper position. The wafers were coated with SPR3012 positive photoresist at the coater station EVG120. The standard recipe "Co-3012-zero layer" was used which consists of the following steps: First, the wafers are treated with HMDS vapor, with nitrogen as a carrier gas. Next, they are spin-coated with positive photoresist (Shipley SPR3012) dispensed by a pump and they are soft baked for 90 sec at 95 °C. The sub-process finishes with an automatic edge bead removal with a solvent in order to clean the edges of the substrate from the accumulation of coating material that can cause contamination in the next steps of the process.

The exposure process of alignment marks includes two steps the alignment and the exposure. It is important each layer of the wafer to be aligned properly and within specifications to the previous and next layers otherwise the wafer and the desired structures will be destroyed. The wafer was aligned to the mask along with the x and y coordinates. The ASML PAS5500/80 automatic wafer stepper was used for this procedure and the name of the exposed masks for the zero layer was COMURK. During the exposure process, the positive resist layer was exposed in ultraviolet (UV) light with an exposure energy of 125mJ, causing a chemical reaction between the positive resist and the light.

Using the developer station EVG120 the wafers were developed according to the following steps. A post-exposure bake took place at 115 °C for 90 seconds. In the development process, parts of the photoresist were dissolved by Shipley MF322. Due to the fact that we used positive photoresist, the exposed resist was dissolved while the unexposed resist was still on the wafer. After the developing stage, a hard bake at 100 °C for 90 seconds took place. The wafers were optical inspected under the microscope to check the line width of the alignment marks and if there was still photoresist in the exposed areas, something that is not allowed after exposure.

Plasma etching was implemented as a method to etch 120nm deep alignment markers into the Si (zero layer). For this process, the Trikon Omega 201 plasma etcher was used and the sequence URK NPD. The total etched time was defined at 50sec.

After the alignment marks were etched into the Si, the photoresist must be stripped from the surface by oxidizing it in an oxygen plasma using the Tepla Plasma 300 system. The wafers were then cleaned properly before the continuation of the processing. In particular, the wafers were cleaned in HNO3, 99% and 69.5%. Rinse and dry of wafers took place in Quick Dump Rinser with the standard program until the resistivity is $5M\Omega$.

Since there were structures in the backside of the wafer, alignment marks were also placed in the backside following exactly the same procedure which was described in detail previously.

The fabrication process continued with the definition of a SiO2 hard mask for the pillars. Thus, first, an oxide layer was grown using Thermal oxidation (Figure 5.2, step 1). It is known that when a Si wafer is exposed to oxygen the surface of the silicon wafer starts to oxidize in order to create silicon dioxide. The silicon dioxide which is created is a good insulator and can be also used as a barrier material in the impurity deposition. Wet oxidation was applied as a type of thermal oxidation. By using wet oxidation, less time to reach the highest temperature was needed. The exact time of thermal oxidation was calculated accordingly to the desired thickness of the oxide layer (2.7um), the temperature (1100°C), and the type of wafer. Thus, the wafers were placed in the furnace for 14 in total hours.

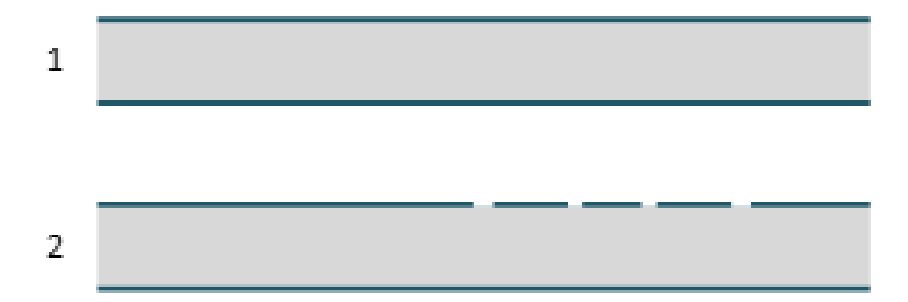


Figure 5.2: Silicon oxide deposition (step 1) and patterning oxide in the front side (step 2)

When this step was completed the oxide thickness was measured in order to verify that the desired oxide thickness was achieved. Using the Leintz MPV-SP ellipsometry system the oxide thickness was measured 2.69um in the back and front sides of the wafer.

As a next step, a hard mask for Si Deep Reactive Ion Etching (DRIE) was created. Therefore, before the exposure of wafers on the pillars mask, 3.3um SiO2 layer was deposited in the front side of the wafer. The principal aim of this step is to create a hard mask for Si DRIE that is going to take place in the next steps of the process. In this process, the deposition of oxide happened by inserting reactant gasses between two electrodes which were in parallel, a ground electrode and an RF energized electrode (Figure 5.3)[90]. This way a capacitive coupling was created, something that causes the chemical reaction. The total amount of oxide on the front side of the wafer where the mask will be exposed was 6um. Novellus Concept One PECVD reactor and undoped oxides (recipe xxxsiostd) was utilized for this procedure. The process conditions were defined according to the selected recipe. The specification of the time parameter was essential for this procedure in order to get the desired thickness (3.3um). Thus, the time was defined at 42sec/station.

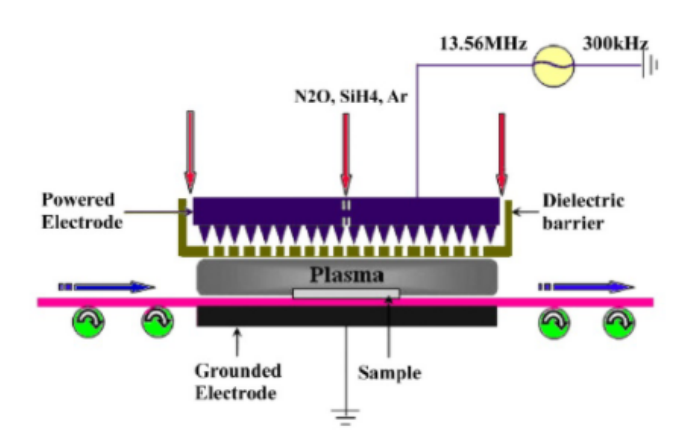


Figure 5.3: Schematic of PECVD reactor [90].

Later, an already designed foil mask was used for Contact Aligner exposure, to transfer the pattern with the pillars on the wafer during lithography. First, the wafers were coated with a 3um positive photoresist following the corresponding recipe (flowchart) on the front side. The "3ulpillars" mask was used with hard contact for 20sec to transfer the pillars pattern on the front side of the wafer. After finishing the development step, an inspection with the microscope is considered essential, in order to ensure that there are no residues of photoresist above the structures of pillars but also to verify that the patterning of structures was good.

Moving on to the fabrication process, the plasma etching of oxide was performed by using Drytek Triode 384T plasma etcher. The purpose was to pattern SiO2 which was deposited with thermal oxidation first and then with the PECVD process. The STDOXIDE recipe was used to etch the oxide layer with a soft landing on the layer underneath while the total etching time was defined at 7.5 min. The remaining photoresist was then removed in an oxygen plasma.

Deep Reactive Ion Etching (DRIE) is a highly anisotropic dry etching process, aiming to create a deeper penetration than in Reactive Ion Etching, developing etching cavities with high aspect ratios [91]. The most widely known technology called the Bosh process, consists of repeated steps until the desired shape of the cavity is achieved. The first step is the plasma etching process, using Sulfur Hexafluoride (SF6), which attacks the substrate from a nearly vertical direction; The second step includes the deposition of a passivation layer, using Octafluorocyclobutane (C4F8). This creates a substance similar to Teflon on the surface of the substrate. It is important to highlight that the duration of each step is for several seconds[92]. The principal function of the passivation layer is to protect the substrate from chemical etching. Despite the functionality of the passivation layer, during the etching phase, the ions that bombard the substrate, bombard also the passivation layer at the bottom of the surface. The passivation layer is sputtered off by the etching. This way, the substrate is exposed to chemical etching[92][91].

The etching of the holes (pillars) in Si wafers using Deep Reactive Ion Etching (DRIE) took place (Figure 5.4). Rapier Omega i2L DRIE etcher was used for this process. This process is typically used for etching deep holes in Si wafers with high aspect ratios and it consists of three steps: deposition of the passivation layer, breakthrough etching, and final etching of the Si wafer. The Deep Reactive Ion Etching of silicon is applied in order to etch 660um of silicon establishing the DRIE of pillars. The number of cycles for etching is inserted as a parameter to the system and it depends on the depth $(660 \, \text{um})$ and the dimensions of the holes. The following Figure 5.4 shows the profile measurement for $633 \, \mu \text{m}$ etched structure. The image was captured with Keyence microscope.

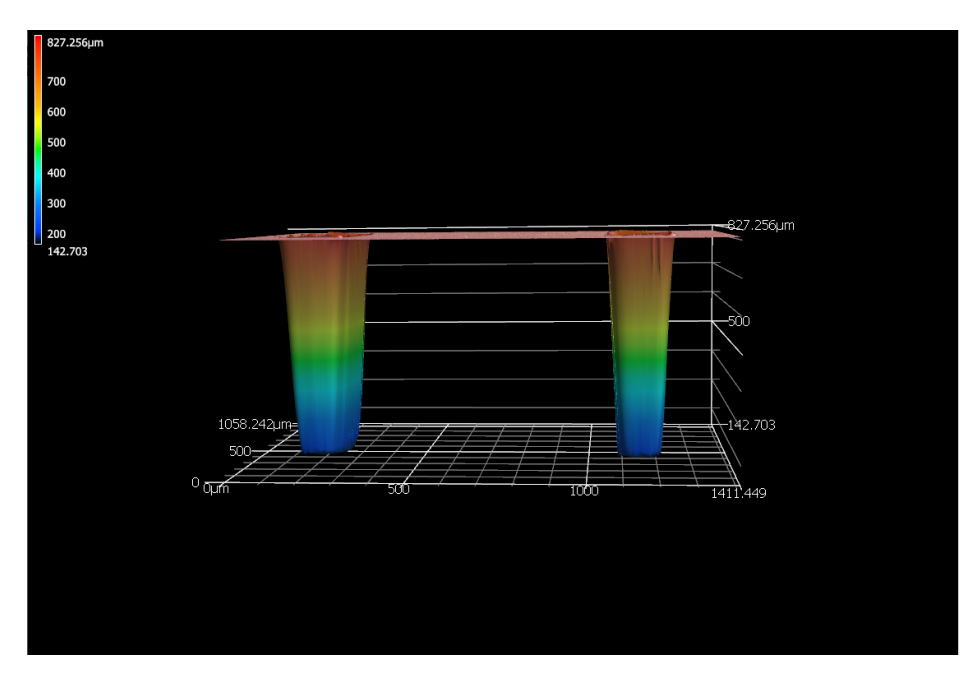


Figure 5.4: 3D illustration of pillar's depth after observing under the microscope.

The etching process was established in many steps. In the following Figure 5.5 the achieved depth at the end of procedure is presented.

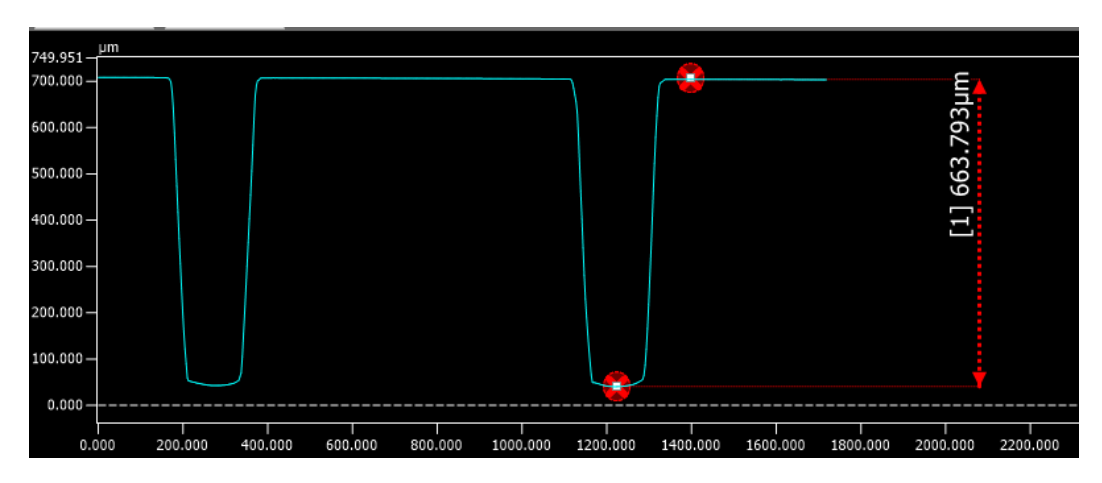


Figure 5.5: Profile of etched structures in Si wafers. The total depth of pillars after etching was measured at 663um.

As it is visually analyzed in the next Figure 5.6, the next step included the growth of SiO2 in the backside of the wafer as a stopping layer. For this reason, 3um of thermal oxide was performed to create a thin layer of oxide. The desired oxide thickness in the backside was at around 8.5um. Thus, the PECVD process was conducted in order to deposit approximately 5um more oxide layer in the backside of the wafer. Similarly to the previous sub-process, the Novellus Concept One PECVD reactor was used and the selected recipe is undoped oxides (recipe xxxsiostd). The only parameter that was necessary to be changed in this recipe was the time. The time depends on the desired level of thickness and it was calculated at around 60sec/station.



Figure 5.6: Growth Si oxide as a stopping layer.

Having created the proper oxide layer as a stopping layer for wet etching later, the process then includes the transfer of pattern in backside using lithographic processes. Specifically, the backside of the wafer was firstly coated with 3um positive photoresist because we had a thicker layer of oxide dispensed by a pump. Then, the "backside" mask was exposed for 25sec to the wafer using the Mask Alignment system. The wafers were developed in the backside structures at the developer station of the EVG120 system.

The following step includes the etching of oxide from the backside of the wafer (Figure 5.7). Wet etching was implemented in this step. The wet etching process consists of various chemical and physical processes. Figure 5.8 demonstrates the mechanism of wet etching. During the first step, the etchant species are transferred to the wafer's surface. At this point, diffusion of the etchant towards the surface and penetration of the etchant in active sites on the surface takes place. During the second step, a chemical reaction between the etchant and the exposed surface occurs. After this step, soluble by-products are generated. Finally, the products of the reaction are diffused.



Figure 5.7: Wet etching of oxide from the backside of the wafer.

Wet etching uses liquid-phase etchants in order to remove materials from the wafer[93]. Most wet etchants consist of an oxidizing agent, an agent for dissolving the oxides, and a solvent, such as water. The oxidized layer is for instance NH4OH, NaOH,H2SO4, HF and the agents whose main use is to dissolve the oxides are acid or base. In our case the oxidized layer was buffered HF (BHF)[93].

When the wet etching procedure completed, full cleaning of wafers took place. In particular, the wafers were placed for 10 minutes in fuming nitric acid HNO3 99%. This acid dissolves organic materials. The wafers were rinsed in the Quick Dump Rinser with the standard program until the resistivity is 5 Mohm. They were placed then for 10minutes in concentrated nitric acid at 110°C in order to dissolve the metal particles. Again rinse was performed as it was described previously and they were dried using rinser-drier with the standard program.

During the wet etching of the backside of the wafer, the front side of the wafer with the pillar profiles must be protected from wet etching. For this reason, a layer of PDMS was deposited on the front side of the wafer as a protection layer. After the wet etching procedure, of course the layer of PDMS must be removed. Therefore, we firstly coated the wafers with CH4 (Teflon), to be able later to remove the PDMS. Then, we prepared the PDMS in the polymer lab according to the following recipe:For the PDMS mixture, elastomer PDMS Sylgard 184 and its curing agent were mixed. Particularly, for three wafers 10 g of the PDMS elastomer in the disposable cup and 1 g of curing agent by using a pipette. The ratio between the elastomer and curing agent must be kept at 10:1. A relatively thick layer of PDMS was poured on the wafers in order to cover 2/3 parts of the wafer and it spin-coated in the Polos Manual Spinner 1. Then the wafer was placed carefully inside the vacuum chamber for 20 minutes until all the bubbles from the surface disappear. The valve was slowly opened to increase

the pressure in the chamber until the atmospheric and remove easily the wafers. The PDMS then was cured for 60min at 90°C in an Memmert Oven with the dedicated carrier (PDMS).

A test wafer was used at the beginning for determining the total time of wet etching. The initial thickness of the oxide layer was approximately 8.5um. After completing the wet etching process the thickness of the holes (etched points) must be exactly zero.

5.4.3 Filling the Pillars with PDMS

In order to create the pillars from PDMS material, as a next step, the holes of the pillars were filled with PDMS (Figure 5.8). The PDMS was prepared at the polymer lab of the EKL cleanroom. For the PDMS mixture, elastomer PDMS Sylgard 184 and its curing agent were mixed. Particularly, 5 g of the PDMS elastomer in the disposable cup and 0.5 g of curing agent by using a pipette. Depending on the number of wafers to be processed these amounts could vary. However, the ratio between the elastomer and curing agent must be kept at 10:1. For the first layer, a thick layer of PDMS was poured on the wafer and then it was slowly spin-coated to ensure that the PDMS was enough to cover the holes. The wafer was placed very carefully inside of the vacuum chamber. The pump was turned on and the process duration was around 20minutes until all the bubbles disappear. Using a sharp object but very carefully not to damage the wafer, the extra PDMS was uniformly removed from the wafer. After the removal of extra PDMS from the wafer, it was cured for 60minutes in the Memmert Oven at 90°C.



Figure 5.8: Filling the pillars structures with PDMS.

5.4.4 Etching PDMS

Due to delays caused by COVID and tool downtimes (*Omega*) the etching of PDMS and the integration of electrodes in the structure were not completed. The steps for the completion of the process is described in the following section. However, in separate test wafer the TiN electrode structures were successfully fabricated. The steps for this sub-process are also described in detail. The next paragraph and until the end the rest of the fabrication process is described.

After filling the holes of the microstructures with PDMS, the next step is to deposit and pattern Al on the PDMS (Figure 5.9). To pattern the PDMS, an aluminum (Al) layer is coated with sputtering onto the PDMS at room temperature.

Sputter deposition is a physical vapor deposition (PVD) method in which a thin film of metal are deposited by sputtering. In particular, the material is ejected from a target into a substrate in this case into the silicon wafer.

More specifically, 1000nm Al is deposited on PDMS. Before that LUR test carried out in order to ensure that the wafer would not be degassing enough, something that can lead to sputtering failure. The wafers are first coated with 1.4um positive photoresist(noEBR, noSB, noHMDS). A soft baking of the wafer is occurred at 95°C for 90sec.



Figure 5.9: Deposition of Al layer on the PDMS.

Openings for TiN electrodes must be created, and for this reason the alignment and exposure of hard mask for TiN openings are performed using the EVG420 contact alignment system. First, the wafers are coated with photoresist. Thus, 1.4um positive photoresist is dispensed by a syringe and spin-coating. The wafers are soft-baked for 1min and 30sec at °C. The wafers are exposed for 8sec and then they are developed using the recipe "devSP, noHB, noPED". A post exposure baking took place for 1min and 30sec. Visual inspection of wafers takes place to ensure that the process of TiN openings for contact pads is successful. PDMS is going to be etched by implementing plasma etching at TiN openings (Figure 5.10). The next picture demonstrates the aforementioned steps.

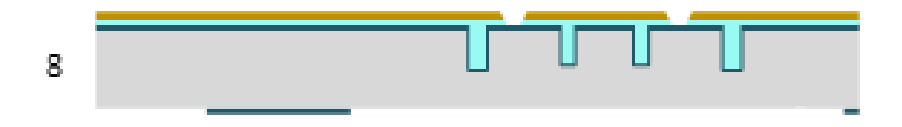


Figure 5.10: TiN openings for electrodes and PDMS etching at TiN openings.

5.4.5 Al etching for Contact Pads

Moving on to the procedure, the layer of Al which was sputtered previously must be now etched in order to create the desired contact pads for the electrodes. Therefore, 1.4um of positive photoresist dispensed by syringe is spin-coated to the wafers. Soft baking at 90 degrees for 1 min and 30 seconds is performed and then the wafer is exposed for 8sec in the mask "Al contact pads". This way the pattern is transferred to the wafer. The developer made the pattern to appear and post-exposure baking at 90 degrees for 1 min and 30 seconds happens. At the end of this sub-process Al was etched by implementing wet etching in the PES solution for 34minutes. The photoresist must be removed in an oxygen plasma. Tepla Plasma 300 system is used for this procedure (Figure 5.11).

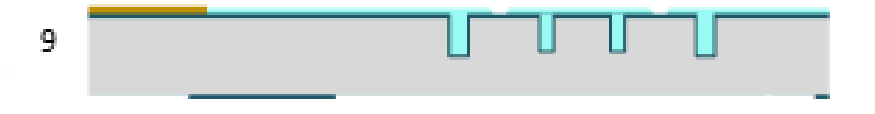


Figure 5.11: Al etching for contact pads creation.

5.4.6 First Layer of Polyimide

Subsequently, metal lines extending from the contact pads to the electrodes are created. These metal lines consist of a 200nm thick layer of sputtered TiN, encapsulated between two layers of

polyimide (Figure 5.12). The preparation of polyimide was performed in the polymer lab at EKL. The TiN interconnects are encapsulated with polyimide in order to be insulated. PI is often used in microelectronics and medical devices due to the fact that presents good thermal resistance [94], chemical resistance [95], good mechanical properties [96], and low dielectric constant [97]. Particularly, PI has been used in several medical devices as an insulation layer such as in neural implants [98] and catheters [99] It is known that different processes of PI layers deposition exist. Among them, the most well known are the vapor deposition polymerization [100], the lamination (with Kapton- type PI) [101] or spin-coating [98]. In this microfabrication process the FUJIFILM 9F305PI was deposited with spin-coating since thin film of PI was desired. The next sketch presents the layer of polyimide (PI).

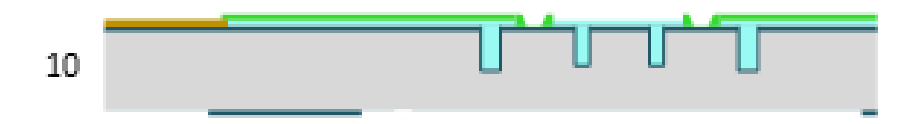


Figure 5.12: First layer of polyimide (PI).

At this point it is important to highlight that before spin coating the first layer of polyimide, a good adhesion between PDMS and polyimide must be created. Thus, in order to activate PDMS and improve its adhesion properties O2 plasma treatment on low pressure, for 40sec and 75W energy is performed. Oxygen plasma treatment has been widely implemented by many research teams in the fabrication of PDMS devices for various purposes. The oxygen plasma treatment on PDMS creates polar functional groups for instance the silanol group (SiOH)[102]. This group has the ability to change properties on the surface of PDMS. In particular, convert the hydrophobic properties to hydrophilic properties [102]. The preparation for polyimide is described in detail in the flowchart at the end of the thesis. Firstly, 900nm polyimide is spin-coated manually using the program 30:60sec at 6000RPM, and before the baking step the wafer is inspected. The back side of the wafer is cleaned with acetone while the edges with Q-tip with HTRD2 developer. Using a hot plate of manual coater system the wafer is soft-baked at 85°C for 120sec. In the next step the wafer is exposed to the mask 'First PI' (see Appendix for Masks) for 10 sec to transfer the electrode patterns. A post-exposure baking process was carried out by placing the wafer to a Memmert oven for 120s at 90 degrees. The developing stage is conducted manually. Two special glasses for polyimide are used to one of them developer is poured and to the other stopper (RER 600). We place for 1min and 30sec the wafer to the developer and afterward for more 1min and 30sec to the glass with the stopper which is dilute solution of acetic acid or citric acid, that halts the action of the developer. The sub-process is finishing with baking the wafer at 100°C for 1min and 30sec. Finally, the polyimide is cured in a vacuum and under N2 flow for 2hours and 30min.

After the first layer of polyimide and due to the fact that TiN will be encapsulated between two layers of polyimide, TiN metal is sputtered by using Trikon Sigma (Figure 5.13). Again like the previous process of Al deposition, before the TiN deposition, the LUR test must be conducted to ensure that the metal deposition will be successful. The layer of TiN should be thick because is above the polymer but also not too thick because then a lot of cracks in the surface of the wafer will be observed. For this reason, the first 200nm Ti was deposited and then 50nm of TiN. After coating with positive photoresist the wafers, we exposed them in a hard mask of TiN for 8sec due to the fact that the amount of positive photoresist was 1.4um. The same recipe and techniques of wafers coating with a photoresist that were used before the Al etching are used now for this coating procedure. The developing process (recipe: dev SP, noHB, no HMDS) reveals the pattern of TiN electrodes on the wafer. Afterward, TiN is etched using plasma in Trikon Omega 210 plasma etcher for 18sec. The total time of etching depends on the layer thickness, which was 250nm in our case. Using Oxygen Plasma Tepla the photoresist from the wafer is fully removed.



Figure 5.13: TiN metal sputtering above the first layer of PI.

The process that follows for the deposition of the second layer of polyimide is exactly the same as the first layer of polyimide. Visually, the process is demonstrated in the following figure (Figure 5.14)



Figure 5.14: Deposition of second layer of PI above the TiN metal.

The last steps of this long process include the deposition of a second layer of PDMS (Figure 5.15). Then TiN is sputtered on the wafer, the main goal of which is to protect the PDMS (Figure 5.16). Trikon Omega is used for TiN plasma etching with endpoint detection. Then, anisotropically wet etching is proposed as a technique in order to etch the backside of the membrane and contact pads. In this process the wafers are immersed in an etching TMAH solution. Specific areas of the surface are protected by a mask layer and in the openings of the mask the active solution reacts chemically with the single crystal material. The final step includes the wet etching of silicon oxide in the backside of the wafer in order to release the membrane and reveal the PDMS pillars. The process duration is around 30minutes and it lasts until all the oxide layer is removed. After finishing the microfabrication process the wafer is going to be diced and the platform to be characterized. Although most of the steps were conducted successfully during the thesis, unfortunately, the whole procedure was not completed. Nevertheless, in a separate wafer the electrode structures were fabricated and this procedure was completed aiming to characterize the electrode's properties by implementing Electrochemical Impedance Spectroscopy. The procedure for the electrode's structure fabrication is analyzed in the following sub-section.

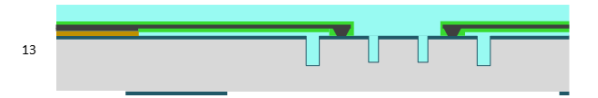


Figure 5.15: The last steps of the microfabrication process including the release of membrane and the reveal of PDMS pillars.

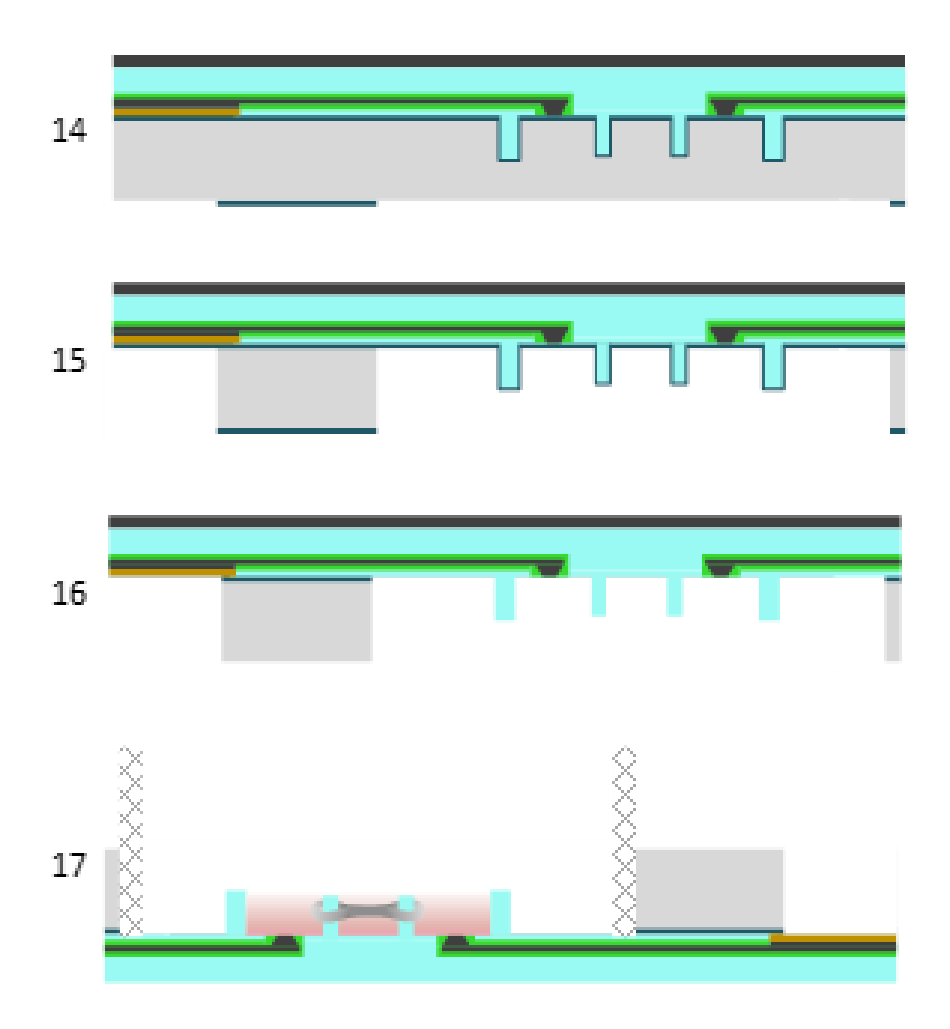


Figure 5.16: The last steps of the microfabrication process including the release of membrane and the reveal of PDMS pillars.

5.5 Fabrication Process for Test Electrode structures

This paragraph explains the process of developing the test electrodes structures in a separate test wafer for electrical characterization purposes, without integrating into the whole EHT platform. For this sub-process, 1mm thick wafers were used. The first step of this sub-process includes the preparation of PDMS which is going to be poured on the wafer creating the first layer. The preparation of PDMS based on the same principles with the microfabrication of the EHT platform.

More specifically, in this step, the preparation of the PDMS is carried out using the elastomer PDMS Sylgard 184 and its curing agent. Depending on the number of wafers to be processed the ratio between the elastomer and curing agent must be kept at 10:1. Thus, in our case for one wafer 5g of Elastomer was mixed with 0.5g of curing agent. For mixing the PDMS elastomer and curing agent the Thinky Speedmixer is used. The total weight of the cup and the holder are determined and the holder of the machine must be adjusted according t this value. A relatively thick layer of PDMS roughly 10um was poured on the wafer and it is slowly spin-coated. Degassing of PDMS performed by placing the wafer in a vacuum chamber, and the duration of the process is around 20 minutes. It is obvious that the process is finished when all the bubbles disappear from the surface of the wafer. Then the wafer was cured in the Memmert Oven at 90°C. Before the creation of the polyimide layer above the PDMS membrane, the PDMS treatment is considered essential due to the fact that it enhances the adhesion of the polyimide layer that is going to be poured on PDMS. Therefore, oxygen plasma treatment of PDMS in low pressure was carried out. Afterward, the wafer was ready for the deposition of polyimide layer. As it was analyzed also in the previous section oxygen plasma treatment is usually performed while introducing oxygen to the plasma chamber. Oxygen is often used to clean surfaces prior to bonding. In this case, because the next layer was the polymer polyimide, oxygen treatment facilitated the adhesion of polyimide to PDMS. The wafer was placed for 0xygen plasma for 40sec at 75W.

The next layer of the wafer consists of polyimide. For this reason, Fujifilm LTC9305 negative polyimide dispensed on a wafer with a manual syringe, was spin-coated above the PDMS in the program 30: 60sec at 6000RPM using Brewer Science manual coater system. The wafer was soft-baked for 120s at 100°C and then it was exposed in hard mask contact with the electrodes shape for 10sec. This time depends on the thickness of the polyimide. After transferring the pattern through lithography the wafer was developed manually. Specifically, two glasses were used for this process. One of them contained the developer and the other the stopper. The wafer was placed for 1min and 30sec to the developer and then for 1min and 30sec to the stopper. The electrodes pattern was revealed. Post- exposure baking takes place for 1min and 30sec at 100°C. The wafer is observed under a microscope and its structure is captured. The following figure shows the electrode structure after this step (Figure 5.17). The layer of polyimide was then cured in a vacuum and under low N2 flow at 150 degrees for 2hours and 30 minutes. As it was tested if we increase the temperature at 200 degrees then the PDMS was cracked.

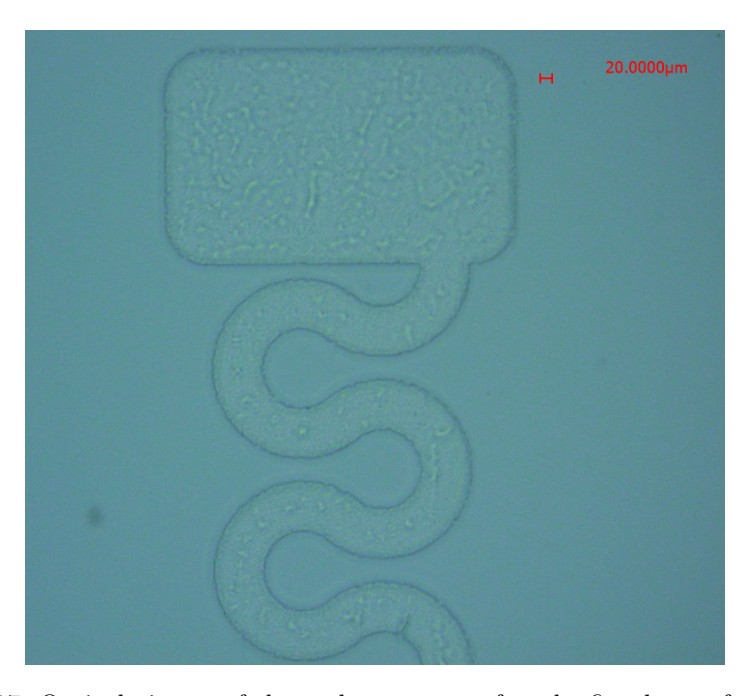


Figure 5.17: Optical picture of electrode structure after the first layer of polyimide.

Before the sputtering of the metal for the electrodes, the LUR test is requested. This happened in order to ensure the efficiency of metal deposition. Due to the fact that there are polymers in the wafer, it is possible these polymers to release gasses during the procedure which influence the environment of deposition. If the leak rate is higher Than 2*10pi6 Torr*L/sec, measured 10 minutes after placing the wafer in the chamber, the wafer can not be characterized compatible with the sputtering procedure.

The thickness of the metal deposition is 250nm. More specifically, because we need a relatively thick layer of metal above the polymer, it is not the best solution to deposit directly TiN. For, this reason firstly a deposition of 200nm Ti is performed because the process is faster and then in total 50nm TiN.

As a next step, the wafer was coated with positive photoresist 1.4um without EBR, and HDMS. It was placed for soft-baking at 90degrees for 1minute and 30seconds. Because of the photoresist (1.4um) the wafer was exposed for 8sec in hard mask contact (TiN electrodes). Post-exposure baking was conducted at 90°C for 1 minute and 30 seconds. Afterward, using Omega 210 plasma etcher the 250nm TiN was etched. For this procedure, the platen temperature is set at 25degrees and according to the thickness of the metal which was 250nm the total time was set at the machine at 20sec. When this procedure finished, the photoresist was totally removed in oxygen plasma after etching by placing the wafer to Tepla Plasma 300 System.

For the deposition of the second layer of polyimide exactly the same procedure as the first layer was followed. After the second layer of polyimide the wafer is optically observed under the microscope and its figure was captured (Figure 5.18, 5.19).

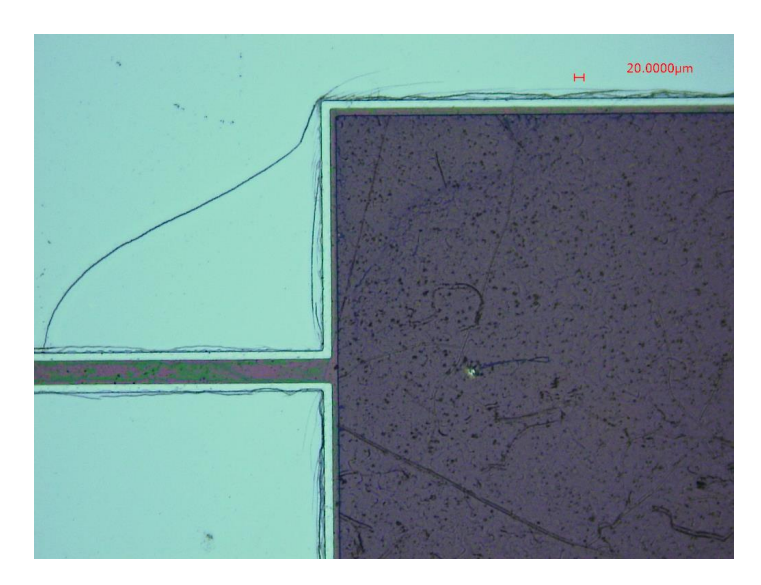


Figure 5.18: Illustration of two TiN contact of Electrode encapsulated between two layers of polyimide above PDMS polymer.

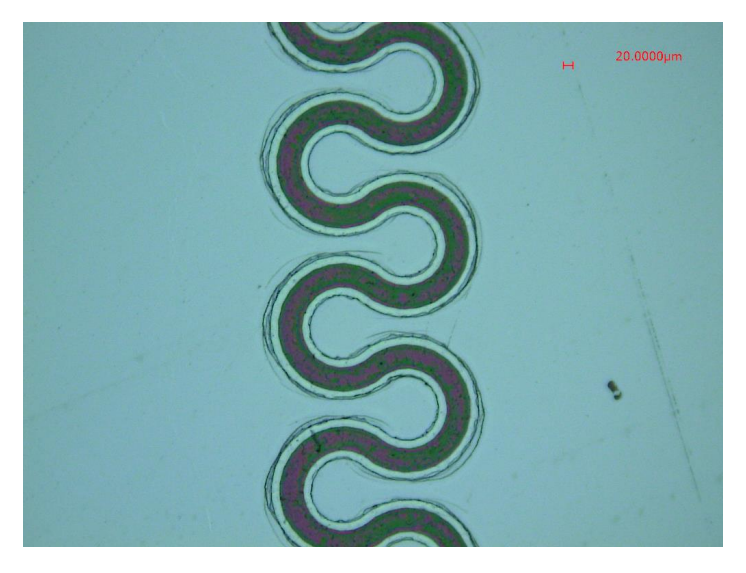


Figure 5.19: Illustration of two TiN contact of Electrode encapsulated between two layers of polyimide above PDMS polymer.

The contact pads of the electrodes were made by Al. Therefore, the Al deposition considered essential for the next step. Using Trikon Sigma Machine firstly LUR test was performed in the same way as previously described and then 100nm of Aluminum was deposited following the same process as it was described in previous section. The wafer was coated with 1.4um positive photoresist dispensed by a syringe. It was spin coated then, using the recipe 1.4um no-EBR, no-SB, no-HMDS. Soft baking at 90degrees for 1minute and 30 seconds follows. Afterwards, the wafer was exposed for 8sec in the mask 'Al contacts' and then post- baking process for the same amount of time and at 90 °C takes place. The wafer was placed in a developer liquid(no HB, no PEB) and at the end was baked again for 1min and 30 sec. The selected method for etching was wet etching of Al. Specifically, the wafer was placed in a PES solution for around 34 minutes until the Al was completely etched. The photoresist was removed by placing the wafer in acetone for 10minutes and for 5 minutes in IPA.

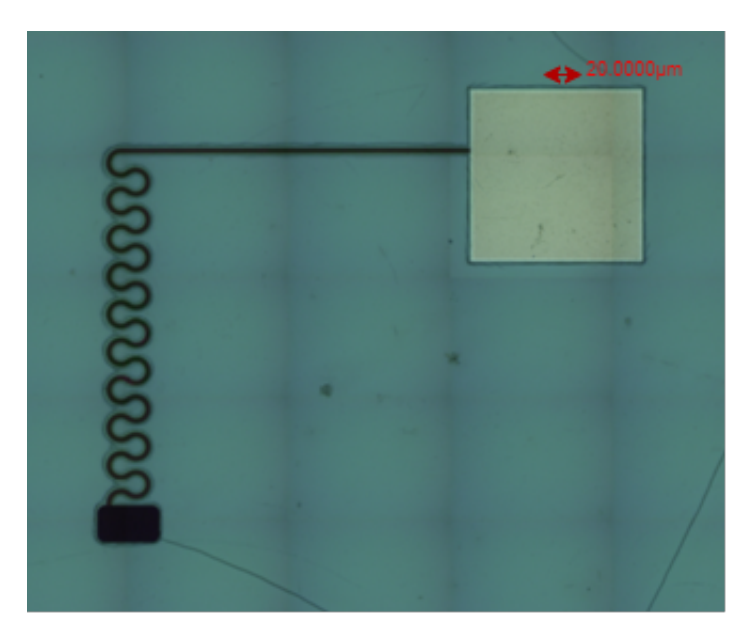


Figure 5.20: Illustration of two TiN contact of Electrode encapsulated between two layers of polyimide above PDMS polymer.

5.5.1 Conclusion

To sum up, the fabrication process of the EHT platform was completed successfully. The first steps for the integration of electrodes on this platform were also performed. However, the entire procedure of integration could not be completed. Instead, the electrodes structures were fabricated successfully. The electrode structures were fabricated using micromachining techniques at the EKL cleanroom. The electrodes were made of TiN, a material that can be characterized biocompatible with the cardiac cells. Furthermore, the TiN electrodes were encapsulated between two layers of polyimide and the whole structure was developed on a PDMS layer. The next steps include the electrical characterization of the TiN integrated electrodes using Electrochemical Impedance Spectroscopy (EIS).



6.1 Design of 16-channel Electrical Stimulator

An electrical stimulator device for electrical stimulation of cardiomyocytes in an EHT platform was designed successfully according to the initial requirements. The proposed circuit is able to work in both modes: voltage-controlled voltage source and voltage-controlled current source. The second one as it was discussed in the previous chapter provides better control of the injected current since the current remains stable and independent of possible tissue changes. The generated rectangular biphasic pulses can reach up to 15V voltage amplitude. Due to the fact that the selected method of biphasic pulse generation was the use of a microcontroller and an operational amplifier, the transition time of the pulse is quick enough and the signal output presents a clear view without possible spikes or noise that the use of an H-Bridge method can cause according to the literature findings (Chapter1).

As far as the design of the measurement circuits is concerned, that provides feedback regarding the applied voltage and current, it operates in a precise way. The current measurement circuit behaves in exactly the same way as in the simulations. On the other hand, the voltage measurement circuit presented a different and not expected behavior than in simulations (LTSpice). This is maybe related to the voltage reference we created for the needs of the circuit by using a zener diode. Although the breakdown region according to the data-sheet was specified at 2.5V in the actual experiments, it measured at 3.03V. Therefore, the gain and the offset of the designed circuit based on an operational amplifier, calculated again according to the new values of resistors, was specified after many experimental trials. After that, the system was tested again and finally was able to give a good voltage measurement. In the voltage-controlled current source mode a small error of up to 10mV. Regarding the voltage-to-current converter (Howland Charge Pump), the actual experiments were in full agreement with the simulations. Thanks to the selection of high precision resistors and attributes of the operational amplifier the voltage circuit can provide stable current in the range of the frequencies that we are interested in (0.5-5Hz). The results from the measurements verify its efficiency. In the current source mode the current amplitude is controlled by controlling the voltage amplitude using the manual potentiometer. Due to the fact that we estimated approximately the load of the cardiac cells but we can't be pretty sure until the actual experiments take place, to protect the cardiac cells from damage a resistor of 500 Ω was placed in series with the cardiac cells.

A user-interface was developed based on the serial monitor of the Arduino microcontroller. There the user can set the parameters of the stimulation (Frequency, duty cycle, the channel of stimulation) and activate the desired channel of stimulation, (one from the 16-EHT platforms).

Until now the monitor of the voltage amplitude is feasible using a manual potentiometer. In the

future this can be improved and replaced by a digital one. This way the precision in the selection of voltage amplitude values will be higher.

Furthermore, a graphical user interface can be developed. Until now the control of the signal parameters is feasible through a user interface based on the serial monitor of the arduino. There the user sets the stimulation parameters and then the current and voltage amplitude can be seen through it. Although, graphical user interface (communication between Matlab and Arduino) to make a nice graphical environment with virtual buttons was tried to be developed the communication between these two software tools was really slow. Therefore, the first method based on the serial monitor was finally used. In the future, for the development of a nice and high-speed graphical user interface a replacement of Arduino nano with another microcontroller such as Rasberry Pi is recommended.

6.2 Integrated Electrodes and read-out interface

In this part of the thesis, electrodes were fabricated using microfabrication techniques in the EKL cleanroom. The EHT platform in which the electrodes are going to be integrated was also developed successfully. The full integration of electrodes in this platform could not be completed. The electrode structures were fabricated in a separate wafer, on a PDMS layer, encapsulated by two layers of polyimide for insulation purposes. The electrical characterization of the TiN electrodes was not completed. Since the integrated electrodes will be in contact with the cardiac tissue, the recommended way to accurately characterize the electrodes and specify their behavior is the Electrochemical Impedance Spectroscopy(EIS). EIS is implemented by applying a sinusoidal electrical voltage across electrodes connected to a solution at a wide range of frequencies. Then the impedance of the electrodes is calculated for each frequency value. In our case, since the electrodes are integrated into a read-out interface and the cell culture will be above the electrodes, a glass is going to be glued on the top of the electrode chips. One of the two integrated electrodes will be the reference electrode and the other will be the working electrode on which the AC signal will be applied in a wide range of frequencies. This way the electrode's impedance will be calculated in high frequencies but also in very low frequencies 1-5Hz which is the frequency area we are interested in.

For the developed electrode chips, a read-out interface was also designed . The read-out interface can host up to 16-chips being in full agreement with the designed 16-channel electrical stimulator. The read-out interface designed in a way that can fit to the bottom of a 96-well plate that biologists use in their experiments. For this reason 6mm diameter holed were created in the PCB for transparency reasons, to facilitate the optical observation of cardiac cells culture through the microscope.



7.1 Conclusion

This thesis presented the entire design, fabrication, and characterization of an electrical stimulation set up(electrical stimulator and Integrated Electrodes) for an EHT platform. Regarding the design and fabrication of the electrical stimulator, all the system requirements were fulfilled. The fully-controlled electrical stimulator is able to provide perfect rectangular biphasic pulses up to 15V, to loads up to 2 kOhm. Since the pulses were produced by using an operational amplifier architecture, no spikes were observed after measuring the signal with an oscilloscope, verifying the quality of the selected method. The voltage amplitude, the frequency, and the duty cycle of the pulse can be adjusted allowing the user to have full control of the electrical stimulation of cardiomyocytes in the EHT platform. A user interface was developed through programming, giving the ability to the user to select the desired channel of stimulation and to set the corresponding pulse parameters. The frequency can be adjusted in a range of 0.5-5Hz by step of 0.1Hz, and the duty cycle can be set accordingly. The two modes of the system: voltage-controlled and current-controlled stimulation giving the flexibility to switch between them and select the best method of electrical stimulation of cardiomyocytes. A Howland Converter Hardware architecture was used for converting voltage source stimulation to current source. The efficiency of the selected method was tested, proving its accuracy. In particular, the functionality of the converter tested for different values of resistors and in all cases, the biphasic rectangular pulse remained stable and independent of the load changes. Current Measurement and Voltage Measurement circuits were integrated into the electrical stimulator facilitating the user to be aware of the imposed voltage and current on the cardiac cells. Last but not least, the electrical stimulator was programmed to detect possible over-current applied to the cells (more than 12mA) and freeze the stimulation until the user lower the value of the applied voltage by rotating the potentiometer.

As far as the fabrication of the TiN electrodes is concerned, the electrodes were developed using microfabrication techniques in the cleanroom. The EHT platform in which the electrodes are going to be integrated was also developed successfully. The full integration of electrodes in this platform could not be completed. The electrode's structures were fabricated in a seperate wafer, on a PDMS layer, encapsulated by two layers of polyimide for insulation purposes. A read out interface (PCB) for 16-electrode chips was designed in KiCad software tool, in a way to fit in the bottom of a 96-well plate which is used by biologists for the actual experiments with the cardiac cells.

7.2 Future Recommendations

The proposed electrical stimulation set up introduces a novel system for electrical stimulation of cardiomyocytes in an EHT platform. Future work and optimization on the system would probably enhance its performance and functionality.

- Currently, the MCU of the electrical stimulator is connected through a USB with a computer. The selection of stimulation parameters is feasible through a user interface based on the serial monitor of the Arduino Nano. In the future, it is recommended to replace the microcontroller with one that can support wireless connectivity. This in combination with an integrated camera, will allow biologists to have full control of the electrical stimulation of cardiomyocytes without a USB connection but rather using an app in their mobile phones!
- Until now, a manual potentiometer is used to control the voltage of the applied signal. Although, this is an easy way of amplitude regulation for the user, it occupies enough space to the PCB. Therefore, it should be replaced by a digital one. This way instead of manual control of voltage amplitude, the amplitude will be controlled digitally through the user-interface.
- The 16-channel electrical stimulator is connected through wire cables with the 16-electrode chip holder(PCB). In the future it is suggested to combine these two devices to one and integrate all the electronics in the same PCB unit where the electrode chips are hosted.
- Finally, the integrated TiN electrodes need to be characterized by using Electrochemical Impedance Spectroscopy(EIS). Since the electrodes will be in touch with the cardiac cells, EIS is recommended as a method to evaluate the functionality of the integrated electrodes.

BIBLIOGRAPHY

- [1] Lorna Ewart et al. "Application of microphysiological systems to enhance safety assessment in drug discovery". In: Annual review of pharmacology and toxicology 58 (2018), pages 65–82.
- [2] Massimo Mastrangeli, Sylvie Millet, Janny van den Eijnden-van Raaij, et al. "Organ-on-chip in development: Towards a roadmap for organs-on-chip". In: (2019).
- [3] Aleksander Skardal, Thomas Shupe, and Anthony Atala. "Organoid-on-a-chip and body-on-a-chip systems for drug screening and disease modeling". In: *Drug discovery today* 21.9 (2016), pages 1399–1411.
- [4] Anja van de Stolpe and Jaap den Toonder. "Workshop meeting report Organs-on-Chips: human disease models". In: *Lab on a chip* 13.18 (2013), pages 3449–3470.
- [5] Yu Shrike Zhang et al. "Multisensor-integrated organs-on-chips platform for automated and continual in situ monitoring of organoid behaviors". In: *Proceedings of the National Academy of Sciences* 114.12 (2017), E2293–E2302.
- [6] Marc N Hirt, Arne Hansen, and Thomas Eschenhagen. "Cardiac tissue engineering: state of the art". In: *Circulation research* 114.2 (2014), pages 354–367.
- [7] Hesam Parsa, Kacey Ronaldson, and Gordana Vunjak-Novakovic. "Bioengineering methods for myocardial regeneration". In: Advanced drug delivery reviews 96 (2016), pages 195–202.
- [8] Rimantas Kodzius et al. "Organ-on-chip technology: Current state and future developments". In: (2017).
- [9] Nikolas Gaio et al. "Cytostretch, an organ-on-chip platform". In: Micromachines 7.7 (2016), page 120.
- [10] Kayla Duval et al. "Modeling physiological events in 2D vs. 3D cell culture". In: *Physiology* 32.4 (2017), pages 266–277.
- [11] Ahmad Rezaei Kolahchi et al. "Microfluidic-based multi-organ platforms for drug discovery". In: *Micromachines* 7.9 (2016), page 162.
- [12] Kacey Ronaldson-Bouchard and Gordana Vunjak-Novakovic. "Organs-on-a-chip: a fast track for engineered human tissues in drug development". In: Cell stem cell 22.3 (2018), pages 310–324.
- [13] Yishai Avior, Ido Sagi, and Nissim Benvenisty. "Pluripotent stem cells in disease modelling and drug discovery". In: *Nature reviews Molecular cell biology* 17.3 (2016), page 170.
- [14] LM Griep, F Wolbers, and B De Wagenaar. "PM terBraak, BB Weksler, IA Romero, PO Couraud, I. Vermes, AD van der Meer and A. van den Berg". In: *Biomed. Microdevices* 15.1 (2012), pages 145–150.
- [15] Balabhaskar Prabhakarpandian et al. "SyM-BBB: a microfluidic blood brain barrier model". In: Lab on a Chip 13.6 (2013), pages 1093–1101.

- [16] Jiu Deng et al. "Engineered liver-on-a-chip platform to mimic liver functions and its biomedical applications: A review". In: *Micromachines* 10.10 (2019), page 676.
- [17] Yu-Shih Weng et al. "Scaffold-free liver-on-a-chip with multiscale organotypic cultures". In: *Advanced materials* 29.36 (2017), page 1701545.
- [18] Hüseyin AVCI et al. "Recent advances in organ-on-a-chip technologies and future challenges: a review." In: *Turkish Journal of Chemistry* 42.3 (2018).
- [19] Sangeeta N Bhatia and Donald E Ingber. "Microfluidic organs-on-chips". In: *Nature biotechnology* 32.8 (2014), pages 760–772.
- [20] Yu Shrike Zhang et al. "From cardiac tissue engineering to heart-on-a-chip: beating challenges". In: Biomedical Materials 10.3 (2015), page 034006.
- [21] Genevieve Conant et al. "High-content assessment of cardiac function using heart-on-a-chip devices as drug screening model". In: Stem Cell Reviews and Reports 13.3 (2017), pages 335–346.
- [22] João Ribas et al. "Cardiovascular organ-on-a-chip platforms for drug discovery and development". In: Applied In Vitro Toxicology 2.2 (2016), pages 82–96.
- [23] Alexandra Eder et al. "Human engineered heart tissue as a model system for drug testing". In: Advanced drug delivery reviews 96 (2016), pages 214–224.
- [24] T Eschenhagen. "Fink C, Remmers U, Scholz H, Wattchow J, Weil J, Zimmermann W, Dohmen HH, Schafer H, Bishopric N, Wakatsuki T, and Elson EL". In: *Three-dimensional reconstitution of embryonic cardiomyocytes in a collagen matrix: a new heart muscle model system. FASEB J* 8 (1997), pages 683–694.
- [25] Yosuke K Kurokawa and Steven C George. "Tissue engineering the cardiac microenvironment: Multicellular microphysiological systems for drug screening". In: Advanced drug delivery reviews 96 (2016), pages 225–233.
- [26] Thomas Eschenhagen et al. "3D engineered heart tissue for replacement therapy". In: Basic research in cardiology 97.1 (2002), pages I146–I152.
- [27] Arne Hansen et al. "Development of a drug screening platform based on engineered heart tissue". In: Circulation research 107.1 (2010), page 35.
- [28] Marc N Hirt et al. "Increased afterload induces pathological cardiac hypertrophy: a new in vitro model". In: *Basic research in cardiology* 107.6 (2012), page 307.
- [29] J Hudson et al. "Functional screening in human cardiac organoids reveals a metabolic mechanism for cardiomyocyte cell cycle arrest". In: *Heart, Lung and Circulation* 26 (2017), S207–S208.
- [30] Milica Dostanić et al. "A Miniaturized EHT Platform for Accurate Measurements of Tissue Contractile Properties". In: *Journal of Microelectromechanical Systems* (2020).
- [31] Maureen Wanjare and Ngan F Huang. "Regulation of the microenvironment for cardiac tissue engineering". In: Regenerative medicine 12.2 (2017), pages 187–201.
- [32] Gaetano J Scuderi and Jonathan Butcher. "Naturally engineered maturation of cardiomyocytes". In: Frontiers in cell and developmental biology 5 (2017), page 50.
- [33] SS Nunes. "Approach Summary". In: ().
- [34] Nina Tandon et al. "Characterization of electrical stimulation electrodes for cardiac tissue engineering". In: 2006 International Conference of the IEEE Engineering in Medicine and Biology Society. IEEE. 2006, pages 845–848.
- [35] Raymond Van De Berg et al. "The vestibular implant: quo vadis?" In: Frontiers in neurology 2 (2011), page 47.
- [36] Angelina Peñaranda et al. "Cardiac dynamics: a simplified model for action potential propagation". In: Theoretical Biology and Medical Modelling 9.1 (2012), page 50.
- [37] Qi Xu et al. "A programmable multi-channel stimulator for array electrodes in transcutaneous electrical stimulation". In: The 2011 IEEE/ICME International Conference on Complex Medical Engineering. IEEE. 2011, pages 652–656.
- [38] Xiaoran Li, Shunan Zhong, and James Morizio. "16-Channel biphasic current-mode programmable charge balanced neural stimulation". In: *Biomedical engineering online* 16.1 (2017), page 104.

- [39] PM Biesheuvel and JE Dykstra. "The difference between Faradaic and Nonfaradaic processes in Electrochemistry". In: arXiv preprint arXiv:1809.02930 (2018).
- [40] N Gaio. "Organ-on-Silicon". In: (2019).
- [41] L Wang et al. "Multi-electrode monitoring of guided excitation in patterned cardiomyocytes". In: *Microelectronic engineering* 111 (2013), pages 267–271.
- [42] Alan L Hodgkin and Bernard Katz. "The effect of sodium ions on the electrical activity of the giant axon of the squid". In: *The Journal of physiology* 108.1 (1949), page 37.
- [43] DR Curtis, JW Phillis, and JC Watkins. "Chemical excitation of spinal neurones". In: *Nature* 183.4661 (1959), pages 611–612.
- [44] Alfred Stett et al. "Biological application of microelectrode arrays in drug discovery and basic research". In: Analytical and bioanalytical chemistry 377.3 (2003), pages 486–495.
- [45] Stuart F Cogan. "Neural stimulation and recording electrodes". In: Annu. Rev. Biomed. Eng. 10 (2008), pages 275–309.
- [46] S Khoshfetrat Pakazad et al. "A stretchable Micro-Electrode Array for in vitro electrophysiology". In: 2011 IEEE 24th International Conference on Micro Electro Mechanical Systems. IEEE. 2011, pages 829–832.
- [47] Michael Q Chen et al. "Current-controlled electrical point-source stimulation of embryonic stem cells". In: Cellular and molecular bioengineering 2.4 (2009), page 625.
- [48] Burak Dura et al. "High-frequency electrical stimulation of cardiac cells and application to artifact reduction". In: *IEEE transactions on biomedical engineering* 59.5 (2012), pages 1381–1390.
- [49] R Hollis Whittington, Laurent Giovangrandi, and Gregory TA Kovacs. "A closed-loop electrical stimulation system for cardiac cell cultures". In: *IEEE Transactions on Biomedical Engineering* 52.7 (2005), pages 1261–1270.
- [50] Kirsi Kujala et al. "Electrical field stimulation with a novel platform: effect on cardiomyocyte gene expression but not on orientation". In: *International journal of biomedical science: IJBS* 8.2 (2012), page 109.
- [51] Hoi Ting H Au et al. "Interactive effects of surface topography and pulsatile electrical field stimulation on orientation and elongation of fibroblasts and cardiomyocytes". In: *Biomaterials* 28.29 (2007), pages 4277–4293.
- [52] Kacey Ronaldson-Bouchard et al. "Advanced maturation of human cardiac tissue grown from pluripotent stem cells". In: *Nature* 556.7700 (2018), pages 239–243.
- [53] Hesam Parsa, Bryan Z Wang, and Gordana Vunjak-Novakovic. "A microfluidic platform for the high-throughput study of pathological cardiac hypertrophy". In: *Lab on a Chip* 17.19 (2017), pages 3264–3271.
- [54] Amandine FG Godier-Furnémont et al. "Physiologic force-frequency response in engineered heart muscle by electromechanical stimulation". In: *Biomaterials* 60 (2015), pages 82–91.
- [55] Mohamed A Mohamed et al. "Electrical Stimulation of Artificial Heart Muscle: a look into the electrophysiological and genetic implications". In: ASAIO journal (American Society for Artificial Internal Organs: 1992) 63.3 (2017), page 333.
- [56] Samad Ahadian et al. "Interdigitated array of Pt electrodes for electrical stimulation and engineering of aligned muscle tissue". In: Lab on a Chip 12.18 (2012), pages 3491–3503.
- [57] Ning Zhang et al. "Multifunctional 3D electrode platform for real-time in situ monitoring and stimulation of cardiac tissues". In: *Biosensors and Bioelectronics* 112 (2018), pages 149–155.
- [58] KW Eric Cheng et al. "Development of a circuit for functional electrical stimulation". In: *IEEE Transactions on neural systems and rehabilitation engineering* 12.1 (2004), pages 43–47.
- [59] Delmar Carvalho de Souza et al. "Power amplifier circuits for functional electrical stimulation systems". In: Research on Biomedical Engineering 33.2 (2017), pages 144–155.
- [60] Jim Simpson and Maysam Ghovanloo. "An experimental study of voltage, current, and charge controlled stimulation front-end circuitry". In: 2007 IEEE International Symposium on Circuits and Systems. IEEE. 2007, pages 325–328.

- [61] Aizan Masdar, BSKK Ibrahim, and M Mahadi Abdul Jamil. "Development of wireless-based low-cost current controlled stimulator for patients with spinal cord injuries". In: 2012 IEEE-EMBS Conference on Biomedical Engineering and Sciences. IEEE. 2012, pages 493–498.
- [62] S Khosravani, N Lahimgarzadeh, and A Maleki. "Developing a stimulator and an interface for FES-cycling rehabilitation system". In: 2011 18th Iranian Conference of Biomedical Engineering (ICBME). IEEE. 2011, pages 175–180.
- [63] Hongen Qu et al. "Development of a network FES system for stroke rehabilitation". In: 2011 Annual International Conference of the IEEE Engineering in Medicine and Biology Society. IEEE. 2011, pages 3119–3122.
- [64] Sahar Elyahoodayan et al. "A Multi-Channel Asynchronous Neurostimulator With Artifact Suppression for Neural Code-Based Stimulations". In: Frontiers in Neuroscience 13 (2019), page 1011.
- [65] Chandrashekhar Shendkar et al. "Design and development of a low-cost biphasic charge-balanced functional electric stimulator and its clinical validation". In: *Healthcare technology letters* 2.5 (2015), pages 129–134.
- [66] Christophor J Poletto and Clayton L Van Doren. "A high voltage, constant current stimulator for electrocutaneous stimulation through small electrodes". In: *IEEE Transactions on Biomedical Engineering* 46.8 (1999), pages 929–936.
- [67] Maxime Yochum et al. "A mixed FES/EMG system for real time analysis of muscular fatigue". In: 2010 Annual International Conference of the IEEE Engineering in Medicine and Biology. IEEE. 2010, pages 4882–4885.
- [68] F Brunetti et al. "Enhancing functional electrical stimulation for emerging rehabilitation robotics in the framework of hyper project". In: 2011 IEEE International Conference on Rehabilitation Robotics. IEEE. 2011, pages 1–6.
- [69] T Ragheb and LA Geddes. "The polarization impedance of common electrode metals operated at low current density". In: *Annals of biomedical engineering* 19.2 (1991), pages 151–163.
- [70] Wendy Franks et al. "Impedance characterization and modeling of electrodes for biomedical applications". In: *IEEE Transactions on Biomedical Engineering* 52.7 (2005), pages 1295–1302.
- [71] Nick Sperelakis and T Hoshiko. "Electrical impedance of cardiac muscle". In: Circulation Research 9.6 (1961), pages 1280–1283.
- [72] ET McAdams et al. "Characterization of gold electrodes in phosphate buffered saline solution by impedance and noise measurements for biological applications". In: 2006 International Conference of the IEEE Engineering in Medicine and Biology Society. IEEE. 2006, pages 4594–4597.
- [73] Low Noise Dual Supply Inverting Charge Pump. Technical report.
- [74] Step down DC-DC converter. Technical report.
- [75] Pulse Width Modulation. Technical report.
- [76] ATMEGA328P. Technical report.
- [77] SecretsOfArduinoPWM. URL: https://www.arduino.cc/en/Tutorial/SecretsOfArduinoPWM.
- [78] ADG1408-DEMUX. Technical report.
- [79] Fundamentals of Current Measurement. https://www.digikey.com/en/articles/fundamentals-of-current-measurement-part-2-current-sense-amplifiers. 2018.
- [80] Cristy M Schade et al. "Assessment of patient preference for constant voltage and constant current spinal cord stimulation". In: Neuromodulation: Technology at the Neural Interface 13.3 (2010), pages 210–217.
- [81] Jinwen Zhou et al. "Surface modification for PDMS-based microfluidic devices". In: *Electrophoresis* 33.1 (2012), pages 89–104.
- [82] I Beaulieu-Boire and A Fasano. "Current or voltage? Another Shakespearean dilemma." In: European Journal of Neurology 22.6 (2014), pages 887–888.
- [83] Aaron S Tucker, Robert M Fox, and Rosalind J Sadleir. "Biocompatible, high precision, wideband, improved Howland current source with lead-lag compensation". In: *IEEE Transactions on Biomedical Circuits and Systems* 7.1 (2012), pages 63–70.

- [84] DH Sheingold. "Impedance & admittance transformations using operational amplifiers". In: Lightning Empiricist 12.1 (1964), pages 1–8.
- [85] Amin Mahnam, Hassan Yazdanian, and Mohsen Mosayebi Samani. "Comprehensive study of Howland circuit with non-ideal components to design high performance current pumps". In: *Measurement* 82 (2016), pages 94–104.
- [86] Jinwen Zhou et al. "Surface modification for PDMS-based microfluidic devices". In: *Electrophoresis* 33.1 (2012), pages 89–104.
- [87] DM Zhou and RJ Greenberg. "Electrochemical characterization of titanium nitride microelectrode arrays for charge-injection applications". In: Proceedings of the 25th Annual International Conference of the IEEE Engineering in Medicine and Biology Society (IEEE Cat. No. 03CH37439). Volume 2. IEEE. 2003, pages 1964–1967.
- [88] Anna Norlin, Jinshan Pan, and Christopher Leygraf. "Investigation of electrochemical behavior of stimulation/sensing materials for pacemaker electrode applications: I. Pt, Ti, and TiN coated electrodes". In: *Journal of the Electrochemical Society* 152.2 (2004), J7.
- [89] Stuart F Cogan. "Neural stimulation and recording electrodes". In: Annu. Rev. Biomed. Eng. 10 (2008), pages 275–309.
- [90] Meysam Zarchi, Shahrokh Ahangarani, and Maryam Zare Sanjari. "Properties of silicon dioxide film deposited by PECVD at low temperature/pressure". In: *Metallurgical and Materials Engineering* 20.2 (2014), pages 89–96.
- [91] WI Wu et al. "Materials and methods for the microfabrication of microfluidic biomedical devices". In: *Microfluidic devices for biomedical applications*. Elsevier, 2013, pages 3–62.
- [92] Frédéric Marty et al. "Advanced etching of silicon based on deep reactive ion etching for silicon high aspect ratio microstructures and three-dimensional micro-and nanostructures". In: Microelectronics journal 36.7 (2005), pages 673–677.
- [93] M Elwenspoek et al. "Wet chemical etching mechanism of silicon". In: Proceedings IEEE Micro Electro Mechanical Systems An Investigation of Micro Structures, Sensors, Actuators, Machines and Robotic Systems. IEEE. 1994, pages 223–228.
- [94] Der-Jang Liaw et al. "Advanced polyimide materials: syntheses, physical properties and applications". In: Progress in Polymer Science 37.7 (2012), pages 907–974.
- [95] S Diaham, ML Locatelli, and R Khazaka. "BPDA-PDA polyimide: synthesis, characterizations, aging and semiconductor device passivation". In: *High Performance Polymers-Polyimides Based-From Chemistry to Applications* (2012), pages 15–36.
- [96] Thomas Stieglitz, M Schuetter, and Klaus Peter Koch. "Implantable biomedical microsystems for neural prostheses". In: *IEEE engineering in medicine and biology magazine* 24.5 (2005), pages 58–65.
- [97] Masaru Kotera et al. "Microstructures of BPDA-PPD polyimide thin films with different thicknesses". In: *Polymer* 54.9 (2013), pages 2435–2439.
- [98] Juan S Ordonez et al. "Silicone rubber and thin-film polyimide for hybrid neural interfaces—A MEMS-based adhesion promotion technique". In: 2013 6th International IEEE/EMBS Conference on Neural Engineering (NER). IEEE. 2013, pages 872–875.
- [99] Benjamin Mimoun et al. "Residue-free plasma etching of polyimide coatings for small pitch vias with improved step coverage". In: Journal of Vacuum Science & Technology B, Nanotechnology and Microelectronics: Materials, Processing, Measurement, and Phenomena 31.2 (2013), page 021201.
- [100] JR Salem et al. "Solventless polyimide films by vapor deposition". In: Journal of Vacuum Science & Technology A: Vacuum, Surfaces, and Films 4.3 (1986), pages 369–374.
- [101] Roy D Kornbluh et al. "Shape control of large lightweight mirrors with dielectric elastomer actuation". In: Smart Structures and Materials 2003: Electroactive Polymer Actuators and Devices (EAPAD). Volume 5051. International Society for Optics and Photonics. 2003, pages 143–158.
- [102] Say Hwa Tan et al. "Oxygen plasma treatment for reducing hydrophobicity of a sealed polydimethylsiloxane microchannel". In: *Biomicrofluidics* 4.3 (2010), page 032204.



A.1 Design Schematics of Electrical Stimulator

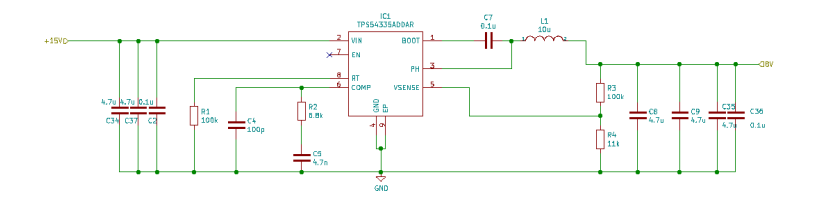


Figure A.1: Schematic of the buck converter chip which converts $30\mathrm{V}$ to $8\mathrm{V}$ and supplies the microcontroller

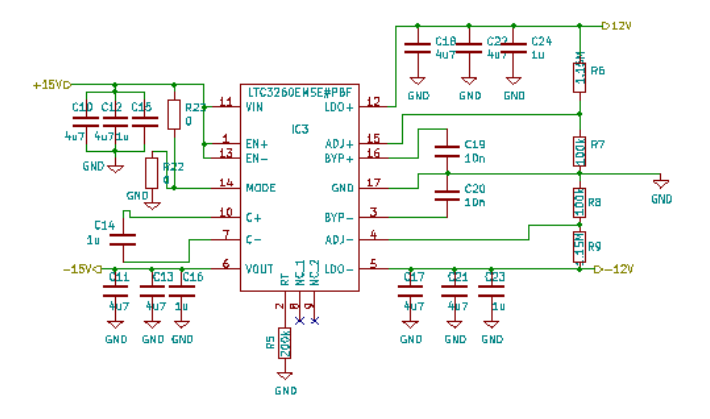


Figure A.2: Schematic of the Charge Pump Converter which converter which converts $30\mathrm{V}$ to +- $15\mathrm{V}$ and supplies the amplifiers

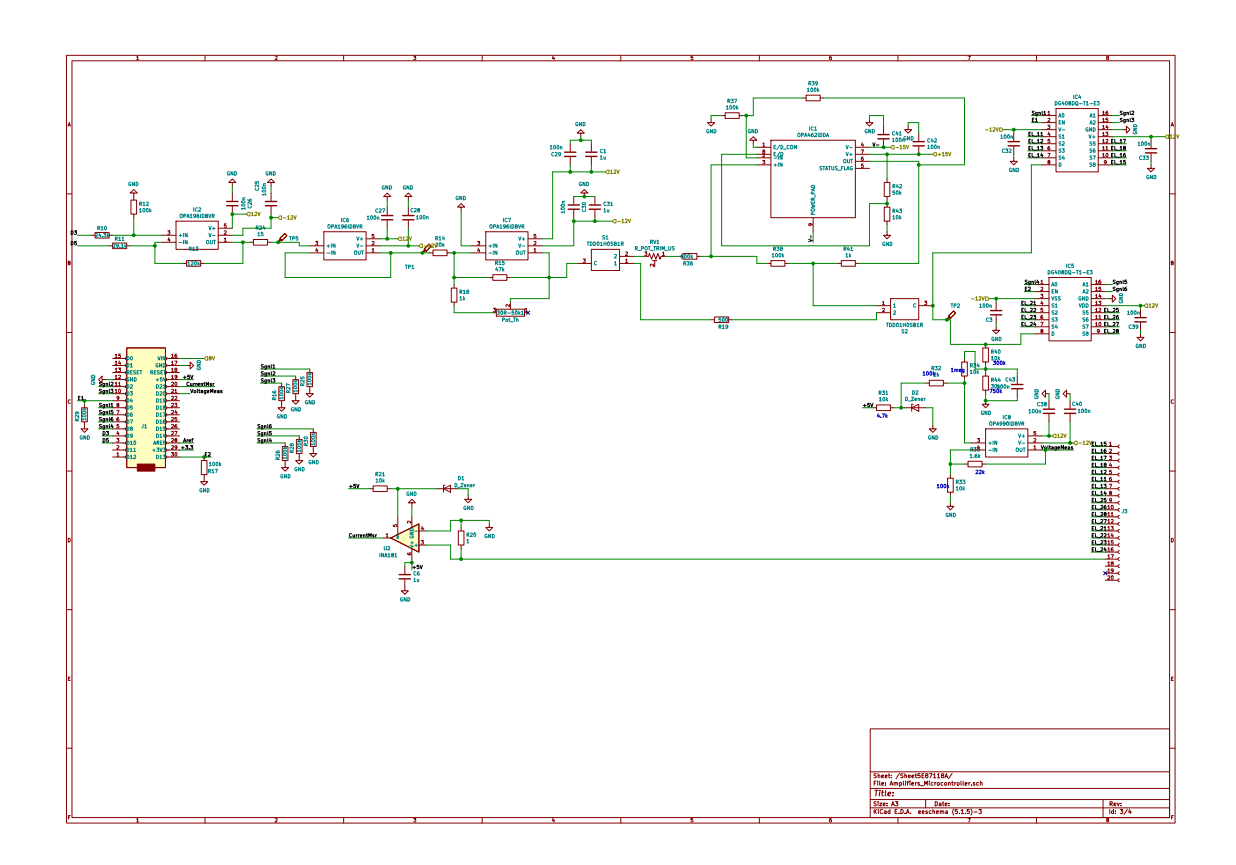


Figure A.3: Entire Schematic of Electrical Stimulator Circuit

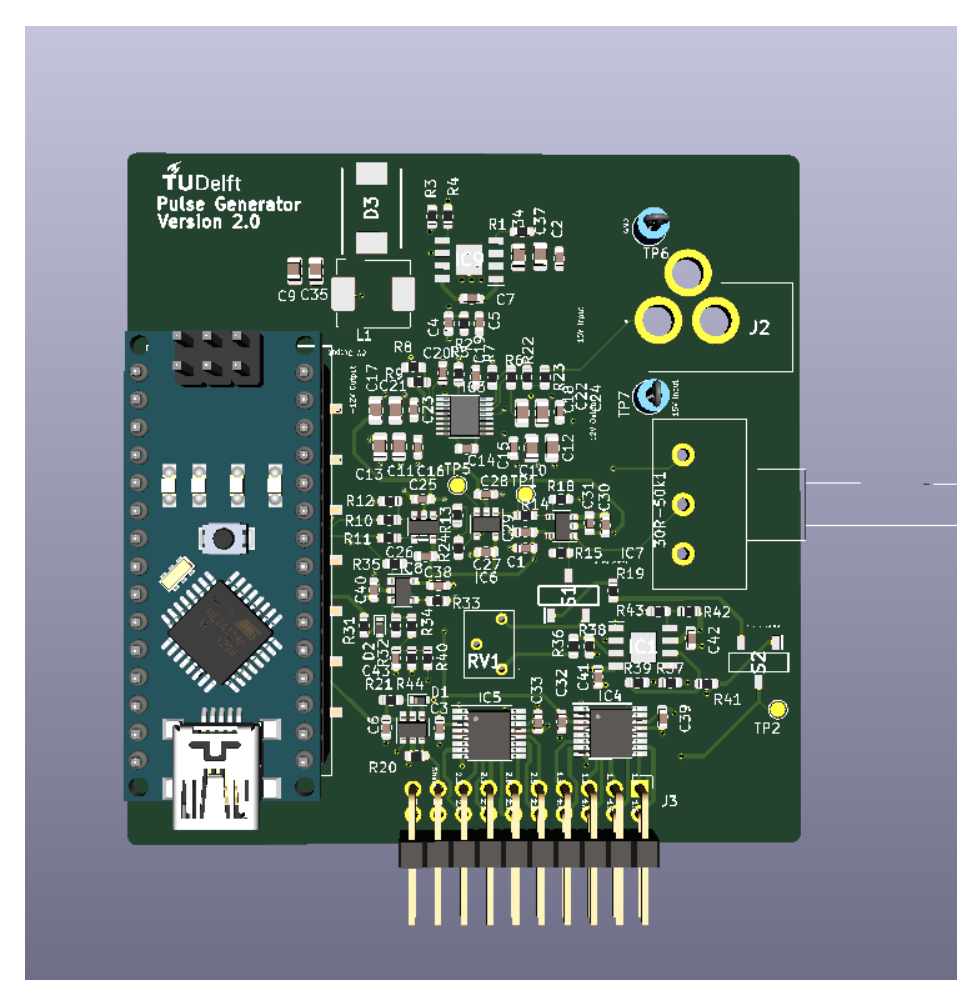


Figure A.4: 3D Version of Electrical Stimulator

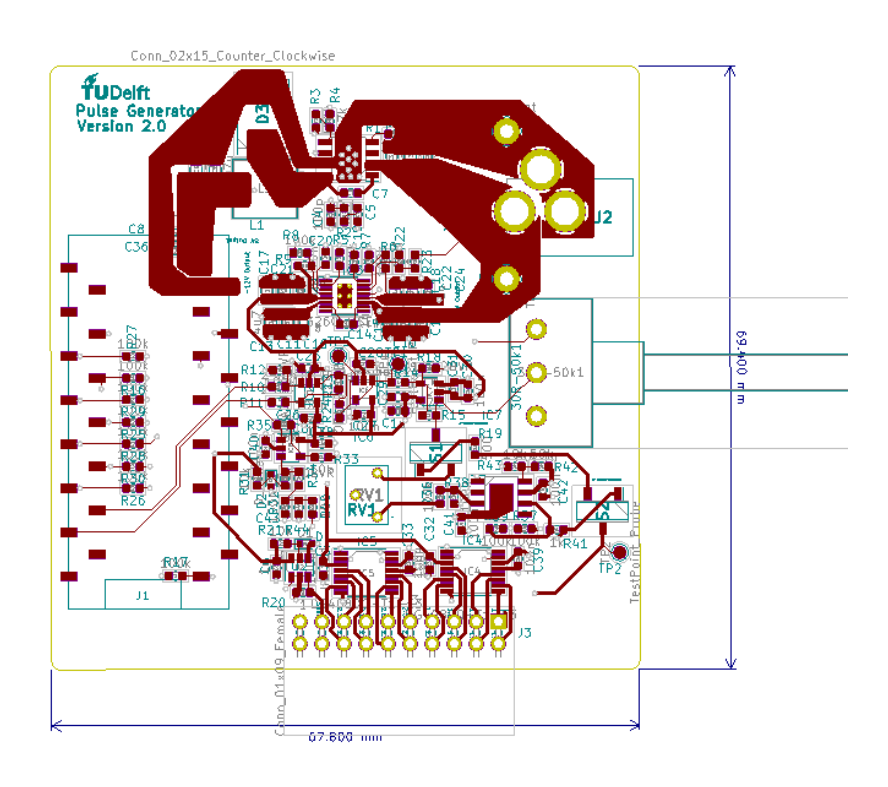


Figure A.5: The KiCad schematic of the front layer of the PCB

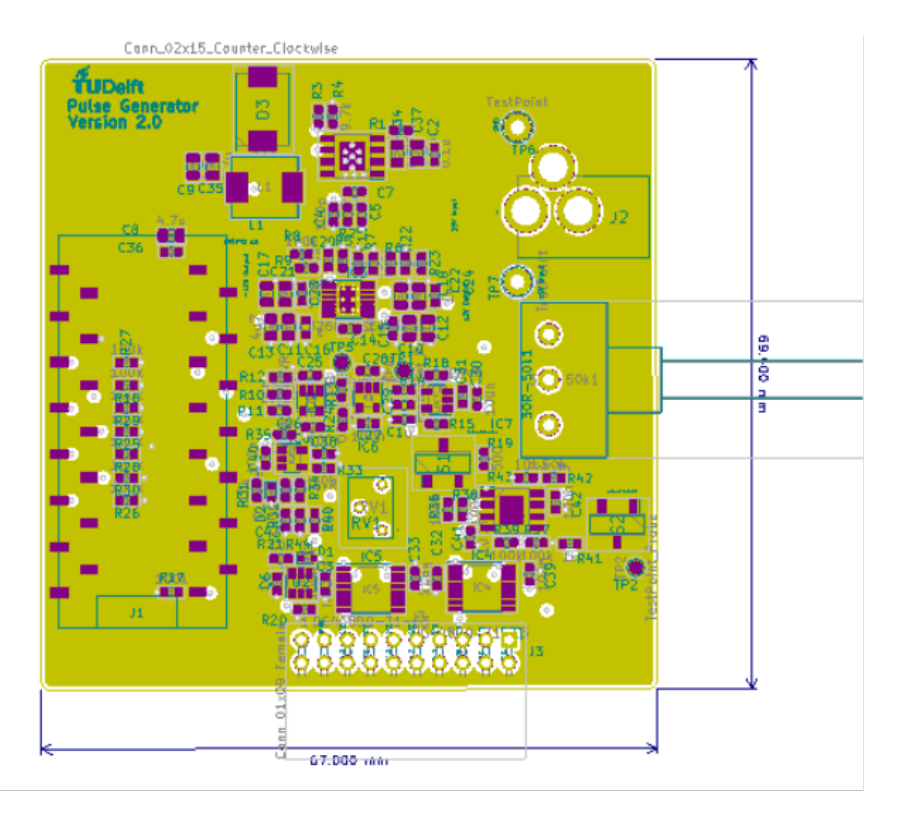


Figure A.6: The KiCad schematic of the second layer of the PCB

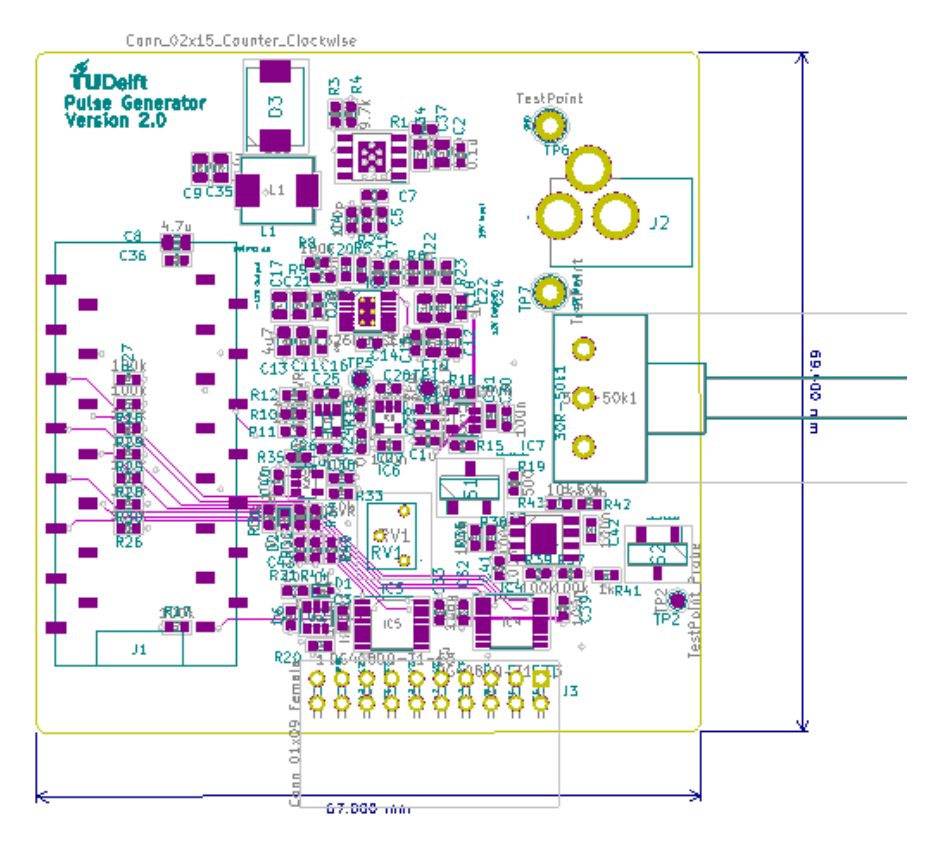


Figure A.7: The KiCad schematic of the third layer of the PCB

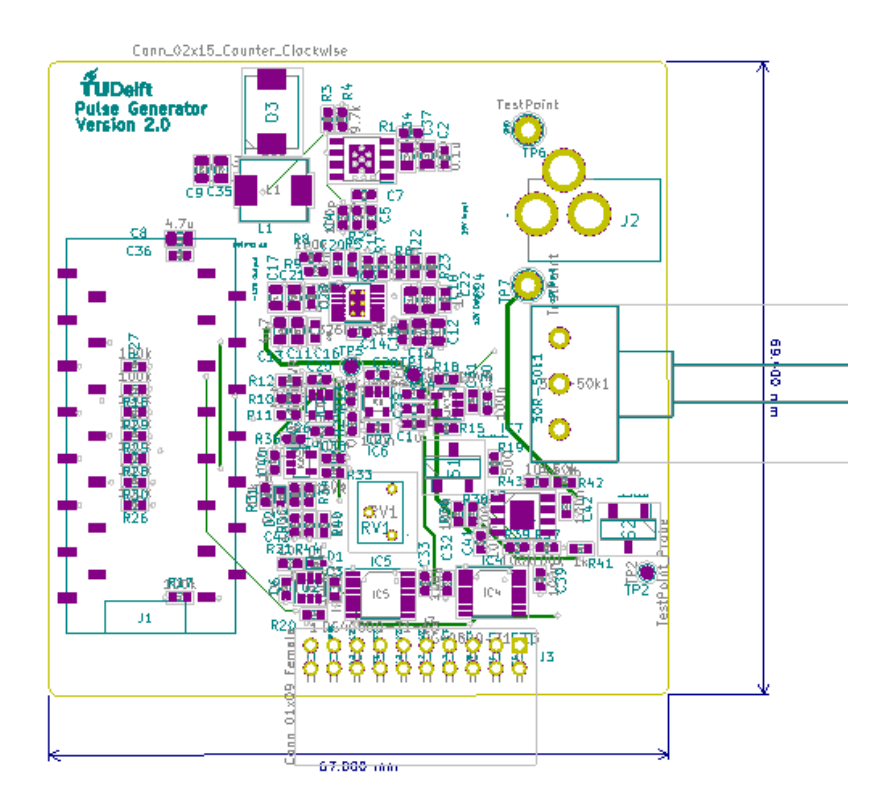


Figure A.8: The KiCad schematic of the back layer of the PCB



PROGRAMMING CODE IN C/C++ FOR CONTROLLING THE ELECTRICAL STIMULATOR

```
The Serial Degin (9600); //This command starts the serial communication between the serial monitor and the microcontroller

printed (ENI, COTPUT); planded (ENI, COTPUT); // selection pin of the demultiplexer is defined as output planded (ENI, COTPUT); // selection pin of the demultiplexer is defined as output planded (ENI, COTPUT); // selection pin of the demultiplexer is defined as output planded (ENI, COTPUT); // selection pin of the demultiplexer is defined as output planded (ENI, COTPUT); // selection pin of the demultiplexer is defined as output planded (ENI, COTPUT); // selection pin of the demultiplexer is defined as output planded (ENI, COTPUT); // selection pin of the demultiplexer is defined as output planded (ENI, COTPUT); // selection pin of the demultiplexer is defined as output planded (ENI, COTPUT); // selection pin of the demultiplexer is defined as output planded (ENI, COTPUT); // selection pin of the demultiplexer is defined as output planded (ENI, COTPUT); // selection pin of the demultiplexer is defined as output planded (ENI, COTPUT); // selection pin of the demultiplexer is defined as output planded (ENI, COTPUT); // selection pin of the demultiplexer is defined as output pland
```

Figure B.1: Set up and initialization of parameters.

```
//Initialization of registers for CTC mode and Timeri
TCCRIA***O;
TCCRIA**O;
TCCRIA
```

Figure B.2: Set up and initialization of parameters.

Figure B.3: Channel selection-automated the user just type the desired channel of stimulation in the serial monitor and the pulse is directed to it.

Figure B.4: Channel selection-automated the user just type the desired channel of stimulation in the serial monitor and the pulse is directed to it.

```
// This function defines the biphasic pulse according to the value of the duty cycle that the user set as a parameter at the beggining
IRR(IMER1_COMPA_vect) {

if(i >= 0 && i <= (duty_cycle-1)) {

    PORTB = _BV(PB2);

}
else if(i > (duty_cycle-1) && i <= ((2*duty_cycle)-1)) {

    PORTB = _BV(PB1);

//Measuring the current circuit and print it in serial monitor

    float Vout=analogRead(A7);
    float Vo=Vout*(5.0/1023.0);
    float I=(Vo-Vvef)*1000/(gain*R);
    Serial.println("To=");
    Serial.println(I);

//Measuring the voltage circuit and print it in serial monitor

float V_out=analogRead(A6);
    float V_out=analogRead(A6);
    float v_ov=V out*(5.0/1023.0);
    float bo=(V_o-3.39)*1.33/0.109;
    Serial.println("Vo=");
    Serial.println("\n");
    Serial.println(Bo=");
    Serial.println(Bo=");
```

Figure B.5: Voltage Measurement and Current Measurement circuits and

```
//Safety Module that checks the maximum applied current to the cardiac cells
   if(I>=12){
        digitalWrite(EN1, LOW);
        digitalWrite(EN2, LOW);
        PORTB = 0;}
}
else if(i > (2*duty_cycle-1) && i <= 100){
        PORTB = 0;}

i++;
   if(i==100){
        i=0;
    }
}</pre>
```

11_9_20_final §

if(I>=12)[
digitalWrite(EN1, LOW);
digitalWrite(EN2, LOW);
PORTB = 0;)

Figure B.6: Safety Module

APPENDIX C

_SIMULATION CIRCUIT OF SECOND METHOD OF BIPHASIC PULSE GENERATION

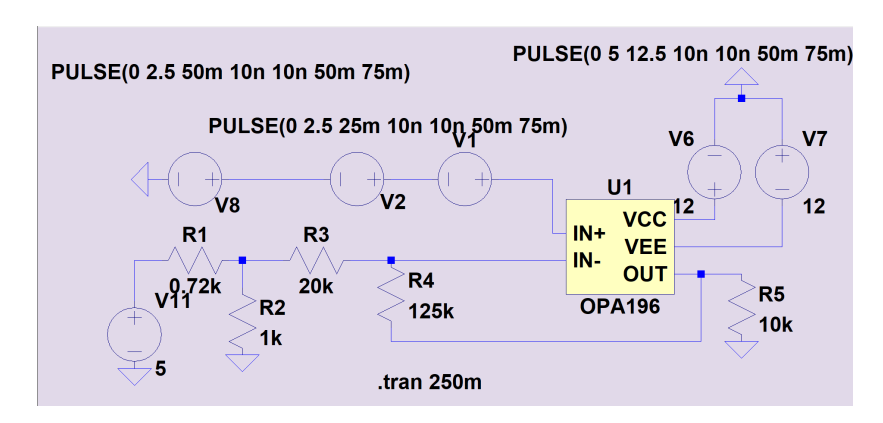


Figure C.1: Simulation circuit of second method of biphasic pulse generation

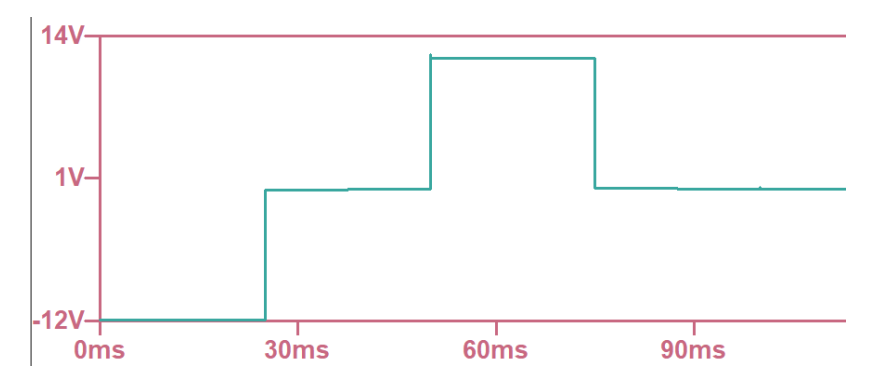


Figure C.2: Result from simulation of second method of biphasic pulse generation



Table D.1: Component List fo DC Buck Converter

Part number	Description	Manufacturer
TPS54360BDDAR	60-V input, 3.5-A, step-down DC/DC converter	Texas Instruments
ASPI-0630LR-100M-T15	Inductor_SMD:L_Abracon_ASPI-0630LR	ABRACON
B560C-13-F	D_Schottky	Diodes incorporated
C0805C475J3RACTU	4.7u Capacitor	KEMET
C0603C101K1HACAUTO	100p Capacitor	KEMET
CRCW0603100KFKEAC	100k Resistor	Vishay
CHP0603-FX-6801ELF	6.8k Resistor	Bourns
C0603C104J3REC7411	0.1u Capacitor	KEMET
CRCW060311K0FKEA	9.7k Resistor	Vishay

Table D.2: Component List fo DC Buck Converter

Part number	Description	Manufacturer
LTC3260EMSE#PBF	LTC3260,Charge Pump Inverter,MSOP EP-16	Linear Technology
CRCW06031M15FKEA	$\begin{tabular}{ll} Resistor_SMD:R_0603_1608Metric~1.15M \\ \end{tabular}$	Vishay
CRCW0603100KFKEAC	Resistor_SMD:R_0603_1608Metric 100k	Vishay
CRCW0603200KFKEAC	$\begin{tabular}{ll} Resistor_SMD:R_0603_1608Metric~200k \\ \end{tabular}$	Vishay
C0805C475J3RACTU	Capacitor_SMD:C_0805_2012Metric 4.7u	KEMET
TMK107BJ105KA-T	Capacitor_SMD:C_0603_1608Metric 1u	Tayo Yuden
CGA3E1C0G2A103J080AE	Capacitor_SMD:C_0603_1608Metric 10n	TDK

Table D.3: Component List for Biphasic Pulse Generation Unit

Part number	Description	Manufacturer
OPA196IDBVR	36V, Low Power, All-Purpose Amplifier	Texas Instruments
OPA462IDDA	Operational Amplifiers - Op Amps 180-V	Texas Instruments
TDD01H0SB1R	SIP Switches Jumper Switch 2 positions	C & K COMPONENTS
OPA990IDBVR	36V, Low Power, All-Purpose Amplifier	Texas Instruments
CRCW060324K3FKEA	24.3k	Vishay
RN731JTTD2912F100	29.1k	KOA Speer
AC0603FR-10120KL	120k	Yageo
CRCW060315R0FKEA	15 ohm	Vishay
PDB181-K415F-503B	Potentiometer_Omeg_PC16BU_Horizontal	Bourns
AC0603FR-1020KL	20k	Yageo
CC0603MRY5V9BB104	100n	Yageo
RC0603FR-0747KL	47k	Yageo

Table D.4: Component List for Howland Converter

Part number	Description	Manufacturer
OPA462IDDA	Operational Amplifiers - Op Amps 180-V	Texas Instruments
R_POT_TRIM_US	R_POT_TRIM_US	Vishay
ERA-3ARW104V	Resistor_SMD:100k	Panasonic
TNPU0603500RAZEN00	Resistor_SMD:500	Vishay
RT0603BRD0750KL	Resistor_SMD:50k	Yageo
CRCW06031K00FKEAC	Resistor_SMD:1k	Vishay

Table D.5: Component List for Voltage Measurement and Microcontroller

Part number	Description	Manufacturer
OPA990IDBVR	Operational Amplifiers , 44V	Texas Instruments
Diode_SMD:D_SOD-523	CMOZ2L7 TR PBFREE	Central Semiconductor
APC0603B10K0N	Resistor_SMD:10k	ARCOL/Ohmite
RR0816P-162-D	Resistor_SMD:1.6k	Susumu
ERJ-UP3F3002V	Resistor_SMD:30k	Panasonic
CC0603MRY5V9BB104	Capacitor_SMD:100n	Yageo
ATMEGA328	MCU	Arduino